# DEVELOPMENT AND EVALUATION OF POSTURAL CONTROL MODELS FOR LIFTING MOTIONS AND BALANCE CONTROL

Xingda Qu

Dissertation submitted to the faculty of the
Virginia Polytechnic Institute and State University
in partial fulfillment of the requirements for the degree of

DOCTOR OF PHILOSOPHY
In
Industrial and Systems Engineering

Dr. Maury A. Nussbaum, Chair
Dr. Kari L. Babski-Reeves
Dr. Michael L. Madigan
Dr. Miguel A. Perez
Dr. John P. Shewchuk

March 28, 2008
Blacksburg, Virginia

Keywords: Postural Control, Lifting, Balance Control, Fuzzy Logic, Optimal Control

# DEVELOPMENT AND EVALUATION OF POSTURAL CONTROL MODELS FOR LIFTING MOTIONS AND BALANCE CONTROL

Xingda Qu

**(ABSTRACT)**

Accurately simulating human motions is a major function of and challenge to digital human models and integrating humans in computer-aided design systems. Numerous successful applications of human motion simulation have already demonstrated their ability to improve occupational efficiency, effectiveness, and safety. In this dissertation, a novel motion simulation model using fuzzy logic control is presented. This model was motivated by the fact that humans use linguistic terms to guide their behaviors while fuzzy logic provides mathematical representations of linguistic terms. Specifically in this model, fuzzy logic was used to specify a neural controller which was generally considered as the part in the postural control system that plans human motions. Fuzzy rules were generated according to certain trends observed from actual human motions. An optimization procedure was performed to specify the parameters of the membership functions by minimizing the differences between the simulated and actual final postures. This research contributed to the field of human movement science by providing a motion simulation model that can accurately predict novel human motions and provide interpretations of potential human motion planning strategies.

Understanding balance control is another research focus in this dissertation. Investigating balance control may aid in preventing unnecessary fall-related incidents and understanding the postural control system. Since human behaviors are generally effective and efficient, balance control models (both two- and three-dimensional) based on an optimal control strategy were developed to aid in better understanding balance control. Specifically, the neural controller was considered as an optimal controller that minimizes a performance index defined by physical quantities relevant to sway. Free model parameters, such as weights of relevant physical quantities and sensory delay time, were determined by an optimization procedure whose objective was to minimize a scalar error between simulated and experimental center-of-pressure (COP) based measures.

Many factors, such as aging, localized muscle fatigue, and external loads, have been found to adversely affect balance control. At the same time, behaviors during upright stance are commonly characterized by COP-based measures. Thus, changes in COP based measures with aging, LMF, and external loads were addressed by using the proposed models, and possible postural control mechanisms were identified by interpreting these changes. Findings from these studies demonstrated that the proposed models were able to accurately simulate human sway behaviors and provide plausible mechanisms regarding how the postural control system works when maintaining upright balance.

## ACKNOWLEDGMENTS

First, I would like to gratefully and sincerely thank my advisor, Dr. Maury A. Nussbaum, for his advice, guidance, encouragement, and most importantly his friendship during my graduate studies at Virginia Tech. His remarkable mind and admirable personality have taught me what a great professor should be.

I would also like to thank my committee members, Dr. Kari L. Babski-Reeves, Dr. Michael L. Madigan, Dr. Miguel A. Perez, and Dr. John P. Shewchuk, for their constructive advice and efforts in my dissertation research. Special thanks to Dr. Thurmon E. Lockhart for his willingness to discuss any aspect of my research work.

Thanks to my best friends at Virginia Tech, Bochen, Boon Kee, Dingding, Hongbo, Jian, Xiaoyue, and Yu-Hsiu. I cannot list all your names here, but thank you all for making my time full of fun. Thanks to my lab mates, Kevin, Linsey, Jung Yong, and Sunwook for being so helpful. Further thanks to my parents and family for their love and care, without which this dissertation would not have been possible.

# Table of Contents

## List of Figures

## List of Tables

# Chapter 1 Introduction

## 1.1 Motivation

The motion strategy adopted by human beings is affected by tasks and products, an undesirable design of which can impair efficiency, effectiveness, and safety. Therefore, measures should be taken in order to improve task and product design, and human motion is a key factor that should be considered.

Two methods can be used to gather human motion data (Robertson et al., 2004). The first is experiment-based, in which human participants are instructed to perform specified tasks in a real or replicated work environment and actual human motion behaviors are captured. The second is simulation-based, in which humans and the work environment are modeled by mathematical algorithms and predicted motions can be obtained through the computation of these algorithms given input data describing the tasks and human participants. The first method can provide more realistic human motion data; however, it is only useful in the particular scenario under which the motion was captured, is only applicable for a single person's behavior, and may be restricted by safety and ethical issues. If a simulation model is accurate, the second method can be a more efficient means to obtain relatively accurate motion data, and can be generally used to predict different motion scenarios for different individuals.

Interest in simulating human motions spans diverse disciplines, including motor control, animation, and consumer product design. Extensive work has been conducted for occupational activities, in particular, with several modern computer aided design (CAD) systems including

humans widely used for task and product design. Accurately simulating human motions is a major function and challenge of human CAD systems (Park et al., 2004), yet Chaffin (2005) offered three major reasons underlying the value of human motion simulation and simulation models/methods. First, such simulations can reveal possible motion strategies and biomechanics that are used to control motions. Second, such simulations can predict motions between different groups of people and different tasks. Third, simulations can predict motions under novel situations. Therefore, human motion simulation is a major area of interest in the application of biomechanics and ergonomics.

Numerous successful applications of human motion simulation have already demonstrated their ability to improve occupational efficiency, effectiveness, and safety (Chaffin, 2001, 2005). Specifically, lifting simulation may be very helpful to understand and prevent occupational low-back pain (LBP) incidents. LBP is one of the most common and costly occupational injuries, and about 5% of American adults experience an episode of LBP every year (Frymoyer and Cats-Baril, 1987). LBP is frequently associated with lifting activities that impose high loads on the lumbosacral and the lumbar intervertebral joints. Body posture is an important factor affecting loads on these joints during lifting (Chaffin, 1999). Use of lifting motion simulation can help estimate dynamic human postures, thus avoiding in the need for collecting actual postural data in the process of tasks evaluation or design.

Balance control modeling is also an area of interest for my dissertation. Falls are a major cause of occupational injuries. In 2003, it was reported that falls accounted for 272,988 nonfatal occupational injuries and 691 fatalities (Department of Labor, 2005). In 1999 alone,

fall-related injuries resulted in $3.7 billion in direct costs (Department of Labor, 2005). Fall-related injuries are even more prevalent and serious for older people. About a third of Americans over 65 experience fall-related injuries annually and 32% of Americans over 85 die from traumatic falls (Shin et al., 2005).

From biomechanical and psychophysiological perspectives, a substantial number of fall injuries are thought to result from loss-of-balance (Hsiao and Simeonov, 2001). Thus, better understanding balance control may aid in preventing unnecessary fall-related incidents. In essence, maintenance of upright stance is a complex control problem. More specifically, the upright posture, by itself, is unstable in the field of gravity. Without internal control, any minute amplitude disturbances can comprise its stability due to the existence of gravity. In addition, stability of the human body requires that the projection of its center of mass (COM) lies within the area of the base of support (BoS) (Loughlin et al., 2003). However, the area of the BoS is only on the order of one square foot. This relatively small area requires fine tuning of the interaction between movements of different body joints in order to maintain upright balance (Latash, 1993). This fact greatly challenges our understanding of any practical control systems.

Theoretically, the task of maintaining upright balance is performed by the human postural control system. However, based on existing knowledge, it is hard to completely understand how the human postural control system works. Balance control models are a powerful tool to investigate potential mechanisms indirectly. A mathematical model usually has the advantage of providing an intuitive understanding of how the entire system functions and how individual components influence the overall system's response (Peterka, 1995). In addition, balance

control models may predict human physiological reactions used in maintaining balance.

Aging can decrease strength (Vandervoort, 2002) and the speed of a response to loss of balance (Thenlen et al., 1996), both of which result in an increased fall risk (Mackey and Robinovitch, 2006). At the same time, some studies have suggested that localized muscle fatigue (LMF) at some joints (e.g. the ankle, hip, and shoulder) increased postural sway (Gribble and Hertel, 2004; Yaggie and McGregor, 2002). Increases in postural sway are an indicator of greater postural instability (Cavanaugh et al., 2005). Thus, LMF may lead to increased fall risks as well (Pline et al., 2006). In addition, carrying external loads is commonly involved in everyday actions and occupational activities, and such loads appear to adversely affect postural balance (Ledin et al., 1993; Kincl and Odkvist, 2002). Identifying changes in the control of upright stance with aging, LMF or external loads has been considered an important initial step in developing interventions to reduce fall risks (McClenaghan et al., 1996). A balance control model can be used to predict these changes, and thus may be a useful tool for the development of intervention strategies for the improvement of balance.

## 1.2 Research objective

This dissertation research primarily focused on two areas. The first area is on human motion simulation. The second, and more extensive, is on balance control modeling. Overall, the objectives of the research were as follows:

- To develop a new human motion simulation model that can accurately simulate and predict human lifting motions.

- To develop a new balance control model that can accurately simulate and predict spontaneous sway behaviors.
- To investigate, and in some cases predict, how different individual and task factors (e.g. aging, localized muscle fatigue, and external loads) affect balance control by using the proposed balance control model.

# Chapter 2 Literature Review

## 2.1 Human Motion Simulation

Due to the redundancy of the human musculoskeletal system, when simulating human motions, ill-posed problems have to be faced. This means that solutions to some problems during simulation are not unique (Kawato, 1996; Faraway et al., 1999). During a simple arm reaching motion, for example, there are an infinite number of possible trajectories connecting the initial and target positions. Several approaches have been proposed to solve the ill-posed human motion simulation problems. These approaches will be reviewed in more detail in the following sections.

### 2.1.1 Inverse Kinematics

Inverse kinematics (IK) is the process of determining what angles are required among the joints of a linked structure, given the final position of the end-effector. IK deals with the study of the geometry of motion, without considering the forces and moments (i.e. the kinetics) that cause the motion. Unlike forward kinematics, inverse kinematics usually has many or infinitely many solutions.

Inverse kinematics has already been widely used in robotics (Craig, 1989). For example, it can lead a multi-link robotic arm to grab an object. The human body can also be simplified into a linked structure, so human motion simulation was simply considered as an inverse kinematics problem in some cases (Beck and Chaffin, 1992; Verriest et al., 1994; Jung et al., 1995; Dysart and Woldstad, 1996).

Since humans may have “preferences” for certain postures, and inverse kinematics algorithms, by themselves, have no ability to specify what the preferred postures are (Perez, 2005), inverse kinematics is usually facilitated by some other tools to select the preferred posture from a feasible solution set (Guez and Ahmad, 1990). Optimization is one such tool, and the one most commonly used in recent investigations. Another popular tool is statistical regressions, which are usually derived from a large set of real motion data (Verriest et al, 1994).

### 2.1.2 Optimization-based Motion Simulation

When using optimization-based approaches, researchers assume that the neural controller plans human motion based on certain performance criteria (Hicheur et al., 2003; Ohta et al., 2004). These criteria are used to define objective functions, and optimization procedures are performed to find the optimal motion trajectory by minimizing or maximizing these objective functions. Exactly how the neural controller works is still unknown in most respects, so it is impossible to specify the exact performance criteria the neural controller adopts. Therefore, different criteria have been suggested to define different cost functions for different types of motion.

Specifically, a minimum jerk criterion for arm reaching motion was proposed some time ago (Flash and Hogan, 1985). This criterion requires that the trajectory of the arm motion minimizes the time integral of the square of jerk (rate of change in acceleration). The predicted trajectory for point-to-point reaching was a straight line and characterized by a symmetrical bell-shaped speed profile. These results qualitatively agreed with obtained experimental data. However, the minimum jerk model can only produce a single unique trajectory without regard to

diverse external working conditions. At the same time, this model is only a kinematics model. It cannot reflect the dynamic characteristics of human motion since the kinetics causing the motion are not considered.

Uno et al. (1989) first presented a minimum torque change model based on the idea that motion optimization should be related to motion dynamics. The performance measure was the time integration of the sum of the squared torque change rate. This model gave a curved path and an asymmetrical speed profile which more closely agreed with the obtained experimental data. However, using the minimum torque change model is more difficult than using the minimum jerk model because a dynamical human body model has to be developed first.

Both the minimum jerk model and minimum torque change model focused on trajectory formation without adding approach angle and speed as constraints. Breteler et al. (2001) adjusted these two models so that the final part of the generated trajectories had a specific direction and speed. After comparing the simulation results from the minimum jerk and minimum torque change models, the trajectory formed by minimum torque change model was found to be more similar with the observed trajectory than that formed by the minimum jerk model.

In general, motion optimization can be reasonably considered as a dynamic optimization problem. Due to the complexity of available dynamic optimization algorithms, some studies have disregarded the complex musculoskeletal dynamics, and simplified a dynamic motion as a set of sequential static postures. For example, Jung et al. (1995) developed an analytical inverse kinematics algorithm to predict arm reaching motion. In this study, the upper limb was

modeled as a four-link system with a total of eight degrees of freedom. To solve such a redundant manipulator problem, the solved motion method, which is a static optimization algorithm, was selected for local optimization. Joint range availability was employed to define the performance function, the minimum of which, coupled with the solved motion method, was used to guarantee kinematic optimality and to simulate human reach. The results showed that there were no significant differences in both joint angles and distances between the real postures and those from the model (at $\alpha = 0.1$).

Another example was given by Dysart and Woldstad (1994, 1996) who used inverse kinematics to specify all mathematically feasible postures of humans performing sagittal lifting tasks, and then adopted different performance criteria to select the static optimal postures. The performance criteria used included minimum overall effort, minimum local effort or fatigue, and maximum body stability. Their simulation results indicated that all of the prediction errors were significantly greater than zero, but use of minimum total torque led to the best predictions. Woldstad (1997) then modified the model, including two new performance criteria (the sum of cubed muscle intensities and the sum of squared joint torques), additional links representing head and neck, and improvements to the optimization procedure etc., and found the new models could produce better results.

Models described by Jung et al. and Dysart et al. were able to account for human motions to some extent. However, an important distinction has been found between a static posture and an instantaneous posture sampled from a continuous movement (Zhang and Chaffin, 1997), which challenges these earlier approaches. To specify an optimal dynamic posture and avoid

overly complex dynamic optimization algorithms, some studies (Zhang et al., 1998, 2000; Wang et al., 1998, 1999; Hsiang and McGorry, 1997; Lin et al., 1999; Mi, 2004) have pre-determined joint trajectories or pre-defined a set of equations representing the joint trajectories when simulating human motions. Some details on these studies are given below.

Zhang et al. (1998, 2000) and Chaffin et al. (1999) proposed an optimization-based differential inverse kinematics (ODIK) approach to model in-vehicle seated reaching movements. A weighted pseudoinverse was used in the joint angular velocity domain to resolve kinematic redundancy. Weights were assigned to different joint angles according to their relative movement contributions to an instantaneous postural change. These weighting parameters were estimated through a numerical optimization procedure based on simulated annealing, such that the predicted movement trajectory best matched the observation. Using this model, Zhang and Chaffin (2000) predicted in-vehicle seated reaching movements, and the overall mean and median time-averaged errors in joint angle were 5.2° and 4.7°, respectively.

Wang et al. (1998, 1999) presented a geometric inverse kinematics algorithm to simulate arm reaching motion. This algorithm was based on the minimization of the norm of joint angular velocities, and hand trajectory had to be specified in advance. The elbow position predicted by the proposed algorithm was compared with the actual elbow position to validate the model. The distance between them was within 42 mm on average. Also, the results indicated that the predicted motion was dependent on initial arm posture.

Hsiang and McGorry (1997) simulated dynamic lifting motion using three different objective functions. Five eighth-order polynomials were assumed to represent the trajectories

of selected joint angles (i.e. elbow, shoulder, hip, knee, and ankle). Coefficients of these polynomials were specified by minimizing or maximizing the objective functions which corresponded to different lifting patterns. Participants were instructed to lift a load using the specified optimal lifting pattern. During lifting, compressive forces on the L5/S1 were measured and compared, and the 'mobilization' pattern was found to be the best considering the peak compressive force on L5/S1.

Lin et al. (1999) developed a dynamic planar motion simulation model (DPMS) and used it to simulate various lifting tasks. DPMS includes three sub-models which are the biomechanical model, optimization model, and trajectory model. In the optimization model, an objective function was defined to minimize the time integral of the sum of square of relative joint strength. The form of the trajectory was approximated by a polynomial function of time. During simulations, possible joint angle trajectories were generated first, and then the optimal trajectory was specified by solving the biomechanical model and the optimization model. Their simulation results were compared with experimental data. The mean squared error (MSE) between the predicted and actual trajectories for different joints angles was in the range of 0.0046 $rad^2$ to 0.095 $rad^2$.

A 15-degree-of-freedom (DOF) model of the human body was developed to predict human motions (Abdel-Malek, 2006). This model first determined a desired Cartesian path for the end-effector using the minimum jerk criterion (Flash and Hogan, 1985) over the duration of motion. Then, B-spline curves were formulated to represent joint trajectories. Such curves were used because of their several robust properties such as differentiability, local control and

convex hull. Coefficients of these B-spline curves provided the decision variables for an optimization procedure whose objectives were defined by discomfort and smoothness, and whose constraints were defined by joint angle ranges of motion and distances to the desired path at selected points. However, the predicted motion was slightly unnatural. The authors suggested that a higher DOF model might improve the results.

Even though the studies mentioned above (Zhang et al., 1998, 2000; Wang et al., 1998, 1999; Hsiang and McGorry, 1997; Lin et al., 1999; Mi, 2004) were able to specify dynamic motions, they are restricted since joint trajectories usually cannot be known or formulated in advance. To address this problem, an approach based on timespace optimization (Chang et al., 2001) was proposed. In this approach, the duration of a lifting motion is divided into equal discrete time intervals. Using the finite difference method, the objective function and constraints of an optimization procedure are represented as functions of joint angles at the discrete points. The joint angles at the discrete points are independent variables and are solved by using sequential quadratic programming. It is not necessary to know the joint trajectories in advance when using this approach. However, angular kinematics may not be a continuously differentiable function, which will result in invalid application of the finite difference method.

Martin et al. (2006) reported an original optimization approach for the prediction of periodic movement such as postural sway. In the proposed optimization procedure, a minimum torque change criterion was adopted. Angular displacement was described by a non-harmonic Fourier series and the coefficients of the Fourier series were optimized. Equilibrium constraints were also considered in the model. This optimization model was able to predict in-phase

coordination between the hip and ankle joint for low motion frequencies and anti-phase coordination for higher motion frequencies. These results were consistent with the observed experimental results.

All the applications of optimization-based approaches mentioned above only apply one criterion for an entire motion. Existing evidence, however, indicates that the neural controller probably plans the motion by using more than one criterion, and different criterion may be adopted at different stages of a motion (Chang et al., 2001; Ohta et al., 2004; Hermens and Gielen, 2004). Combining potential energy and discomfort performance criteria, Marler (2004) used multi-objective optimization (MOO) to predict arm reaching motion, with results that were more accurate than those obtained from a single criterion. Gundogdu (2000) evaluated objective functions employing minimum jerk, work, moment, and a combination of these three for human motions, using a two-dimensional sagittally symmetric five-link human body model. The linear combination objective function proved to be the most effective. Ohta et al. (2004) simulated a constrained arm movement in a crank-rotation task. The formation of the trajectory was explained at both the joint level and the muscle level. At the joint level, the minimum torque change criterion, the minimum hand force change criterion, and the combined criterion were considered. At the muscle level, the minimum muscle force change criterion, the minimum hand force change criterion, and the combined criterion were considered. At both levels, after a comparison between the simulation and experimental data, the combined criterion proved able to predict the motion more accurately. Hence, the authors argued that the neural controller might adopt a combination of different optimal criteria when planning motions.

### 2.1.3 Data-based Motion Simulation

Chaffin (2005) argued that human motion models should be based on real motion data to assure validity for complex task simulations. Data-based motion simulation is another contemporary approach that can solve the ill-posed human motion problem. In the data-based approach, no assumptions are necessarily made with respect to the minimization or maximization of some performance functions the neural controller may adopt, and computational requirements are relatively low. Fundamental to this approach is the creation of a database of a certain types of motion within a certain range. Based on this database, a certain model is constructed, which takes the desired initial and target position along with the anthropometry and other features of the human body as inputs and the predicted motion as the output. Faraway (2003) summarized that the data-based approach relies on three main components: a special posture representation, a diverse motion database, and a prediction method.

A functional regression approach based on captured 3D motion data was developed to predict joint angles during an arm reaching motion (Faraway, 1997). This approach uses a quadratic regression form to fit the available data. The coefficient of determination was applied as a measure of the fit, and the value obtained was 80.6% for the proposed quadratic model. One of the limitations of this approach is that it determines the motion postures only in terms of joint angles. When using forward kinematics to specify the final posture, the end-effector position may not coincide with the target. In order to solve this problem, Faraway et al. (1999) proposed a posture rectification approach, in which the predicted joint angles have a minimum

deviation from the initial joint angles obtained from the quadratic regression model, and can satisfy the constraints that the end-effectors lie on the target. However, rectification cannot always improve predictions. Results showed that it might worsen joint center prediction at the sternum and shoulder while improving it at the elbow and hand. For this reason, Faraway (2003) suggested a new formulation for motion prediction which uses stretch pivot coordinates to represent postures. This representation allows for rapid and simple computation of postures. Faraway (2003) designed his model based on large databases of various types of automobile and materials handling motions. He also demonstrated two contrasting prediction methods. One is parametric regression, which is used to predict the stretch pivot coordinates in the posture representation. The other is non-parametric regression. A small number of motions which were similar with the predicted motion were selected and averaged in the stretch pivot coordinates to produce the predicted motion. No simulation results were discussed by the author.

A statistical design of experiments approach was reported by Mavrikios et al. (2006). In this approach, anthropometric parameters were considered as impact factors that influenced human motions. These impact factors were determined by performing analysis of variance (ANOVA) of the experimental motion data. The authors agued that this approach needed a reduced set of experimental motion data, but could predict human motions as accurately as the functional regression approach (Faraway, 1997) that required a larger number of experiments to be executed. Their results showed a difference between the actual and predicted positions of the end-effector in the last motion frame of less than 100mm.

Rosenbaum et al. (1995) proposed a model which specified reaching posture by making use of stored postures. Each candidate stored posture was assigned a weight according to two criteria: accuracy (how closely the candidate posture achieves the task) and efficiency (how costly it is to move from the starting posture to the posture under consideration). The predicted posture was found by treating all of the stored candidate postures as vectors and taking their weighted sum. Their simulation results were considered to be positive since there was no significant difference between the observed and simulated data for most postures (Vaughan et al., 1998). However, this model cannot be used in complex tasks (e.g. avoiding obstacles).

Rosenbaum et al. (2001) also described a model in which every motion was planned using a constraint hierarchy -- a set of requirements ordered by priority. This model was used for a grasping simulation with several constraints (e.g. avoiding collisions). The predicted posture must meet the requirement of the highest-level constraint and then satisfy the second highest level constraint. Also in this model, a two-stage process was established. The first stage is selecting the most promising stored postures from the database, while the second involves generating a potentially better posture to serve as the goal posture. Evaluation of the stored and generated postures should be done with reference to a constraint hierarchy that defines the task to be performed. Mean squared errors (MSE) between simulated and real data were compared. Since the MSE first increased and then decreased as a function of time, this model was concluded to be able to provide a better prediction at the end of a movement than during the course of a movement.

Memory-based motion simulation (MBMS) is a novel simulation approach for motion

prediction (Park 2003; Park et al., 2004; Park et al., 2005), and which is based on generalized motor program (GMP) theory. Symbolic motion structure representation (SMSR) is used to analyze existing motions. With SMSR, multi-joint motion can be represented using a set of symbol strings, in which each symbol stands for a monotonic motion. For example, 'U' stands for monotonically increasing; 'D' stands for monotonically decreasing; 'S' stands for stationary. When a novel motion scenario is submitted to the MBMS system, its motion database is searched to find relevant existing motions. The selected motions, referred to as "root motions", need to be modified by a motion modification algorithm (MoM) such that they can satisfy the novel motion scenario, while retaining the root motion's overall angular movement pattern and inter-joint coordination. Park et al. (2004) used a MoM algorithm to generate side reaching motion and forward, downward reaching motion to new target locations. No statistically significant difference was found between the predicted and observed motions, and the largest mean time-averaged distance difference was 1.3cm at the wrist joint. According to the results of these examples, the MoM algorithm was concluded as able to produce realistic simulated motion for diverse new scenarios.

Park et al. (2006) also described a memory-based posture planning (MBPP) model which can predict reach postures that involve avoiding obstructions. In this model, the task space is partitioned into small regions called cells. Alternative postures for reaching the cell that satisfy joint range of motion and static balance constraints are stored. When a target and an obstruction configuration are given, the model selects collision-free postures from the stored postures, and modifies them so that the hand target acquisition constraint can be met.

Simulation results showed that the MBPP model was able to rapidly and robustly plan collision-free reach postures.

Motion editing is commonly applied in computer graphics to simulate human motions. In general, a pre-existing motion is edited to meet new constraints or impose new qualities while keeping as much of the original quality as possible. Witkin and Popovic (1995), and Gleicher (2001) used a motion-displacement mapping technique to make large scale changes to an original motion while preserving fine details. However, this technique can only check each frame without considering the whole motion. This may lead to the loss of some specific aspects of the original motion. In contrast, spacetime constraint methods (Gleicher, 1997; Witkin and Kass, 1988) are able to determine constraints over the entire motion and compute the optimal motion that meets these constraints. In addition, Gleicher (1997) proposed an approach that can solve numerical constraint problems sufficiently fast so that interactive motion editing for articulated 3D characters is achieved.

Artificial neural networks (ANNs) are computation models commonly used for prediction problems. When training data is available, ANNs have the ability to solve incomplete or little understood problems (Hassoun, 1995). Thus, ANNs are a potential tool for use in motion simulation, and existing methods can be classified as data-based approaches due to their dependence on training data. Jung and Park (1994) used a feedforward backpropagation neural network to predict human reaching motions. Motion trajectories of the upper limb joints were collected and divided into two data sets – a training data set and test data set. Comparisons were made between model-based predictions and actual motions, and no significant differences

were found between the two data sets for all the considered joints.

Ulusoy et al. (2001) presented a neural network system to control a two-link dynamic arm model. Two neural networks were adopted in this system. One was used to predict static joint torques, while the other was used to determine the parameters needed for specification of the torque-time profile for each joint. The two-link arm was then driven by the output of these two neural networks to move from any initial position to any final position in the sagittal plane.

A dynamic neural network for the planning of hitting movements was derived by Dessing et al. (2004). This model implemented continuous required velocity control by extending the Vector Integration To Endpoint model while providing explicit control of effector velocity at interception. The predicted movement trajectories were qualitatively consistent with the kinematics of hitting movements as observed in experiments.

Perez (2005) applied recurrent neural networks to predict whole body lifting kinematics. These networks were trained using an existing set of non-cyclic lifting motions, and took lift characteristics as the input and a set of joint angles as the output. Both static postures and dynamic motion based on target positions were predicted. Root mean square errors were generally smaller than 20 degrees, a magnitude which was similar to the levels of intra-variance in the dataset.

Inverse kinematics, combined with collected motion data, has also been used to predict human motions. Using inverse kinematics, Beck and Chaffin (1992) developed a so-called ‘behavior based model’ to simulate lifting tasks, and Verriest et al. (1994) proposed a linear statistical model to predict arm reaching motion. Both of these approaches are based on

statistical regression equations derived from a large number of real motion data. Compared with the experimental results, these approaches can predict motion quickly, but not accurately.

### 2.1.4 Limitations of the Existing Human Motion Simulation Models

Optimization-based approaches are able to suggest mechanisms by which the neural controller plans motions, based on the fundamental assumption that the neural controller determines motions according to the specified performance criterion. Yet they have an essential drawback, in that the assumption that the neural controller determines motions according to some performance criterion has not been validated. If this assumption is not valid, the optimization-based approach is not valid either. Even if this assumption is valid, different people may adopt different performance criteria to plan the same type of motion, so it is infeasible to specify the exact performance criteria and to use a single objective function for everybody. Also, current optimization-based approaches can only provide a single path for a specific motion task, whereas motion planning likely has a substantial stochastic component. Human subjects may choose their own motion plans randomly. Further, all but the simplest optimization algorithms are computationally intensive. If real-time analysis is critical, these approaches are not appropriate.

Using data-based approaches, a predicted motion is derived from real motion data and no assumptions are made with respect to functions the neural controller attempts to minimize or maximize. Hence, these approaches appear more valid. There are, however, limitations in data-based approaches. First, they depend heavily on the availability of real motion data.

Predictive results will decline in quality as the specified inputs move further away from available data. Faraway (2003) provides an example: for a reaching motion, when the input target was far to the left of the subject, and all the targets in the database were on the right side, good simulation results could not be expected. Second, although anthropometric data and some other features are considered as part of the input, individual differences cannot be sufficiently accounted for because it is impossible for the collected database to include all kinds of motion strategies. In addition, data-based approaches provide only limited information on underlying neural control processes.

Besides the limitations mentioned above, many human motion models have one common limitation. Specifically, most models predict motion trajectories based on motion durations that have to be supplied externally. While durations may be externally specified or predictable in some cases (e.g. assembly line tasks), this is clearly not true for all tasks of interest.

## 2.2 Balance Control Modeling

Balance control during quiet upright standing is particularly well suited for modeling because, in most cases, the human body can be simply and sufficiently modeled as an inverted pendulum. Such a system is then easily represented mathematically. At the same time, balance control modeling is quite difficult, since the human body and underlying control system is so complex that the existing knowledge cannot completely explain how it works. Many researchers have worked toward explaining the control mechanism for quiet upright stance, as a simpler case than more general postural control, and diverse theories have been proposed.

### 2.2.1 Ankle Strategy and Hip Strategy

Recent studies have shown that human beings are able to select distinct strategies to maintain balance according to the magnitude of disturbances (Fujisawa et al., 2005; Gatev et al., 1999; Kuo 1995; Johansson et al., 1988). For small disturbances, the amplitude of sway angles will be small and the neural controller will adopt an ankle strategy, in which only ankle torque is considered to contribute to reducing sway angles. For large disturbances that cause large amplitude of sway angles, the neural controller will adopt a hip strategy, in which hip torque has to be generated in coordination with ankle torque to maintain upright stance. Other studies (McClenaghan, et al., 1996; Winter et al., 1996) have also indicated that in side-by-side stance, anterior-posterior (A/P) balance is totally under ankle control, whereas medial-lateral (M/L) balance is under hip control. Usually, when the ankle strategy is applicable, a single-link inverted pendulum is sufficient to represent the human body (Maurer and Peterka, 2005); when the hip strategy has to be applied, the human body should be considered as a multi-link inverted pendulum (Fujisawa et al., 2005; Jo and Massaquoi, 2004).

### 2.2.2 Passive Control and Active Control

Passive control torques are considered to stem from intrinsic tissue mechanical properties (i.e. stiffness or viscosity), and to act without time delay. In contrast, active control torques are generated by active muscle contraction regulated by the neural controller. A time delay due to sensory transduction, transmission, processing, and muscle activation is necessarily involved in active control torque.

Winter et al. (1998, 2001, and 2003) developed a stiffness control model for quiet standing, in which a stiffness control strategy was adopted. The human body was assumed to behave like an inverted pendulum, and ankle joint torque was assumed to be proportional to the angle of the pendulum from vertical. This model predicted that the center-of-pressure (COP) oscillates essentially in phase with the center-of-mass (COM) during body sway. Also, Winter et al. (2001) directly estimated muscle stiffness from ankle joint torque and sway angle. The average coefficient of correlation between the two was 0.92. Further, based on the stiffness control model, Gage et al. (2004) conducted a series of experiments and found that the mean r-value between COP-COM and COM acceleration in both the A/P and M/L directions were -0.95±0.02 and -0.84±0.05, respectively. They also argued that these results were consistent with the simulation results from the proposed stiffness control model.

Morasso et al. (1999, 2002), Loram and Lakie (2002), and Lakie et al. (2003) questioned the validity of the stiffness control model. They all argued that passive torque alone was not sufficient to stabilize the body as an inverted pendulum, and that additional active torque regulated by the neural controller was necessary. Specifically, Loram and Lakie (2002) indicated that besides the torque from intrinsic mechanical ankle stiffness, repetition of a ballistic-like biphasic pattern of torque generated by the neural controller played an important role in stabilization. Lakie et al. (2003) conducted several novel experiments, the results of which showed that the inverted pendulum body could be stabilized even when intrinsic stiffness was low. Further, they analyzed sway magnitude and found that intrinsic stiffness contributed little to maintaining balance. Morasso and colleagues (1999, 2002) also suggested that the

in-phase relationship between COP and COM trajectories was determined by physics, not by the control pattern.

Casadio et al. (2005) used a motorized footplate mounted on a force platform to measure intrinsic ankle stiffness directly, and then compared the measured intrinsic ankle stiffness with the critical stiffness. If the measured stiffness is below the critical stiffness, an active stabilization mechanism is required to compensate the inadequate stiffness; otherwise, an active stabilization mechanism is unnecessary. Their results showed that intrinsic ankle stiffness during quiet standing was only 64±8% of the critical stiffness, and the authors concluded that active neural control is necessary.

Peterka (2002) also found that active control torque plays a dominant role in balance control. In his work, experiments were designed to collect stimulus-response data for human bipedal upright stance. A simple feedback control model was used to specify the transfer function structure. In this model, it was assumed that the human body behaved like an inverted pendulum and the neural controller was a PID (proportional, derivative, and integral) controller. Postural stiffness, damping and feedback time delay defined in the model were estimated in such a way that the transfer function could best match the collected stimulus-response data in the frequency domain. The passive stiffness and damping parameters obtained from the simulation were only 1/10 the value of active stiffness and damping parameters.

### 2.2.3 Feedforward and Feedback Control

Feedforward control is often considered to be involved in postural control and means that

the neural controller is able to predict an external input or upcoming behaviors, and generate a corresponding control torque to stabilize the body (Fitzpatrick et al., 1996; Gatev et al., 1999). Feedback control is also considered to play a role. For example, in order to maintain an upright posture, movement cues about the deviation of the body from an upright reference position, which are obtained from the sensory systems, are fed back to the neural controller which generates corrective controls to resist the deviation of body position away from upright (Johansson et al., 1988; Peterka, 1995, 2002; Ishida et al., 1997).

Specifically related to feedforward control, Gatev et al. (1999) reported that lateral gastrocnemius muscle activity measured during quiet stance was positively correlated with A/P motion of the COM. They also found that lateral gastrocnemius muscle contractions, which provided the control torque, preceded COM position change by about 200 ms. Based on these findings, the neural controller was considered to be able to generate control torque in anticipation of an upcoming position of the COM. Thus, it was suggested that a feedforward control mechanism is responsible for stabilizing the human body during quiet standing.

Fitzpatrick et al. (1996) recognized the contribution of the feedback control mechanisms to maintaining balance, but also stated that feedback control alone was not able to stabilize the human body. In their study, a reflex response based on a feedforward process was found to be both consistent with experimental results and necessary to counteract a postural disturbance. Fitzpatrick et al.'s results were obtained based on the assumption that the weights of sensory information in different test conditions stayed constant. However, this assumption was challenged by several current investigations which showed the contributions of different sensory

systems to postural steadiness can be re-weighted when the goal of a movement task or the environmental context changes (e.g. Cenciarini and Peterka, 2006; Horak, 2006).

Several lines of evidence support that such re-weighting occurs. For example, the contribution of proprioceptive input from the ankles is increased with eye closure (Ishida et al., 1997), and the use of vestibular cues was shown to increase with an increase of visual and proprioceptive perturbations (Peterka, 2002). Further, Brumagne et al. (2004) reported that during upright standing the focus of proprioceptive sensitivity would be changed from the trunk to the ankle with aging or the occurrence of low back pain. Peterka and Loughlin (2004) developed a control model that took a weighted combination of sensory-orientation cues as the input of a PID neural controller, and used this to investigate two possible explanations – the sensory-reweighting hypothesis and a load-compensation hypothesis. Their simulation results showed that predictions from the sensory reweighting hypothesis were consistent with experimental results whether sway-referencing was ideal or not. Cornilleau-Peres et al. (2005) proposed a measure of the visual contribution to postural steadiness, the stabilization ratio (SR), which showed significant differences between standing with eyes open and eyes closed. The studies mentioned above all challenged Fitzpatrick et al.'s conclusion.

Peterka (2002) further argued that active torque generated by feedback control mechanisms was the dominant contributor to quiet stance control. He developed a closed-loop control model of upright stance, composed of an inverted pendulum body and a PID neural controller (Peterka, 2000). This model was able to generate realistic stabilogram diffusion functions which summarize the mean square COP displacement as a function of the time interval

between COP comparisons. Peterka (1995) also developed a feedback control model which assumed that somatosensory and visual body orientation cues with different time delays are processed independently. For each sensory feedback loop, human postural control properties are modeled by PID controllers. Their simulation results could reflect the gain and phase of body sway by adjusting the PID parameters in both loops. Thus, it was concluded that feedback control mechanisms were able to explain balance control.

Masani et al. (2006) simulated human quiet stance using an inverted pendulum model regulated by a feedback PD (proportional and derivative) controller. Different pairs of proportional and derivative gains were examined in their simulations. Simulated COM position, velocity and ankle joint torque were compared with those from the experiments using cross-correlation functions. Their feedback PD controller could stabilize bipedal quiet standing even when the closed-loop time delay was as large as 185ms, and generate the preceding motor command that was observed experimentally. Their conclusion was that a feedforward control mechanism is not necessary. As a whole, the evidence reviewed in this section suggests that the postural control system should be a feedback rather than a feedforward control system.

### 2.2.4 Neural Control Strategy

Numerous experimental and simulation results have shown that the neural controller must play a very important role in balance control, by generating active joint control torque according to feedback information about body configuration. However, the true control strategy adopted by the neural controller is still an object of discussion and controversy.

PD or PID strategies are among the most common control strategies used in balance control modeling, since the proportional, derivative, and integral actions are fundamental modes of control systems (Johansson et al., 1988). Johansson et al. (1988) proposed that the stabilizing ankle torque was a linear combination of displacement, velocity, and time integration of joint angles. Based on this, a third-order transfer function among ankle torque, disturbance torque, and vibration were specified. Balance control was quantified with three parameters – swiftness, stiffness, and damping. These parameters were computed from measurements recorded with a force platform. Results from six participants characterized a well-damped regulation system.

Iqbal et al. (2004) presented an inverted pendulum human body model with a stabilizing PID controller. This model included force feedback from Golgi tendon organs and two levels of position and velocity feedback from multiple muscle spindle organs. There were time delays in all the feedback loops, and the PID controller generated the muscle motor command. Pade approximation techniques were used to derive the transfer function of the entire closed-loop dynamics. Stability of the system was analyzed using the Hermiter-Biehler theorem to specify the stabilizing set of controller gains. Their simulation results showed that the proposed model could guarantee stabilization of the inverted pendulum human body, but there was no discussion about the validity of the model.

Maurer and Peterka (2005) used a simple model based on a PID neural controller to interpret spontaneous sway measures. In this model, the human body was represented by a single-link inverted pendulum. Input to the body was the ankle joint torque, composed of a

random disturbance torque and the control torque generated by the neural controller. Outputs of the model were body sway angle and COP displacement. The neural controller received body orientation information with a time delay through a feedback loop. An optimization procedure was applied to estimate the parameters in the model for a given data set. The simulation results showed that all sway measures derived from simulations were well within a one standard deviation range of the mean experimental data, and could be classified into three groups according to their correlations.

The integral component in PID controller is likely negligible, and does not substantially affect the stability of the postural control system. Thus, PID controllers were replaced by PD controllers in some studies (e.g. Masani et al., 2005; Caver et al., 2005, 2006). Specifically, Caver et al. (2005, 2006) modeled the human body as a linearized inverted pendulum controlled by a PD controller, and adopted a state estimator to estimate the angular position of the body away from upright stance. Further, this model was used to identify how sensory weighting alters with changes of sensory information by optimizing some observable sway measures (Caver et al., 2006).

Besides PD and PID control strategies, some other control strategies have also been proposed. Jo and Massaquoi (2004) suggested a recurrent integrator proportional integral derivative (RIPID) control strategy for upright balance modeling. In their model, human body dynamics in the sagittal plane were described by analyzing a three-segment inverted pendulum. The model cerebellar system included a PID part along with a mechanism to provide descending integration. The cerebellar system had two sets of control gains for PID. When imposed

platform disturbances were small, the first set of cerebeller control gains were used to apply an ankle strategy for balance. When the platform disturbances were more violent, the second set of cerebeller control gains were used to apply a mixed ankle-hip strategy for balance. In contrast, the cerebral system had only one set of same-joint linear force feedback gains. The conclusion of this study was that the proposed model based on a RIPID strategy could successfully simulate balancing reactions to a wide range of external disturbances.

Kuo (1995) described an optimal control model for analyzing human balance control. In this model, the neural controller was modeled as a linear quadratic optimal controller. The control weighted matrix in this controller was used to measure the cost of executing the ankle or hip strategy, and the state weighted matrix was chosen by regulating certain physical quantities relevant to posture so that the equations governing the feedback gain matrix were simplified. Three relevant quantities were proposed. The state cost function was represented by a combination of these three physical quantities. The combination that produced behaviors most similar to the experimental results was chosen as the basis to specify the state weighted matrix. The parameters to specify the combination were determined by the control selection center according to the size of disturbances.

van der Kooij et al. (1999) indicated that body orientation information from sensory systems received by the neural controller has a certain time delay, and the neural controller was supposed to be able to estimate the exact body orientation based on the delayed information. Their proposed model included four parts: body dynamics, sensor dynamics, sensory integration center, and action control center. Body dynamics were defined by a three-link inverted

pendulum model; sensor dynamics were represented by the transfer functions of different sensory systems; in the sensory integration center, the best estimates of body orientations were obtained by using a Kalman filter; finally, the action control center selected the muscle actions obtained from a regulator that can minimize a certain objective function. The authors compared the effects of sensory perturbations on total body sway obtained from the model predictions and experimental results. The difference in percentage increase of body sway compared with the body sway when no sensory system was perturbed was less than 12% under all circumstances.

Most of these balance control models are based on the assumption that body sway is forced by some kind of background noise. Bottaro et al. (2005) challenged this assumption. They built a noise-driven model with a PID neural controller and an inverted pendulum body, and found that the simulated average jerk of the COM oscillation in the sagittal plane was twice that of corresponding experimental data. Therefore, they argued that the noise-driven assumption was not valid and could not reflect physiological evidence. Furthermore, Battaro et al. (2005) also proposed a sliding mode control model. Since sway movements obtained from this model were smoother than those obtained from the noise-driven model, they concluded that the sliding mode control model was more consistent with experimental data.

The balance control models mentioned above were established to simulate how human beings maintain balance based on the assumption that the neural controller adopts a particular control strategy such as PID control strategy, optimal control strategy etc. There are also some other models in which the neural controller is completely specified using available experimental data.

As an early example, Ishida et al. (1997) considered the human body as an inverted pendulum with ankle moment as the controlling variable and the sway angle of the body as the controlled variable. The neural controller took the sway angle as its input and generated a stabilizing ankle moment. A prediction error method, which was based on the measured discrete sway angle and the measured discrete ankle moment, was used to identify the transfer function of the neural controller. The order of this transfer function, which in this case was fixed at two, was determined by the Akaike Information Criterion (AIC). Frequency responses under different tasks were then used to analyze the contributions of different sensory systems to balance. It was found that under sway-referenced support conditions, the vestibular system might be dominant, whereas under fixed support conditions, the proprioceptive system contributed most. Fujisawa et al. (2005) applied similar methods to model the human postural control system, but they used a two-link inverted pendulum to describe human body dynamics. Therefore, four feedback paths in the neural controller were characterized by transfer functions connecting the two inputs – ankle and hip joint angles, and the two outputs – ankle and hip joint moments. Their results showed that somatosensory feedback paths might be activated from the hip joint angle to the moments around the ankle and hip joints when postural control became more difficult.

It has also been reported that postural sway can be decomposed into two fundamental dynamic components, a slow nonoscillatory component and a faster damped-oscillatory component, which can be characterized by eigenvalues of the transfer function (Kiemel et al. 2002, 2006). Kiemel et al. (2002) collected a series of postural sway data, based on which the

stochastic structure of postural sway was compared with a PID control model. Eigenvalues of the PID model were found to be consistent with the collected data. Further, Kiemel et al. (2006) investigated the basis for the slow component by providing subjects with sum-of-sine visual motion. The whole human body system was modeled and described by the transfer function from the simulated A/P visual motion and stochastic properties of sway to A/P COM displacement. The Bayesian Information Criterion (BIC) was used to estimate the best order of the model, and the model parameters were specified using the maximum likelihood method so that the model fit the collected experimental data. The final results supported that the slow component was related to errors in state estimation rather than a moving reference, indicating that the slow process was inside the feedback loop.

Yang et al. (1990) used a top-heavy inverted pendulum model depicted in the sagittal plane, which included the three linkages representation (the two shanks, the two thighs and the trunk), to model the standing human. Their simulation procedure was iterative. During each iteration, for a specified disturbance, a joint torque combination within a certain range was chosen. The disturbance and joint torque combination were input into the mathematical equations of the human standing model with a simulation duration of 80ms. After this interval, if all three segments returned within five degrees of the initial position, the joint torque combination was considered as a successful solution. After simulating all possible combinations of the joint torques, the solution space was obtained. The authors regressed the successful solutions in the solution space and found that coefficients for each joint torque were kept nearly constant even when considering the factors that could cause a change in the

successful joint torques. Therefore, they concluded that given the model structure used in this approach, there was a proportional relationship between individual joint torques.

Alexandrov et al. (2001) used eigenmovements, which are the movements along eigenvectors of the motion equation, to interpret equilibrium maintenance in human forward trunk bending. The human body was represented by a three-joint model, and the movements were decomposed into “ankle”, “hip”, and “knee” eigenmovements based on the dominant component in each eigenvector. This modeling approach was able to decouple the complex human body system into a simple linear combination of three independent inverted pendulums. Simulation results showed that the ankle eigenmovement started earlier than the hip eigenmovement, and the ankle eigenmovement contributed the most to equilibrium maintenance, whereas the hip eigenmovement contributed the most to movement.

### 2.2.5 Limitations of the Existing Balance Control Models

As discussed above, existing balance control models can be primarily classified into two groups according to the way in which the neural controller is determined. The models in the first group assume that the neural controller adopts a particular control strategy to maintain balance. Thus, different control strategies were applied in the models. However, since it is still unknown how the neural controller works, it is impossible for us to confirm whether the neural controller does indeed adopt a certain control strategy to maintain balance. Further, there are also some limitations when applying specific control strategies. Currently, a PD or PID control strategy is widely used to stabilize upright stance in balance control models. Both

control strategies are simple and easily modeled, but they lack obvious physiological meaning. So, it is difficult to analyze and assess potential control mechanisms from a physiological perspective if only using a PD or PID control strategy. An optimal control strategy which can easily explain balance control from a physiological perspective was proposed by Kuo (1995), however, no systematic approach that helps to estimate the performance index in the optimal controller was given, and the mathematical properties of the human body system could be specified only when some complex knowledge (e.g. musculoskeletal geometry) was available. Bottaro et al. (2005) reported that sliding mode control theory could effectively model body sway during quiet standing, but the authors also admitted that there were few theoretical and experimental issues that can explain the nature of the switching mechanism used in this approach. When using the RIPID control strategy (Jo and Massaquoi, 2004), muscular responses must be considered, and thus more yet-to-be validated assumptions must be made. For example, one assumption is that the specified muscles are idealized muscles which have certain lines of action.

Unlike the models in the first group, the models in the second group determine a neural controller using experimental data. These models appear more valid, as no assumptions about the controller have to be made. Yet, these models are still limited since they depend on the availability of experimental data. Furthermore, when using these models, the neural controller has to be modeled as a discrete system, and such discretizing likely yields errors when applied to what is in reality a continuous system. In some cases, the upright stance even cannot be stabilized (Ishida et al. 1997).

# Chapter 3 Simulating Lifting Motions using Fuzzy Logic Control


## Abstract

Human motion simulation is an ill-posed problem. In order to predict unique lifting motion trajectories, a motion simulation model based on fuzzy logic control is presented. The human body was represented by a two-dimensional five-segment model, and the neural controller was specified by fuzzy logic. Fuzzy rules were defined with their antecedent part describing the fuzzy variables of scaled positional error and velocity, and with their consequent part describing scaled angular velocity. These rules were generated according to certain trends in the fuzzy variable trajectories observed from actual lifting motions. An optimization procedure was performed to specify the parameters of the membership functions by minimizing the differences between the simulated and actual final postures. Simulations were obtained for 14 novel lifting motions from seven participants. Overall results indicated that the presented model simulated lifting motions with an accuracy that was at least comparable to some previous human motion simulation models. Accuracy of the model simulations differed between joints and was highest near the beginning and end of the motions. Strengths and limitations of the modeling approach are discussed. Use of fuzzy logic control appears to be a fruitful basis for future simulations of lifting and other human tasks.



*Qu, X., Nussbaum, M.A. (2008) Simulating lifting motions using fuzzy logic control. Accepted for publication in *IEEE Transactions on Systems, Man, and Cybernetics, Part A: Systems and Humans.*


## 3.1 Introduction

Interest in simulating human motions spans diverse disciplines, including motor control, animation, and consumer product design. Extensive work has been conducted for occupational activities, in particular, with several modern computer aided design (CAD) systems including humans widely used for task and product design. Accurately simulating human motions is a major function and challenge of human CAD systems (Park et al., 2004), yet Chaffin (2005) offered three major reasons underlying the value of human motion simulation and simulation models/methods. First, such simulations can reveal possible motion strategies and

biomechanics that are used to control motions. Second, such simulations can predict motions between different groups of people and different tasks. Third, simulations can predict motions under novel situations. Numerous successful applications of human motion simulation have already demonstrated their ability to improve occupational efficiency, effectiveness, and safety (Chaffin, 2001, 2005).

However, since the human musculoskeletal system is mechanically redundant, simulating human motions involves ill-posed problems or non-unique solutions (Faraway et al., 1999; Kawato, 1996). During a simple arm reaching motion, for example, there are an infinite number of possible trajectories connecting the initial and target positions. In general, approaches to solving the ill-posed problem of human motion simulation can be classified into two groups. Those in the first group are optimization-based, where it is assumed that the neural controller (or central nervous system) plans motions based on certain performance criteria (Dysart and Woldstad, 1996; Hicheur et al., 2005; Ohta et al., 2004; Uno et al., 1989). These criteria are used to define an objective function, and optimization procedures are performed to find a solution (the optimal motion trajectory) by minimizing or maximizing the objective function value. Optimization-based approaches are able to suggest mechanisms by which the neural controller plans motions, based on the fundamental assumption that the neural controller determines motions according to the specified performance criterion. However, this fundamental assumption cannot be proven based on existing knowledge, which questions whether an optimization-based approach is a valid simulation of the motion planning process (though models developed using this approach may generate simulations with some level of

fidelity and thus have practical utility).

In contrast, approaches in the second group are data-based. They derive simulated motions from pre-existing motion capture data, and no assumptions are made with respect to functions the neural controller may optimize (Faraway, 2003; Park et al., 2004, 2005; Rosenbaum et al., 2001). In general, underlying these approaches is the construction of a database for a certain type of motion from empirical data. From this database, a model is developed, and typically uses some features of the motion (e.g. the desired initial and final positions) and the human body (e.g. segment lengths) as inputs and provides a simulated motion as the output (Faraway, 2003). These data-based approaches depend on the availability of actual motion data and, while they can yield good simulations even for novel motions (Park et al., 2004, 2005), they provide only limited information on the neural control processes.

Developing an alternative to these two traditional approaches is the focus of the present study, the basis for which is fuzzy-logic control. Fuzzy logic grew from fuzzy set theory as a way to represent approximate rather than precise reasoning, as occurs with the use of linguistic descriptors (Zadeh, 1973). It is a common experience that humans use subjective and qualitative linguistic terms to guide their behaviors. For example, when we walk it is hard for us to determine the exact walking speed. Usually, what we can tell is whether it is slow or fast. These linguistic terms cannot be easily described by conventional mathematical methods. In contrast to conventional mathematical methods, fuzzy logic can incorporate and model subjective and qualitative linguistic terms effectively. Hence, it can be inferred that fuzzy logic might be an appropriate basis from which to account for human motion behaviors in a realistic

manner. In addition, the human body is a highly non-linear system. Unlike conventional control methods, fuzzy logic has been widely and effectively used in non-linear control system design. Examples of the applications of fuzzy logic in non-linear control system design include the control of vehicle speed (Bolognani and Zigliotto, 1996), robot motion (Isik, 1987), heat exchange (Ostergaad, 1977), and power systems and nuclear reactors (Bernard, 1988). Based on these arguments, fuzzy logic was considered an appropriate tool for simulating human motions.

Lifting motions are common occupational activities, and the focus of the present model development. Lifting simulation may be very helpful to understand and prevent occupational low-back pain (LBP) incidents. LBP is one of the most common and costly occupational injuries, and about 5% of American adults experience an episode of LBP every year (Frymoyer and Cats-Baril, 1987). LBP is frequently associated with lifting activities that impose high loads on the lumbosacral and the lumbar intervertebral joints. Body posture is an important factor affecting loads on these joints during lifting (Chaffin et al., 1999). Use of lifting motion simulation can help estimate dynamic human postures, thus avoiding the need for collecting actual postural data in the process of task evaluation or design. Hence, the objective of this study was to develop and evaluate a postural control system model based on fuzzy-logic to simulate human lifting motions. The ability of the model to accurately simulate novel lifting motions was determined, and the model itself was examined to identify possible rules by which lifting motions are planned.

## 3.2 Methods

Many lifting motions are bilaterally symmetric (i.e. in the sagittal plane), so this initial model development focused on simulating only two-dimensional motions. Actual motion data were needed to specify the simulation model and to evaluate the quality of simulation results. Such data were obtained from The University of Michigan's HUMOSIM database (www.humosim.org). From the database, kinematic data are available for standing lifts involving moving a load from a standardized 'home' position to different targets (destinations) varying in height and distance. These kinematic data were derived from surface markers which were sampled at 25 Hz. The initial location of the load center was always 1.7 cm to the right, 38 cm anterior, and 11.8 cm superior to the midpoint between the hips (*H*-point). Of these, 28 motions involving symmetric lifting were extracted, and were performed by healthy volunteers (3 male and 4 female), aged 20 – 70 years. Half of these motions had a target set at 10 cm anterior to the initial load center, and the remainder at 36 cm anterior (i.e. close and far targets, respectively). These lifting motions can be also classified into two groups according to their target heights. Specifically, 14 motions had a target 49.0 cm superior to the *H*-point and were used here as 'root motions' to generate fuzzy rules; the rest had a target 16.0 cm superior to the *H*-point and were used as 'novel motions' for the purpose of evaluating the simulation model performance. The same participant was required to lift the same load (a box) in both 'root motions' and 'novel motions', and load mass varied across participants (1.6 – 3.9 kg).

### 3.2.1 Postural control system model

A model of the postural control system (Figure 3.1a) was developed, and consisted of two main parts: a neural controller model and a human body model. The neural controller plans lifting motions, and is assumed to be a fuzzy-logic controller. Lifting tasks have a goal to deliver some object to a prescribed target using the hands. In other words, lifting tasks are performed to make the distance between the target and the hands zero. If the distance between the target and the hands is not zero, the lifting task is not complete and control commands for manipulating the body should be generated by the neural controller to minimize this distance. Otherwise, the lifting task is complete and no neural control outputs are needed. Thus, in this study, the neural controller model generated control commands to manipulate the body based on positional error (Euclidean norm) between the end-effectors (the hands) and the motion (lifting) target. The human body was represented by a five-segment model (Figure 3.1b), consisting of the lower leg, upper leg, trunk, upper arm, and lower arm, with five corresponding single degree-of-freedom joints (ankle, knee, hip, shoulder, and elbow). Segments lengths were specified for each participant, based on kinematics obtained from skin surface markers.

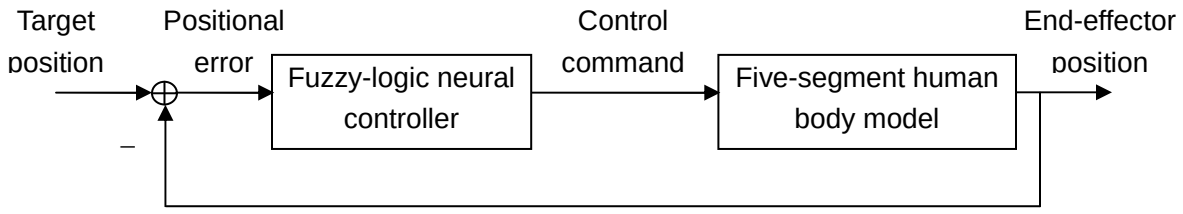


(a)

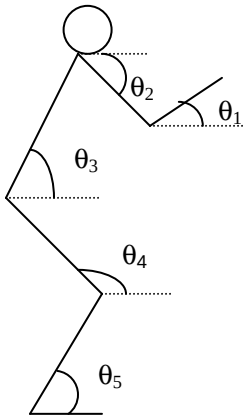


(b)

**Figure 3.1 (a) Model of the postural control system for lifting motions; (b) Five-segment human body model.**

### 3.2.2 Fundamentals of fuzzy logic control

The neural controller was designed as a fuzzy logic controller, consisting of four elements: the fuzzy rule base, fuzzification interface, fuzzy inference machine, and defuzzification interface (Castro, 1995). A fuzzy rule base is the foundation of the application of fuzzy logic, and includes a set of rules defined as 'if… then…' conditional statements, whose antecedent part (if…) and consequent part (then…) are expressed in linguistic terms. Inputs to a fuzzy logic controller are generally quantitative. In order to relate these quantitative inputs to qualitative linguistic terms, the fuzzification interface calculates the membership functions of each input, and provides the corresponding fuzzy input. The membership function is used to

specify the extent to which a quantitative value belongs to a fuzzy set. The fuzzy inference machine is determined by the overall fuzzy relation that is defined by the fuzzy rule base using fuzzy operators. In the fuzzy inference machine, the fuzzy inputs are matched with the overall fuzzy relation using the compositional rule of inference (de Silva, 1995) to generate the corresponding fuzzy outputs. The controlled part in a control system always requires quantitative control commands. Thus, the defuzzification interface translates the fuzzy outputs into quantitative signals.

### 3.2.3 Development of the fuzzy rule base

A fuzzy rule base is usually obtained from expert knowledge and experience (de Silva, 1995). However, unlike many conventional control processes, human postural control mechanisms are not well understood even by experts (Kawato, 1996). Since a rule base is nonetheless needed, root lifting motions (as described above) were analyzed to determine 'reasonable' rules as follows.

It was assumed that the motions of the five joints were independent, so separate fuzzy rule bases were developed for each. The fuzzy logic neural controller was assumed to generate instantaneous joint angular velocity signals according to the distance between the end-effectors and target. Therefore, three variables representing positional error and its velocity and joint angular velocity were adopted for each rule base. Note that positional error here is always positive since it is the distance between the end-effectors and target. In order to minimize the effects of different lifting conditions (e.g. different target locations), instantaneous positional

error and its velocity were scaled by the initial positional error, and instantaneous joint angular velocity was scaled by the error between the initial and final joint angles. Thus, the linguistic terms in the antecedent part of the fuzzy rules were used to describe the fuzzy variables of the scaled positional error (*er*) and scaled positional error velocity (*erv*), and the linguistic terms in the consequent part described the scaled angular velocity (*v*).

Fuzzy rules were generated manually according to observed trends in the fuzzy variable trajectories, in four steps. First, a set of preliminary 'significant' points along the fuzzy variables trajectories were identified. These points were defined by the local optima, or the points at which the fuzzy variable definitely belonged to a specific fuzzy set. Second, significant points at which fuzzy rules were generated were identified. Some preliminary significant points were too closely spaced in time, in which cases only one was chosen as the significant point to generate a fuzzy rule. The rest were considered redundant because the fuzzy rules generated from the nearby preliminary significant points should be the same. Third, at the time when a significant point occurred, a most likely fuzzy set was estimated to which each fuzzy variable might belong. Fourth, corresponding to any significant point, a fuzzy rule was generated according to the estimated most likely fuzzy sets for all fuzzy variables.

An example of the fuzzy rule process is given in Figure 3.2. Preliminary significant points are identified, and represented by a triangle, circle, and square (Figure 3.2a) for *er*, *erv*, and *v*, respectively. Some redundant preliminary significant points were then removed. For example, preliminary significant points *f* and *l* were in close proximity, so point *l* was rejected. The dotted vertical lines indicate the times at which significant points occurred, and fuzzy rules

were generated at these times. For example, at the time indicated by line E, the scaled positional error was estimated as most likely belonging to the medium fuzzy set, the velocity of the scaled positional error most likely belonged to the negative large fuzzy set, and the scaled shoulder angular velocity most likely belonged to the positive large fuzzy set. Thus, a fuzzy rule might be generated as 'If the scaled positional error is medium and its velocity is negative large, then the scaled shoulder angular velocity is positive large'.

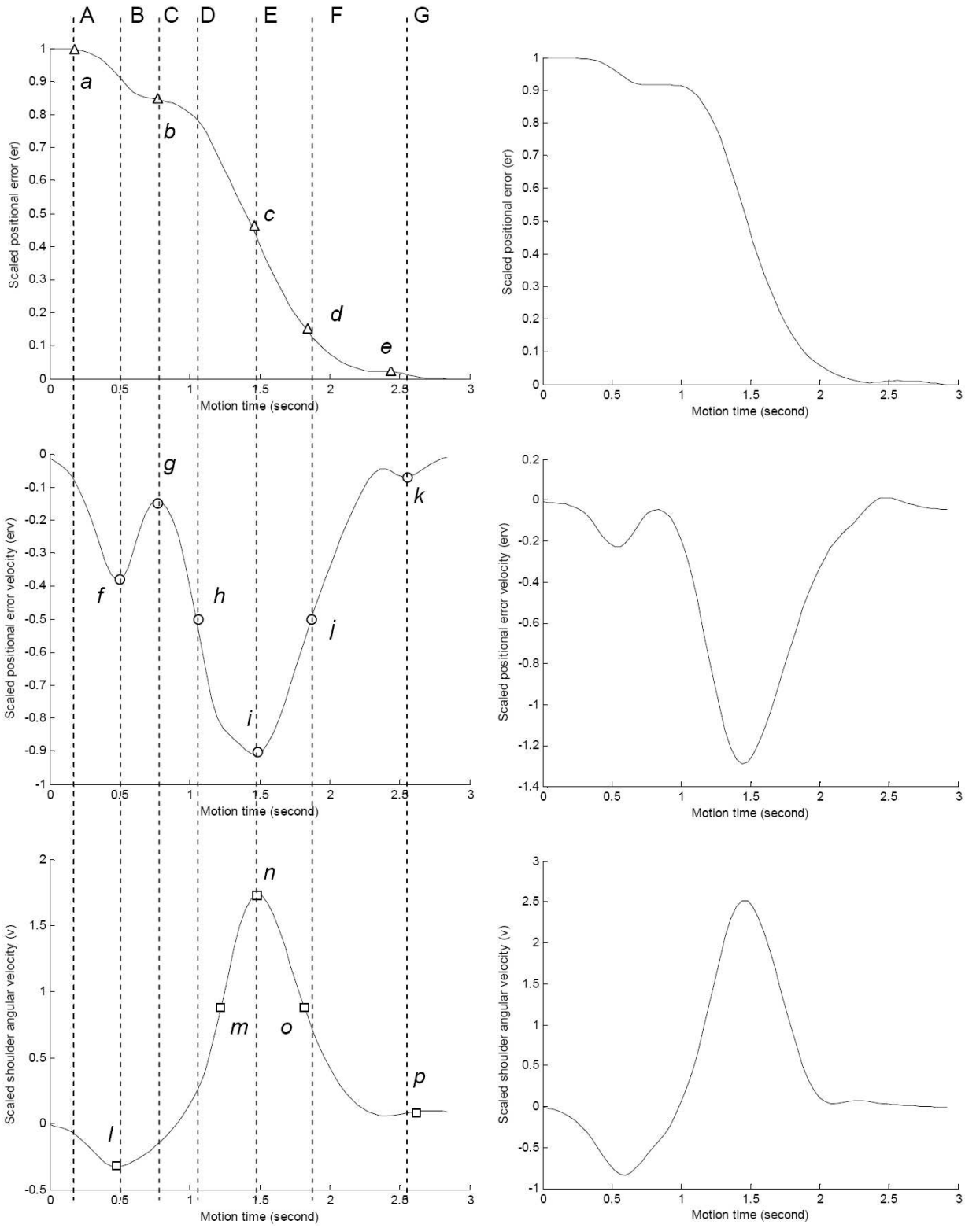


(a) (b)

**Figure 3.2 (a) Trajectories of fuzzy variables from a lifting motion; (b) Trajectories of fuzzy variables from a lifting motion that is different from the motion in (a).**

### 3.2.4 Membership functions

Each fuzzy variable corresponded to a series of fuzzy sets, and these fuzzy sets were defined by membership functions (Fig. 3.3). Specifically, scaled positional error (*er*) corresponded to five fuzzy sets that were small (S), medium small (MS), medium (M), medium large (ML), and large (L); scaled positional error velocity (*erv*) corresponded to four fuzzy sets that were positive (P), negative small (NS), negative medium (NM), and negative large (NL); and scaled joint angular velocity (*v*) corresponded to six fuzzy sets that were negative large (NL), negative medium (NM), negative small (NS), positive small (PS), positive medium (PM), and positive large (PL).

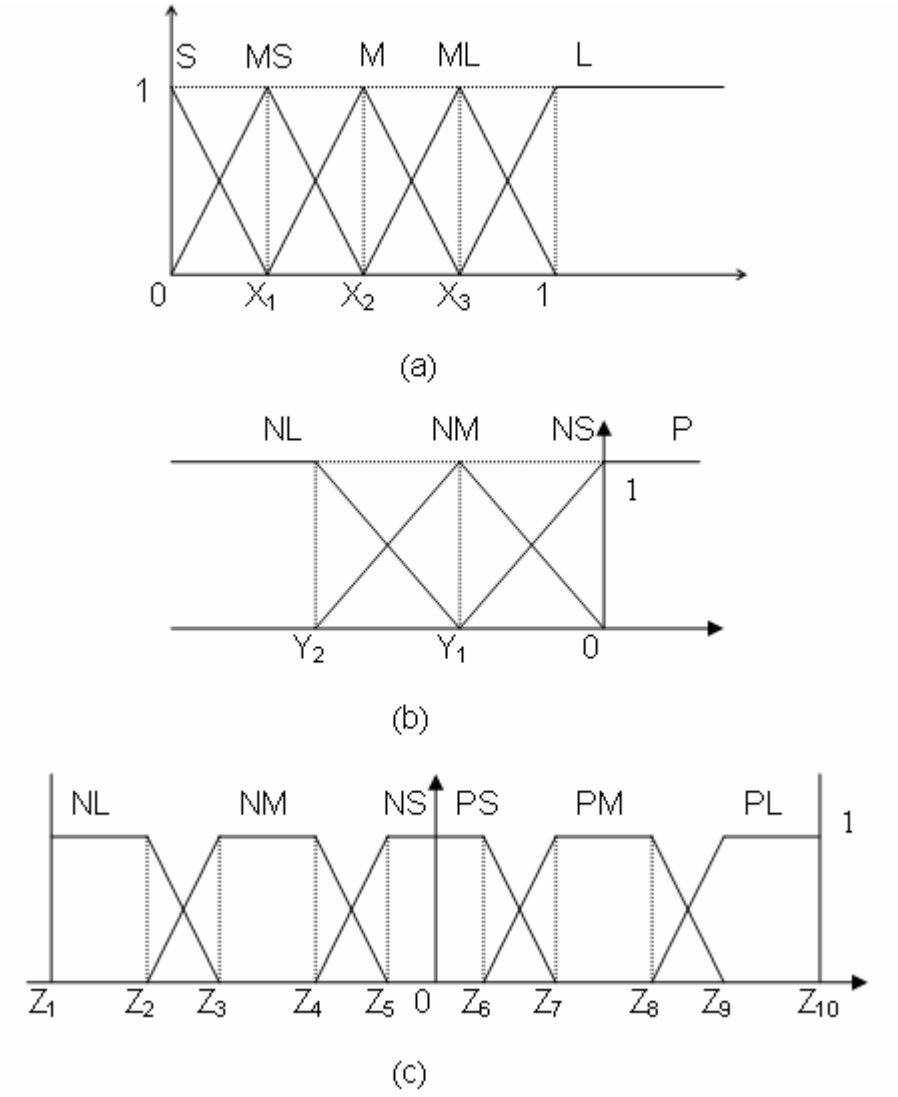


**Figure 3.3 (a) Membership functions for the scaled positional error; (b) Membership functions for the scaled positional error velocity; (c) Membership functions for the scaled joint angular velocity. See text for definitions of abbreviations.**

Parameters of the membership functions (e.g. $X_1$, $Y_1$, and $Z_1$; Figure 3.3), cannot be exactly pre-determined for any novel lifting motion. In order to specify these parameters, an optimization procedure was used, that took the membership function parameters as decision variables and had a cost function given by:

$$f = \sum_{i=1}^{n} | \theta_{fi} - \hat{\theta}_{fi} | \tag{3.1}$$

where n=5 is the number of the joints in the human body model, $\theta_{fi}$ is the simulated final angle of the $i^{th}$ joint, and $\hat{\theta}_{fi}$ is the desired (actual) final angle of the $i^{th}$ joint. Note that it was assumed that the motion duration and the desired initial and final postures for the simulated lifting motion were available in advance. Hence, the model is required to simulate all dynamic postures between the initial and final body configurations.

When applying this optimization procedure, initial values of the decision variables (membership function parameters) were first roughly estimated according to the fuzzy variable trajectories (see Figure 3.2 for examples) used to generate fuzzy rules. Subsequently, the Matlab Optimization toolbox function 'fminsearch' (The MathWorks, Natick, MA) was used to find the optimal set of membership function parameters that minimized the cost function (Eq. 3.1) for the simulated lifting motion. The algorithm 'fminsearch' uses the simplex search method of Nelder-Mead which is a direct heuristic search method without using numerical or analytic gradients. Instantaneous joint angles are limited by the ranges of joint motion. In the optimization procedure, if any predicted instantaneous joint angle was not within predetermined ranges (Table 3.1), the cost function would be set at a large number. This ensured that the current values of membership functions were not optimal and thus could not be selected to predict novel motions. After determining the membership function parameters, the membership functions used in this study can be completely specified.

**Table 3.1 Ranges of included angles (degrees)**

| Joint | Included angle | Lower bound* | Upper bound* |
|---|---|---|---|
| Elbow | $\pi-\theta_1+\theta_2$ | 38 | 180 |
| Shoulder | $\pi-\theta_3+\theta_2$ | -61 | 188 |
| Hip | $\pi-\theta_4+\theta_3$ | 67 | 180 |
| Knee | $\pi-\theta_4+\theta_5$ | 67 | 180 |
| Ankle | $\theta_5$ | 55 | 90 |

Adapted from Lin et al., 1999

### 3.2.5 Model simulation

Empirically, similar motion trajectories have common features (Lin et al., 1999; Ohta et al., 2004). For example, for point-to-point reaching with the arm, the trajectory of the end-effector is nearly a straight line, and characterized by an asymmetrical bell shaped velocity profile (Iguchi et al., 2005; Morasso, 1981). In addition, Figure 3.2 showed the trajectories of the selected fuzzy variables from two different lifting motions. When comparing these and other trajectories, disregarding the amplitude and duration, they were found to have similar trends. Such evidence indicates that similar lifting motions have common features, and it was more specifically assumed here that humans performing comparable lifting motions (e.g. to different target locations) adopt similar fuzzy rules. Thus, fuzzy rules derived from the lifting motion of a single participant were used to simulate a different but similar lifting motion. Based on the available database, fuzzy rules were generated from a root lifting motion, and then these fuzzy rules were used to simulate the novel lifting motion that has the same anterior target distance as the root lifting motion for the same participant.

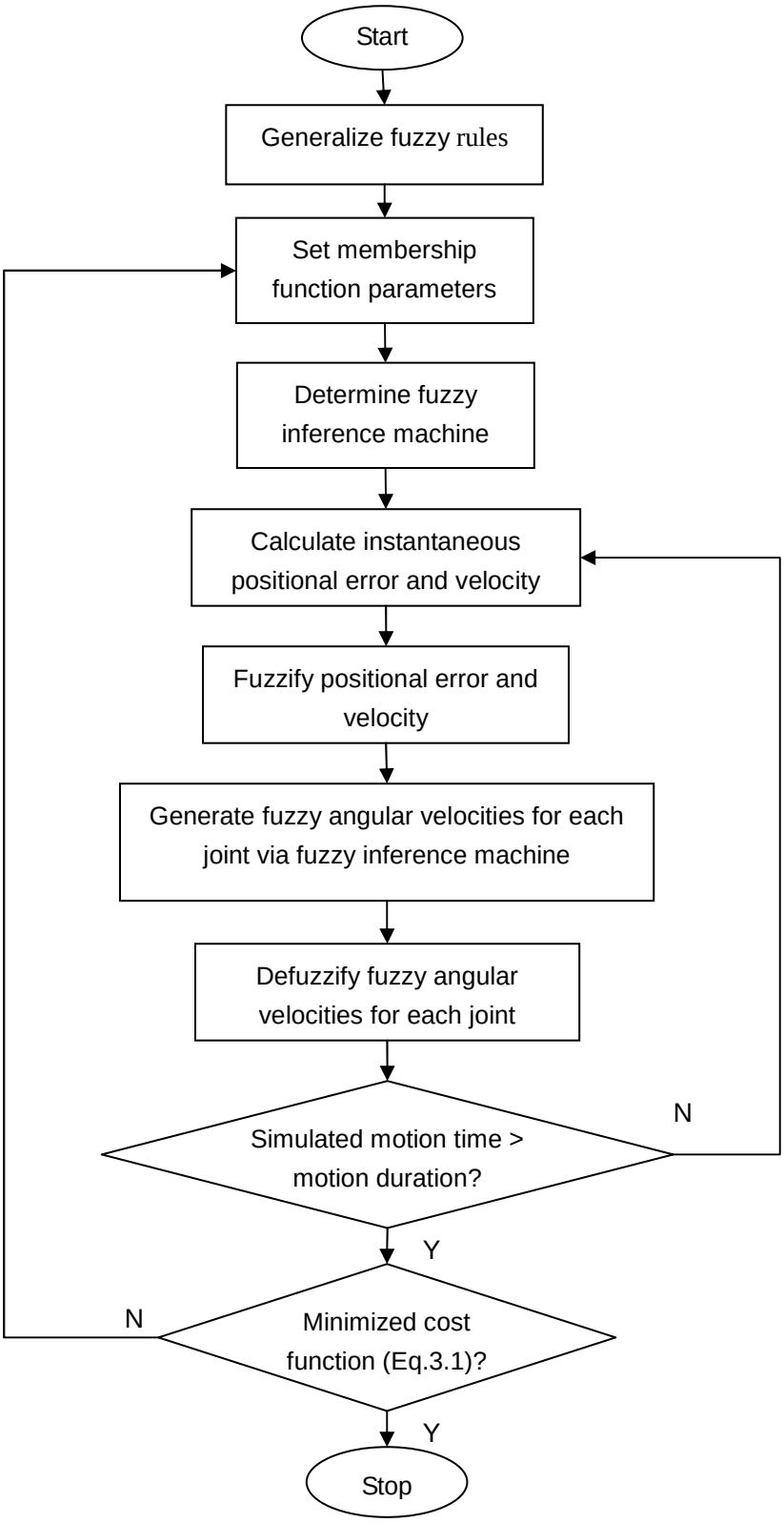


**Figure 3.4 Flow of model simulation.**

Figure 3.4 summarizes the procedures involved in using the model to simulate lifting

motions. Fuzzy rules were generated initially from root lifting motions. Then, the initial values of membership function parameters for the fuzzy variables of *er*, *erv*, and *v* were set according to their trajectories. These two steps were done offline. In the next stage, the fuzzy inference machine was determined according to an overall fuzzy relation, defined as:

$$\mu_R(er, erv, v) = \max_i \mu_{Ri}(er, erv, v) \tag{3.2}$$

where $\mu_{Ri}(er, erv, v) = \min[\mu_{ERi}(er), \mu_{ERVi}(erv), \mu_{Vi}(v)]$ is the membership function of a fuzzy relation derived from a fuzzy rule, and $\mu_R(er, erv, v)$ is the membership function of the overall fuzzy relation.

Subsequently, the instantaneous positional error and its velocity for the simulated lifting motion were calculated and fuzzified. The most common membership functions are the triangular or trapezoidal functions (Castro, 1995). Castro (1995) also proved that fuzzy logic control systems using both triangular and trapezoidal membership functions are able to approximate any real continuous function on a compact set to arbitrary accuracy. Thus, in this study, both trapezoidal and triangular membership functions were used. For a general trapezoidal membership function (Fig. 3.5), the fuzzification algorithm is given by:

$$\mu(x) = \begin{cases} 1 & b \le x \le c \\ (x-a)/(b-a) & a < x < b \\ (d-x)/(d-c) & c < x < d \\ 0 & else \end{cases} \tag{3.3}$$

where a, b, c, and d are the trapezoidal membership function parameters, *x* is quantitative input, and *μ(x)* is the corresponding fuzzy input. For a triangular membership function b=c, and the calculation still follows Eq. 3.3.

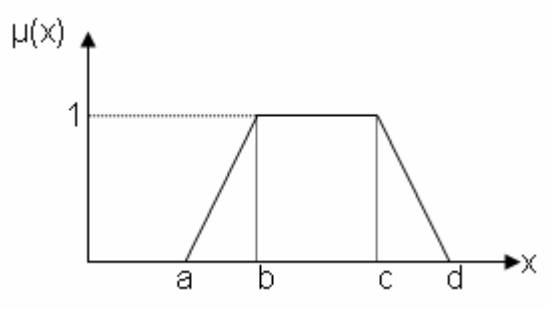


**Figure 3.5 A general trapezoidal membership function.**

After determining the fuzzified positional error and its velocity, the fuzzy inference machine used the compositional rule of inference to match these fuzzy inputs with the overall fuzzy relation, and then generated fuzzy angular velocity (Eq. 3.4).

$$\mu_V(v) = \sup_{er,erv} \min[\mu_{ER}(er), \mu_{ERV}(erv), \mu_R(er, erv, v)] \tag{3.4}$$

Then, a centroid method (Eq. 3.5) (de Silva, 1995) was used to defuzzify the fuzzy output from the fuzzy inference machine.

$$\hat{v} = \frac{\int v\mu_V(v)dv}{\int \mu_V(v)dv} \tag{3.5}$$

where $\hat{v}$ is the defuzzified output, i.e. the quantitative instantaneous joint angular velocity. The simulated motion time was then compared with the motion duration that was specified externally. If the current simulated motion time was less than the motion duration, the instantaneous positional error and its velocity were calculated, and the above procedures were repeated. If the current simulated motion time was larger than or equal to the motion duration, the optimization procedure determined if the cost function (Eq. 3.1) was minimized. If so, the simulation was stopped, and the current results used to predict the lifting motion. Otherwise, the optimization procedure reset the membership function parameters and the above procedures were repeated. Note that the solution obtained from the optimization procedure can not be

expected to be globally optimal since heuristic search was applied in the optimization procedure.

### 3.2.6 Analysis

To evaluate the model, comparisons were made between actual and simulated motions, using only those in the 'novel motion' set. Divergence between the two was quantified using the mean, median, and root mean squared (RMS) absolute joint angular errors. These errors were determined for each lifting motion for all five joints. Previous studies have also used mean squared errors (MSE) between the simulated and actual joint angles to evaluate the performance of a lifting motion simulation (Hsiang and Ayoub, 1994; Lin et al., 1999), and these values were also determined here for each joint. Correspondence between the simulated and actual joint angles was quantified using the bivariate coefficient of correlation ($\rho$). For any novel lifting motion, given the motion duration $T$, instantaneous absolute joint angular errors were extracted from five equally-spaced intervals over T (i.e. T/6, T/3, … , 5T/6). Times $0$ and $T$ were not included because the initial and final postures were specified offline. Analysis of variance (ANOVA) was performed to identify the effects of joint, motion time, and anterior target distance on these instantaneous absolute joint angular errors. Post-hoc pairwise comparisons were conducted using the Tukey's honestly significant difference (HSD) criterion. The level of significance for all statistical tests was set at $p=0.01$.

## 3.3 Results

Comparisons of the actual and simulated human lifting motions for two representative

novel motion trials are illustrated in Fig. 3.6. Summary results regarding absolute joint angular errors (i.e. between the simulated and actual lifting motions) are presented in Table 3.2. Most of the mean and median absolute joint angular errors were < 5°. Across all types of errors, four were in the range of 10-13°. Additionally, these error measures were generally smaller for the motions with a closer target than those with a farther target. MSEs varied across motions and joints (Table 3.3). Overall, the simulated motions of the hip, shoulder and elbow had larger MSEs than did those of the ankle and knee.

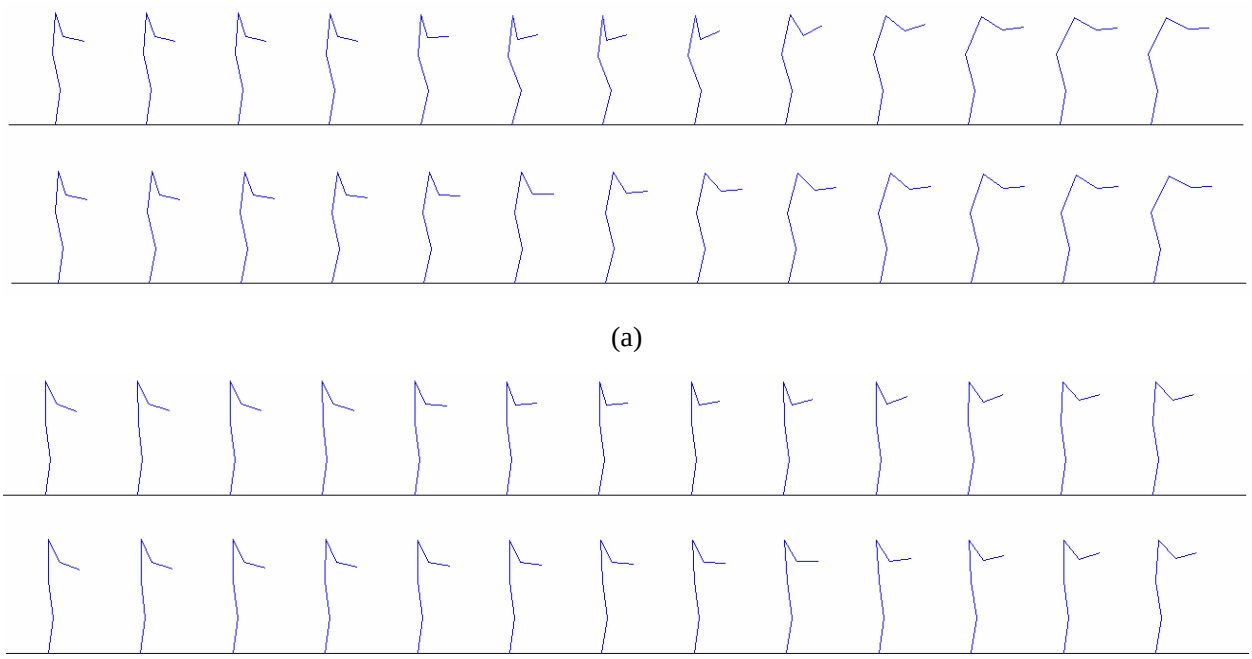

(a)

(b)

**Figure 3.6 (a) Actual (top) and predicted (bottom) lifting motion trajectories with a far target. (b) Actual (top) and predicted (bottom) lifting motion trajectories with a close target. Instantaneous dynamic postures were extracted from 12 equally-spaced intervals over the motion duration.**

**Table 3.2 Absolute angular errors (degrees) between simulated and actual lifting trajectories.**

| | Mean | | Median | | RMS | |
|---|---|---|---|---|---|---|
| Participant # | Close target | Far target | Close target | Far target | Close target | Far target |
| 1 | 3.5 | 5.0 | 3.7 | 4.8 | 6.6 | 8.4 |
| 2 | 3.5 | 5.4 | 2.7 | 5.8 | 6.8 | 10.1 |
| 3 | 3.7 | 7.6 | 3.5 | 8.4 | 5.9 | 12.9 |
| 4 | 2.6 | 4.7 | 2.3 | 3.1 | 4.9 | 7.8 |
| 5 | 3.1 | 9.7 | 1.2 | 10.7 | 6.6 | 13.3 |
| 6 | 2.1 | 7.7 | 1.2 | 6.6 | 4.1 | 12.6 |
| 7 | 2.3 | 5.5 | 1.9 | 5.1 | 4.2 | 9.6 |
| Mean | 3.0 | 6.5 | 2.4 | 6.4 | 5.6 | 10.7 |
| Overall Mean | 4.7 | | 4.4 | | 8.1 | |

**Table 3.3 Mean squared joint angular errors (degree$^2$).**

| Participant # | Ankle | Knee | Hip | Shoulder | Elbow |
|---|---|---|---|---|---|
| Close target | | | | | |
| 1 | 0.4 | 0.0 | 3.0 | 42.0 | 173.4 |
| 2 | 0.7 | 0.6 | 2.6 | 56.1 | 174.4 |
| 3 | 2.0 | 1.0 | 4.3 | 50.7 | 117.0 |
| 4 | 0.0 | 0.0 | 5.2 | 30.8 | 81.7 |
| 5 | 0.2 | 0.0 | 1.9 | 61.9 | 152.2 |
| 6 | 1.1 | 0.2 | 0.7 | 67.0 | 14.3 |
| 7 | 0.1 | 0.1 | 0.5 | 33.5 | 53.4 |
| Mean | 0.7 | 0.3 | 2.6 | 48.9 | 109.5 |
| Far target | | | | | |
| 1 | 0.8 | 0.6 | 36.5 | 137.0 | 176.1 |
| 2 | 1.6 | 0.3 | 18.2 | 189.4 | 296.9 |
| 3 | 1.0 | 0.3 | 57.6 | 628.1 | 139.8 |
| 4 | 3.4 | 18.2 | 7.5 | 172.9 | 105.2 |
| 5 | 3.8 | 285.0 | 179.4 | 185.5 | 226.2 |
| 6 | 50.7 | 0.4 | 58.2 | 446.6 | 236.0 |
| 7 | 0.2 | 0.2 | 30.9 | 162.4 | 266.3 |
| Mean | 8.8 | 43.5 | 55.5 | 274.5 | 206.6 |
| Overall Mean | 4.7 | 21.9 | 29.0 | 161.7 | 158.1 |

Most of the correlations between the simulated and actual joint angles were significantly positive (Table 3.4). Nearly 70% of these correlations were > 0.6, indicating a moderate-high

correspondence between simulated and actual angles. However, there were also some unexpected results. Some simulated and actual joint angles were not significantly correlated, and some were negatively correlated. On average, ρ values increased from the lower extremity to upper extremity, and decreased with an increase in the anterior target distance. Across all novel motions, three had an average $\rho < 0.5$, whereas eight among the rest had an average $\rho > 0.6$.

**Table 3.4 Coefficients of correlation (ρ) between simulated and actual joint angles.**

| Participant # | Ankle | Knee | Hip | Shoulder | Elbow | Mean |
|---|---|---|---|---|---|---|
| Close target | | | | | | |
| 1 | 0.92 | 0.99 | 0.90 | 0.76 | 0.77 | 0.87 |
| 2 | 0.88 | 0.70 | 0.62 | 0.57 | 0.75 | 0.70 |
| 3 | 0.98 | 0.86 | 0.64 | 0.80 | 0.78 | 0.81 |
| 4 | 0.59 | 0.22* | 0.72 | 0.91 | 0.91 | 0.67 |
| 5 | 0.21* | 0.70 | 0.93 | 0.92 | 0.54 | 0.66 |
| 6 | 0.72 | 0.25* | 0.98 | 0.84 | 0.89 | 0.74 |
| 7 | 0.84 | -0.08* | 0.87 | 0.59 | 0.70 | 0.58 |
| Mean | 0.73 | 0.52 | 0.81 | 0.77 | 0.76 | |
| Far target | | | | | | |
| 1 | 0.41 | -0.10* | -0.42* | 0.89 | 0.81 | 0.32 |
| 2 | 0.75 | 0.96 | 0.27 | 0.82 | 0.91 | 0.74 |
| 3 | -0.39* | 0.40 | -0.51* | 0.66 | 0.96 | 0.22 |
| 4 | 0.29 | 0.61 | 0.79 | 0.90 | 0.55 | 0.63 |
| 5 | 0.29 | 0* | 0.88 | 0* | 0.44 | 0.32 |
| 6 | 0* | 0.60 | 0.75 | 0.79 | 0.75 | 0.58 |
| 7 | -0.55* | 0.83 | 0.94 | 0.93 | 0.62 | 0.55 |
| Mean | 0.12 | 0.47 | 0.39 | 0.71 | 0.72 | |
| Overall Mean | 0.42 | 0.50 | 0.60 | 0.74 | 0.74 | |

* indicates that correlation was not significantly positive.

There were significant main effects of joint ($F(4, 316)=49.1$, $p<0.01$) and motion time ($F(4, 316)=14.2$, $p<0.01$) on the instantaneous absolute joint angular errors. The joint × motion

time interaction was also significant ($F(16, 316)=5.0$, $p<0.01$), though it appeared to be relatively unimportant (Figure 3.7). No other main or interaction effects were significant, though there was a trend ($p=0.085$) indicating ~1° larger errors when lifting to far targets. On average, the absolute joint angular errors of the shoulder (9.9°) and elbow (11.2°) were larger than those of the ankle (1.0°), knee (1.8°) and hip (4.0°). Post-hoc comparisons indicated that errors were significantly larger for the shoulder and elbow than the remaining joints. Instantaneous absolute joint angular errors appeared to increase with motion time initially, and then decrease after reaching a peak value near the middle stage of the motion. These errors were significantly larger at the middle stage of lifting motions (*T/2*) than at either the initial or final stage of motions (T/6 or 5T/6).

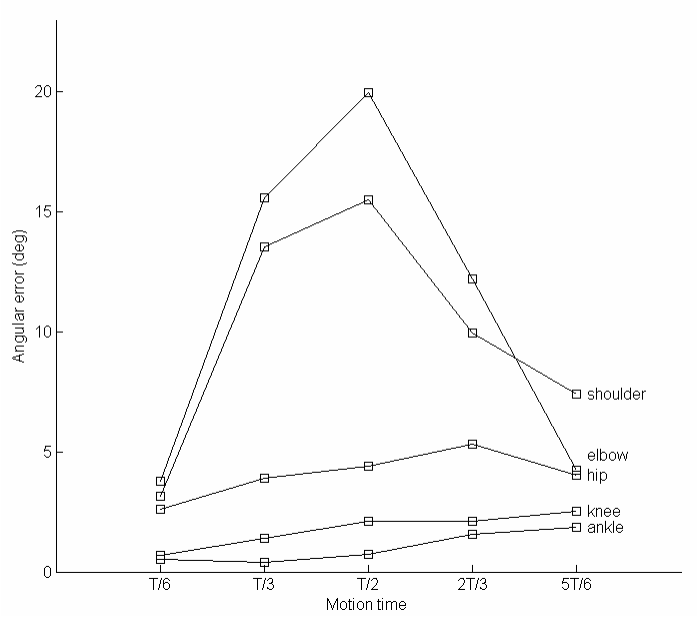


**Figure 3.7 Mean absolute angular errors at different motion times; each curve represents a different joint.**

## 3.4 Discussion

The main purpose of this study was to develop and evaluate a fuzzy-logic-based model

for simulating two dimensional (sagittal plane) lifting motions. A simple two-dimensional five-segment body model was adopted and assumed to be manipulated by a fuzzy-logic neural controller. Fuzzy rules were generated from actual motion data, and then used to predict novel motions on a participant-specific basis. In addition, to specify the parameters of membership functions, an optimization procedure was performed by minimizing the differences between the simulated and actual final postures.

When empirically evaluating human motion simulation models, 10° has been suggested as a criterion value for mean joint angular errors (Beck and Chaffin, 1992; Perez, 2005). From this perspective, the presented model is able to adequately predict lifting motions in the sagittal plane, since the overall mean joint angular errors for the 14 simulated novel motions were all < 10° (Table 3.2). Results from the present model also compare favorably to those from other human motion simulation models. Specifically, Zhang and Chaffin (2000) presented a model based on an optimization-based differential inverse kinematics approach to simulate seated reaching motions. Overall mean and median joint angular errors from their study were 5.2° and 4.7°, respectively, with corresponding values here of 4.7° and 4.4°. Perez (2005) used artificial neural networks to predict lifting motions and found RMS joint angular errors typically less than 20°. Here, these errors were < 14° for all lifting motions (Table 3.2). In addition, except for the elbow, mean MSEs for the ankle, knee, hip and shoulder joints in the current study were smaller than those from Lin et al. (1999) who simulated lifting motions using a dynamic planar motion simulation model (i.e. ankle: 4.7 vs 20.9; knee: 21.9 vs 148.6; hip: 29.0 vs 78.4; shoulder: 161.7 vs 270.2; elbow: 158.1 vs 105.0. unit: degree$^2$). In addition to these error measures,

correlations between simulated and actual joint angles indicated that the presented model can simulate actual lifting motions with good fidelity, since most of these correlations (ρ) were > ~0.6.

Average absolute joint angular errors and mean MSEs were smaller for the ankle, knee and hip than for the shoulder and elbow (Fig. 3.7 and Table 3.3). The former joint angles thus appear to be better predicted than the rest using the current model. However, when considering the relative strength of association between simulated and actual joint angles (ρ, Table 3.4), it appears that predicted ankle, knee, and hip angles were not as good as the predicted shoulder and elbow angles. A possible explanation for this discrepancy is that the shoulder, and elbow joints were more 'active' during novel lifting motions, in the sense that larger angular excursions were observed. Specifically, the average ranges of shoulder and elbow joint angles (41.4° and 43.8°) were substantially larger than those of the ankle, knee and hip (2.8°, 4.8° and 13.8°). A smaller joint motion range can be expected to lead to smaller error measures for that joint. Thus, absolute error measures are limited when determining which joint angles might be better predicted than others. Instantaneous absolute joint angular errors were smaller at the initial and final stages of lifting motions, which is reasonable since the predicted initial and final postures were specified in advance. Thus, the predicted instantaneous postures should contain more information about the actual ones when getting closer to the initial or final posture in time. Lifting to a closer target involves smaller angular excursions. Hence, motions to a closer target should tend to generate smaller error measures, consistent with the results found (though the effect was only marginal).

It has been generally considered that joint torques are the outputs of the neural controller when planning motions (Ferry et al., 2004; Martin et al., 2006). However, in this study, using joint torques as neural control outputs might be less effective and/or less efficient mainly due to two factors. First, joint kinetic data were not available directly (i.e. not included in the HUMOSIM database). Second, since we only adopted a simplified five-segment human body model and each segment was assumed to be rigid, additional errors would be induced using joint torques to calculate lifting kinematics. In contrast to joint torques, joint angular velocities can be derived easily from the HUMOSIM database. More importantly, using joint angular velocities to calculate joint angular displacements would induce much less errors than do joint torques. Thus, the neural control outputs were assumed to be instantaneous joint angular velocities.

When using the current model, it was assumed that initial and final postures are determined in advance. We made such an assumption because initial and final postures are often available (e.g. through photographs, videos, or task simulations) or can be statically estimated (Park et al., 2004). When simulating motions, we were more interested in the dynamic postures occurring between them, and the same assumption has been required for other lifting motion simulation models (Beck and Chaffin, 1992; Chang et al., 2001; Iguchi et al., 2005).

In essence, the presented model is data-based, since recorded motion data are needed to generate fuzzy rules. Yet unlike existing data-based models, potential neural control mechanisms were taken into account in this model. Specifically, the neural controller was

based on fuzzy logic. Fuzzy rules are the basis for application of fuzzy logic. These rules are able to reflect the external properties of the neural controller by describing the relationships between the neural controller's inputs and outputs. In contrast to existing data-based models, the presented model was able to provide information regarding the neural control mechanisms by interpreting fuzzy rules. For example, during model simulation, a fuzzy rule was generated as: "if the scaled positional error is medium and its velocity is negative large, then the scaled shoulder angular velocity is positive large". From this rule, we may speculate that when the neural controller sensed a medium positional error and negative large velocity error, it would generate control signals to adjust shoulder angular velocity to be positive large. It is also important to note that fuzzy rules are not based on any assumptions, but rather stem from observed motion data. Thus, the presented model may have a higher level of construct validity than optimization-based models.

Overall, the presented model was able to simulate two-dimensional lifting motions, and offers some hypotheses regarding how the neural controller works. However, several limitations still exist when using this model. First, due to the properties of linguistic terms, there is no way to obtain the exact rules between fuzzy inputs and outputs. We can only roughly estimate the possible rules by analyzing actual motion trajectories. Second, we assumed that the neural controller adopted the same strategy for different but similar lifting motions. This may not necessarily be true in reality, as humans may have many options to complete a given motion task and the motion planning may have a stochastic component. Third, some features of the predicted motions, such as motion duration, must be specified externally.

While durations may be externally specified or predictable in some cases (e.g. assembly line tasks), this is clearly not true for all tasks of interest. Fourth, this model may be computationally inefficient since an optimization procedure was adopted to determine the values of membership function parameters and fuzzy rules had to be specified manually. Fifth, we made several assumptions during model simulation for simplicity. For example, we assumed that motions of five joints were independent. These assumptions might not be valid in reality, but were required in this initial model development in order to improve computational efficiency. It is also important to note that root motions and their corresponding novel motions were somewhat similar in this study, so fairly good predictions might be expected. However, as has been the case with other data-based models (Faraway, 2003), when the novel motions differ substantially from the available root motions, the quality of these predictions may degrade.

Sensory delay should exist in the postural control system due to sensory transduction, transmission, and processing. As noted earlier, fuzzy rules were specified manually. Sensory delay is typically ~100 ms (Peterka, 2002), which is a relatively small value compared with the motion durations studied here. Hence, we could not easily identify such small time differences when specifying the fuzzy rules. Sensory noise was not considered for the same reason. However, we still suggest that fuzzy rules can reflect some aspects of the neural control mechanisms. Because sensory delay likely introduces a phase difference to the neural inputs, the essential properties of the neural inputs should not be changed.

Besides the ranges of joint motion, lifting motions may also be limited by other constraints such as joint strength and balance maintenance. However, the latter constraints

were not incorporated because neither could be calculated with sufficient accuracy here due to the use of a simplified five-segment body model. However, these and other constraints might be included with adoption of a more complex human body model in the future. Specifically, if either simulated joint strengths exceed their limits or the projection of the whole body center-of-mass goes beyond the base of support (BOS), the cost function of the optimization procedure could be set to a large number as described above, thereby ensuring the current membership function parameters were not optimal.

In this study, simulation of any novel lifting motion used the root lifting motion from the same participant to generate fuzzy rules, and only two-dimensional lifting motions were simulated. The presented model should also be able to simulate motions across individuals (e.g. using a root motion and novel motion from different individuals), and be applicable to two-dimensional and three-dimensional motions of other types (so long as some root motions are available). Thus, in future research, the ability of the presented model to simulate lifting motions across individuals and to simulate two-dimensional and three-dimensional motions of other types should be investigated. At the same time, as noted earlier, we assumed that motions of the five joints were independent. Studies have revealed that different joints were coordinated together to manipulate human postures (Chaffin et al., 1999), so dependence of joint motions should be taken into account when developing future human motion models. Furthermore, sensitivity analyses, generalizability, and investigations of the effects of some tasks attributes on the observable trends in fuzzy variable trajectories are also worthy areas of future investigation.

# Chapter 4 A Balance Control Model of Quiet Upright Stance based on an Optimal Control Strategy


## Abstract

Models of balance control can aid in understanding the mechanisms by which humans maintain balance. A balance control model of quiet upright stance based on an optimal control strategy is presented here. In this model, the human body was represented by a simple single-segment inverted pendulum during upright stance, and the neural controller was assumed to be an optimal controller that generates ankle control torques according to a certain performance criterion. This performance criterion was defined by several physical quantities relevant to sway. In order to accurately simulate existing experimental data, an optimization procedure was used to specify the set of model parameters to minimize the scalar error between experimental and simulated sway measures. Thirty-two independent simulations were performed for both younger and older adults. The model's capabilities, in terms of reflecting sway behaviors and identifying aging effects, were then analyzed based on the simulation results. The model was able to accurately predict center-of-pressure-based sway measures, and identify potential changes in balance control mechanisms caused by aging. Correlations between sway measures and model parameters are also discussed.



*Qu, X., Nussbaum, M.A., Madigan, M.L. (2007) A balance control model of quiet upright stance based on an optimal control strategy. *Journal of Biomechanics 40*: 3590-3597.


## 4.1 Introduction

Upright stance is inherently unstable in that without internal control, even minute amplitude disturbances can compromise stability. Internal control is provided by the postural control system which generates joint torques to control upright stance (Ishida et al., 1997; Peterka, 2000). Thus, investigating balance control mechanisms may aid in understanding the postural control system.

A number of balance control models have been proposed to investigate balance control

mechanisms. The most essential aspect of such models is the model neural controller. In general, methods used to model neural control can be classified into two groups. In the first group, it is assumed that the neural controller adopts a particular control strategy to maintain balance. These include PID (proportional, derivative, and integral) control (Iqbal et al., 2004; Johansson et al., 1988; Maurer and Peterka, 2005), RIPID (recurrent integrator proportional integral derivative) control (Jo and Massaquoi, 2004), and sliding mode control (Bottaro et al., 2005), etc. While these studies have provided a basis for applying control theory to the neural controller, a common concern with such models is that it is impossible to validate the fundamental control assumption since it is still unknown how the neural controller works. In the second group, the neural controller is completely determined by available experimental data (Fujisawa et al., 2005; Ishida et al., 1997; Kiemel et al., 2002). These models appear more valid, as no assumptions about the controller have to be made, yet are limited by a dependence on experimental data. Further, when using models in the second group, the neural controller has to be modeled as a discrete system, which may induce errors related to discretizing continuous data. Such errors can result in instability when modeling upright stance (Ishida et al., 1997).

Human motions are generally effective and efficient. For example, hand paths taken in point-to-point reaching movements are the shortest between the initial hand position and the target since they tend to be straight and smooth (Morasso, 1981; Ohta et al., 2004), and these movements appear to be organized to minimize energy expended (Soechting et al., 1995). Some type of optimization also appears present in the control of muscle recruitment for

generating motions (Fagg et al., 2002). With respect to the control of upright stance, some investigations of sway have been based on the assumption that these motions are planned according to optimal objectives, and have yielded realistic motion trajectories (Ferry et al., 2004; Martin et al., 2006). Thus, we may consider that the neural controller is an optimal controller that is able to optimize the generation of sway motion (though we may not know, *a priori*, what is optimized).

The purpose of this preliminary study was to develop a new balance control model based on an optimal control strategy, and to demonstrate the feasibility of this model in simulating spontaneous sway. Since center-of-pressure (COP) based sway measures are most commonly used to characterize sway behaviors (Baratto et al., 2002; Peterka, 2000; Prieto et al., 1996), this model was expected to be able to accurately simulate sway behaviors characterized by COP-based sway measures. The experimental COP-based sway measures used to specify the proposed model was given by Prieto et al. (1996). Recent studies have shown that older adults have a reduced ability to maintain balance (Du Pasquier et al., 2003), indicating that aging likely compromises balance control. Thus, results are presented on the ability of the model to simulate spontaneous sway measures, to reflect differences in sway associated with age, and to identify potential internal mechanisms that cause these differences.

## 4.2 Methods

### 4.2.1 Human body dynamics and sensory systems

The postural control system was modeled as a feedback control system (Masani et al., 2006; Peterka, 2002). The closed loop in the postural control system model consists of three parts: human body dynamics, the sensory (afferent) feedback, and a neural controller. Human body dynamics was described by a single-segment inverted pendulum model (Fig. 3.1). Sway motion was assumed to be restricted to the sagittal plane. The anthropometry of the simulated subject was set to that of an average adult male (Maurer and Peterka, 2005). The equation of motion for the inverted pendulum model of the body is given by:

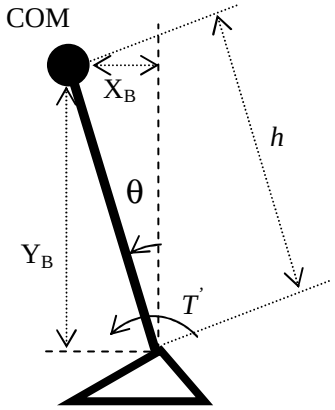


**Figure 4.1 Single-segment inverted pendulum model of sway dynamics.**

The equation of motion for the inverted pendulum model of the body is given by:

$$I\ddot{\theta}(t) - Mgh\sin\theta(t) = T'(t) \tag{4.1}$$

where $I$ = 66kg/m$^2$ is the moment of inertia of the body about the ankle, $M$ = 76kg is body mass, $h$ = 0.87m is the height of the body center of mass (COM), $\theta$ is the sway angle, $T$ is the ankle torque, and $g$ = 9.81m/s$^2$ is the acceleration due to gravity. For spontaneous sway, $\theta(t)$ is small

enough so that $sin\theta(t) \approx \theta(t)$. Thus, Eq. 4.1 can be linearized as:

$$I\ddot{\theta}(t) - Mgh\theta(t) = T^{'}(t) \tag{4.2}$$

The sensory systems were assumed to be able to provide accurate body orientation measures to the neural controller, but with an inherent time delay due to sensory transduction, transmission, and processing (van der Kooij et al., 1999). We assumed that the sensory delay time was time-invariant for a given individual under consistent conditions. In order to linearize the sensory system model, the delayed sway angular displacement, $\hat{\theta}(t) = \theta(t - \tau_d)$, was expanded using a Taylor series (Bajpai et al., 1977), and thereby approximated as:

$$\hat{\theta}(t) \approx \theta(t) - \tau_d \dot{\theta}(t) + \frac{1}{2}\tau_d^2 \ddot{\theta}(t) \tag{4.3}$$

where $\tau_d$ is the time-invariant delay time.

According to Eqs. 4.2 and 4.3, given a zero initial condition, the properties of body dynamics and sensory systems can be represented by the following transfer functions, respectively:

$$\frac{\theta(s)}{T^{'}(s)} = \frac{1}{Is^2 - Mgh} \tag{4.4}$$

$$\frac{\hat{\theta}(s)}{\theta(s)} = \frac{1}{2}\tau_d^2 s^2 - \tau_d s + 1 \quad \text{or} \quad \frac{\dot{\hat{\theta}}(s)}{\dot{\theta}(s)} = \frac{1}{2}\tau_d^2 s^2 - \tau_d s + 1 \tag{4.5}$$

To stabilize the postural control system, so that the body is kept upright, the properties of both body dynamics and sensory systems should be taken into account by the neural controller. Thus, the controlled part in the postural control system includes both body dynamics and sensory systems. In addition, without taking random disturbance torque into account, $T^{'}=T$. Thus, derived from Eqs. 4.4 and 4.5, the transfer function from the torque generated by the neural

controller ($T$) to delayed sway angular displacement ($\hat{\theta}$) is:

$$\frac{\hat{\theta}(s)}{T(s)} = \frac{\frac{1}{2}\tau_d^2 s^2 - \tau_d s + 1}{Is^2 - Mgh} \tag{4.6}$$

Since the Laplace '$s$' can be directly replaced by the differentiation operator, according to Eq. 4.6:

$$\ddot{\hat{\theta}}(t) = \frac{Mgh}{I}\hat{\theta}(t) + \frac{1}{I}T(t) - \frac{\tau_d}{I}\dot{T}(t) + \frac{1}{2}\tau_d^2\ddot{T}(t) \tag{4.7}$$

Thus, we obtained the state equations accounting for the properties of body dynamics and sensory systems as follows:

$$\dot{x}(t) = Ax(t) + Bu(t) \tag{4.8}$$

where $A = \begin{pmatrix} 0 & 1 & 0 & 0 \\ \frac{Mgh}{I} & 0 & \frac{1}{I} & \frac{-\tau_d}{I} \\ 0 & 0 & 0 & 1 \\ 0 & 0 & 0 & 0 \end{pmatrix}$, $B = \begin{pmatrix} 0 \\ \frac{\tau_d^2}{2I} \\ 0 \\ 1 \end{pmatrix}$, the state is $x(t) = \begin{pmatrix} \hat{\theta}(t) \\ \dot{\hat{\theta}}(t) \\ T(t) \\ \dot{T}(t) \end{pmatrix}$, and the control signal is, $u(t) = \ddot{T}(t)$.

The neural controller was designed according to the above state equations, and it assumed to be an optimal controller that incorporates an optimal control processor and two integration units. The optimal control processor generates the optimal control signal (u) according to some performance criterion. Two integration units ensure that the output of the neural controller is the joint torque. We also assumed that spontaneous sway was caused by both the torque generated by the neural controller and a random disturbance torque (e.g. Peterka, 2000). The latter modeled as white noise. The complete postural control system model can thus be illustrated as in Fig. 4.2 (a).

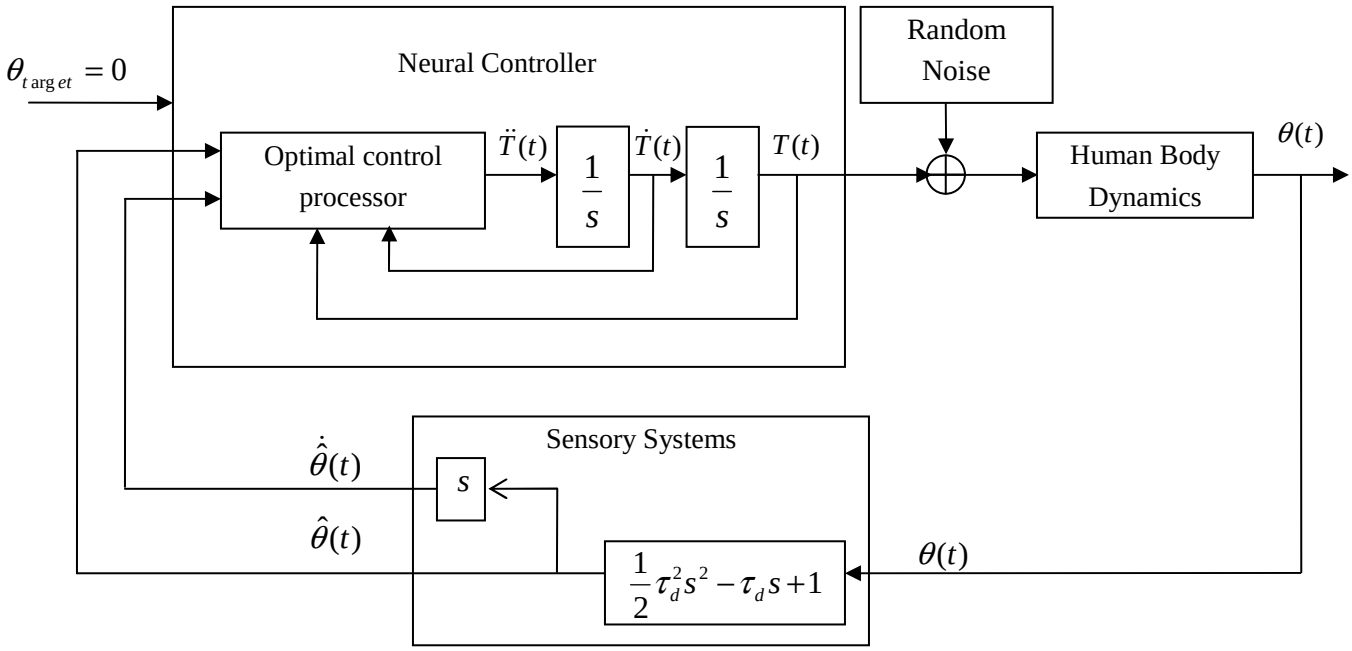


(a)

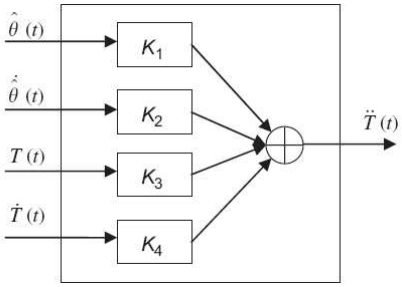


(b)

**Figure 4.2 (a) Human postural control system model of balance control. θ = sway angular displacement; $\hat{\theta}$ = delayed sway angular displacement; *T* = ankle torque; $\theta_{target}$ = target sway angle. Human body dynamics is defined by Eq. 4.4. Sensory systems are defined by Eq. 4.5. (b) Optimal control processor model. {$K_1$, $K_2$, $K_3$, $K_4$} is the optimal feedback gain.**

### 4.2.2 Optimal control processor

The optimal control processor was designed following an optimal control strategy and expected to generate the optimal control signal *u*. Since there is no clear final condition for

spontaneous sway, the optimal control processor is determined by an infinite-time linear quadratic regulator (LQR). The LQR minimizes a performance index of the standard form

$$J = \frac{1}{2}\int_0^\infty (x'(t)Qx(t) + u'(t)Ru(t))dt \tag{4.9}$$

where $Q$ and $R$ are time-invariant weighting matrices for state $x$ and control signal $u$ (see Eq. 4.8), and are chosen by regulating certain physical quantities relevant to sway.

State $x$ and control signal $u$ (see Eq. 4.8) should be able to represent selected physical quantities, and do so in a form that allows the weighting matrices to be easily obtained. Minimum torque change rate is one of the most common criteria used to predict human motion (Chang et al., 2001; Uno et al., 1989). Ferry et al. (2004) and Martin et al. (2006) used this criterion to simulate sway motion and found that it could yield realistic trajectories. Humans may also try to minimize the displacement and velocity of the sway angle, and/or other joint torque measures over time in order to maintain balance effectively and efficiently. Therefore, it was concluded that the relevant physical quantities included ankle torque measures and delayed body orientation measures. From this, the optimal controller's performance index was defined by:

$$J = \frac{1}{2}\int_0^\infty (w_1\hat{\theta}^2(t) + w_2\dot{\hat{\theta}}^2(t) + w_3T^2(t) + w_4\dot{T}^2(t) + w_5\ddot{T}^2(t))dt \tag{4.10}$$

where $w_1$, $w_2$, $w_3$, $w_4$ and $w_5$ are weightings of the respective relevant physical quantities. These weights are not predetermined. Rather, they are determined as described below, and are subsequently interpreted as indicating which physical quantities play a more important role in balance control.

In order to apply formulated optimal control equations, the performance index (Eq. 4.10)

must first be converted into the standard form (Eq. 4.9). Doing so yields the weighting matrices $Q$ and $R$ in Eq. 4.9 as:

$$Q = \begin{pmatrix} w_1 & 0 & 0 & 0 \\ 0 & w_2 & 0 & 0 \\ 0 & 0 & w_3 & 0 \\ 0 & 0 & 0 & w_4 \end{pmatrix} \quad \text{and} \quad R = w_5 \tag{4.11}$$

After determining the weighting matrices of the performance index in the standard form, and state equations of the controlled part in the postural control system, the optimal state feedback gain ($K = \{K_1, K_2, K_3, K_4\}$) is needed. This gain is used to define the optimal control processor (Fig. 4.2 (b)), and can be calculated by solving the Riccati equation (Naidu, 2003). Given the state $x$, the optimal control processor generates the optimal control signal:

$$u(t) = -Kx(t) = -(K_1\hat{\theta}(t) + K_2\dot{\hat{\theta}}(t) + K_3T(t) + K_4\dot{T}(t)) \tag{4.12}$$

Note that when using the Riccati equation to calculate the optimal feedback gain, only the state matrices $A$ and $B$ (see Eq. 4.8), and the weighting matrices $Q$ and $R$ (see Eq. 4.9) were required, and the properties of the random noise were not taken into account. This is appropriate since the random noise is not contained in the closed loop of the postural control system, and thus cannot account for the internal properties of the postural control system.

### 4.2.3 Optimization procedure

Unlike the anthropometry of the simulated subject, some model parameters, e.g. sensory delay time, cannot be specified in advance. At the same time, the balance control model was expected to be able to accurately simulate sway measures. To this end, an optimization

procedure was performed to determine the values of the unspecified model parameters, so that the simulation results can best match the experimental results.

COP-based measures of sway were desired from the model output for comparison with experimental data. From body dynamics, the COP displacement along the A/P direction ($X_{cop}$) was determined using (Maurer and Peterka, 2005):

$$X_{cop} = \frac{(Mh^2 - I)\ddot{\theta} + Mx_B(g + \ddot{y}_B) - My_B\ddot{x}_B - Mh_F\ddot{x}_B + m_F d_F g}{M(g + \ddot{y}_B) + m_F g} \tag{4.13}$$

where $m_F$ = 2.01kg is the mass of the feet, $h_F$ = 0.085m is the height of the ankle, and $d_F$ = 0.052m is the A/P distance between the ankle and the COM of the feet (additional terms are as defined above).

Prieto et al. (1996) systematically presented a set of COP-based sway measures. Maurer and Peterka (2005) classified these measures into three groups. Measures within each group are highly correlated, and between groups have lower correlations. According to Maurer and Peterka's classification, we chose three measures from each group to define the cost function for the optimization procedure. These measures are: mean distance (MD), root mean square distance (RMS), maximum distance (MAXD), mean velocity (MV), mean frequency (MFREQ), 50% power frequency (P50), 95% power frequency (P95), centroidal frequency (CFREQ), and frequency dispersion (FREQD). The cost function is defined a scalar error function of these sway measures (we will provide detailed definition in the following chapters). This optimization procedure is sufficiently complex that heuristic approaches are suitable for searching for a good solution.

The cost function in the optimization procedure is then given by:

$$E = \sum_{i=1}^{N} \left( \frac{COPM_i - \hat{COPM}_i}{\hat{SD}_i} \right)^2 \qquad (4.14)$$

where N=9 is the number of COP-based measures, $COPM_i$ is the mean of the $i^{th}$ COP-based measure from the simulation results, and $\hat{SD}_i$ and $\hat{COPM}_i$ are respectively the standard deviation and mean of the $i^{th}$ COP-based measure from the experimental results. In addition, a genetic algorithm (GA) was implemented to determine the optimal set of model parameters in the optimization procedure.

### 4.2.4 Model simulation and analysis

Figure 4.3 shows the flow of model simulation. Initially, the state equations of the controlled part in the postural control system were determined. Then, the values of the model parameters were randomly set for a simulation trial. Based on the current model parameters, the weighting matrices of the optimal control processor's performance index were determined, and then the corresponding optimal feedback gain was obtained by solving the Reccati equation. This optimal feedback gain was then used to determine the optimal control signal. At this stage, we were able to simulate the kinematics and dynamics during spontaneous sway. Based on the simulation output, the simulated COP-based measures were obtained, and then compared with the experimental COP-based measures. The heuristic approaches were used here to determine whether the cost function was minimized. If so, this simulation trial was stopped, and the current simulation results would be used for further analysis. Otherwise, the GA would aid in

finding another set of model parameters, and the above procedures would be repeated until the cost function was minimized or a stopping criterion was met. In this study, the stopping criterion was the maximum number of generations (iterations) which was set at 50.

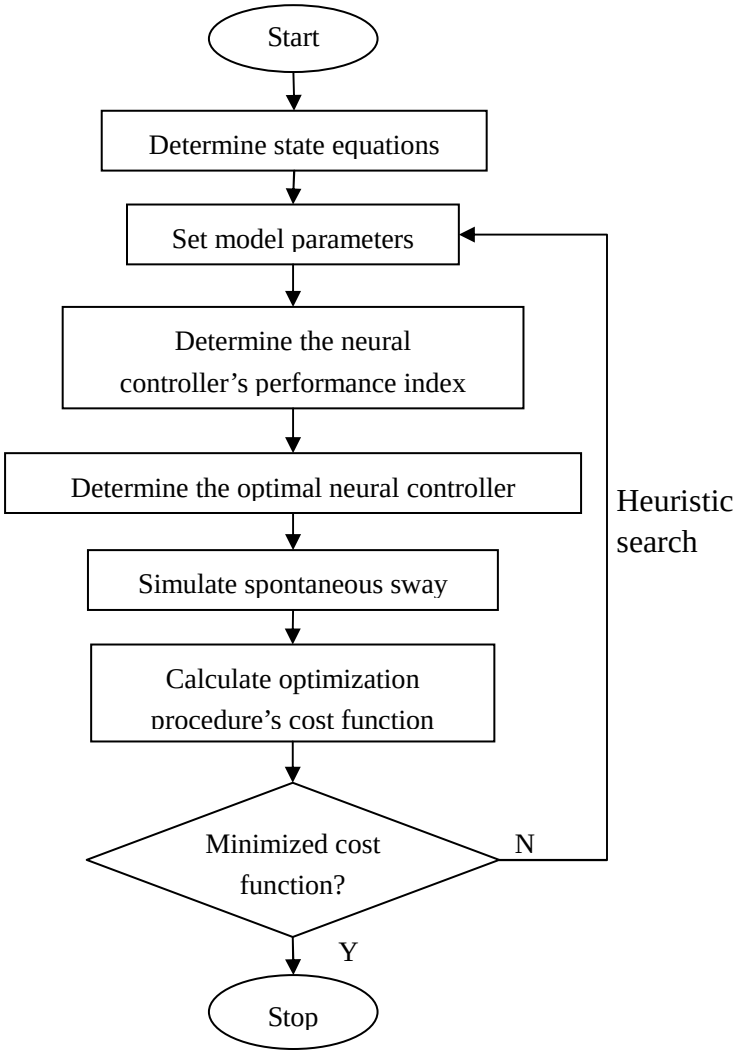


**Figure 4.3 Flow of model simulation.**

In the preliminary study, 32 independent simulations with different initial random disturbance seeds were performed for both younger and older adults. The whole simulation procedure was coded using the Matlab programming language (The MathWorks, Natick, MA), and each simulated sway trial was 40 seconds in duration. After obtaining the simulation

results for all the simulated trials, two-sample *t*-tests were used to identify significant ($P<0.05$) differences in any model parameters between younger and older adults. We also determined linear correlations between model parameters and simulated sway measures.

## 4.3 Results

### 4.3.1 Simulated sway measures

Nearly all the simulated sway measures from the 64 simulation trials were within the one standard deviation ranges of the corresponding experimental data (Fig. 4.4). The only exception occurred in the measure of MFREQ, but it was still very close to the upper bound of the one standard deviation range of the experimental results.

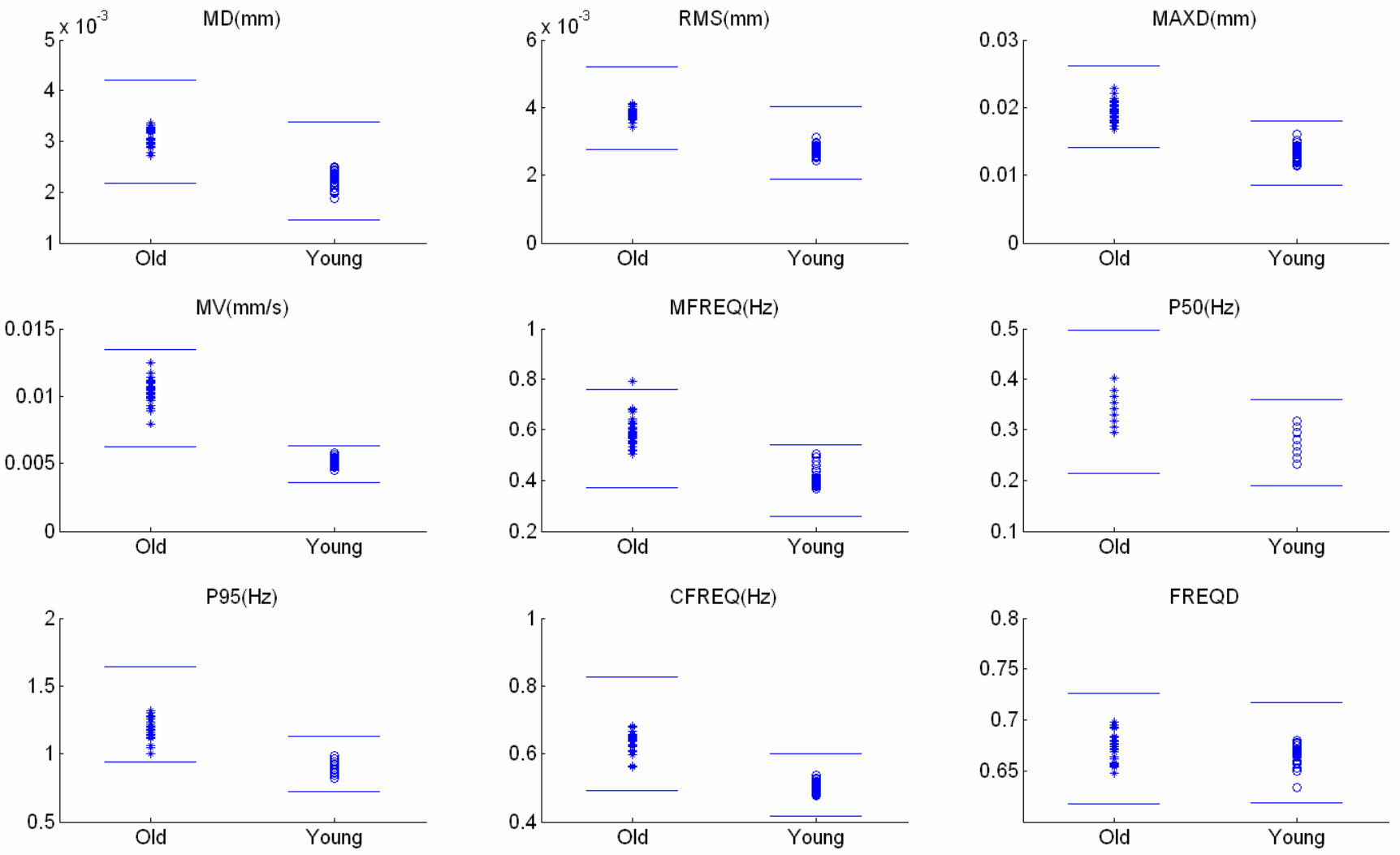


**Figure 4.4 Simulated sway measures obtained from 32 simulation trials of both younger and older adults. Horizontal solid lines represent the one standard deviation ranges of the corresponding experimental data given by Prieto et al. (1996).**

### 4.3.2 Model parameters

Several modeled parameters differed between younger and older adults (Table 4.1). Significant differences were found in the weights of sway angular velocity ($w_2$), ankle torque ($w_3$), ankle torque acceleration ($w_5$), and random disturbance gain ($k_n$). More specifically, $w_2$ and $w_5$ were significantly larger in younger adults, while $w_3$ and $k_n$ were significantly larger in older adults. In addition, some differences in the parameters approached significance, including the weight of sway angular displacement ($w_1$) and sensory time delay ($\tau_d$) which were both larger in the older group.

**Table 4.1 Model parameter means (SD) for younger and older adults (p-values given for age-related differences)**

| | Younger adults | Older adults | p-value |
|---|---|---|---|
| Weight $w_1$ | 0.330 (0.195) | 0.397(0.188) | 0.083 |
| Weight $w_2$ | 0.540 (0.198) | 0.434 (0.177) | <0.05 |
| Weight $w_3$ | 0.072 (0.050) | 0.098(0.063) | <0.05 |
| Weight $w_4$ | 0.053 (0.038) | 0.069 (0.066) | 0.123 |
| Weight $w_5$ | 3.84 (3.00) $\times 10^{-3}$ | 1.96 (2.97) $\times 10^{-3}$ | <0.05 |
| Disturbance gain $k_n$ | 151.8 (23.1) | 356.1 (83.3) | <0.05 |
| sensory delay $\tau_d$ (ms) | 25.6 (18.0) | 33.3 (23.0) | 0.073 |

### 4.3.3 Correlations between the simulated sway measures and some model parameters

Typically, the simulated sway measures were positively correlated with $w_1$, $w_3$, $w_4$, $k_n$, and $\tau_d$, and negatively correlated with $w_2$ and $w_5$ (Table 4.2). Two exceptions were that FREQD was positively correlated with $w_5$, and P95 was uncorrelated ($r=0.003$) with $\tau_d$. Not all of these correlations were significant. For example, although $w_1$ seemed positively correlated with all of the simulated sway measures, none of these correlations was significant. However, most of the sway measures (MAXD, MV, MFREQ, P95, CFREQ) were significantly correlated with $w_2$, $w_3$, $w_5$, and $k_n$. In addition, MD and RMS were significantly correlated with $w_2$, $w_5$, and $k_n$, P50

with $w_5$, $k_n$, and $\tau_d$, and FREQD with $w_4$ and $k_n$.

**Table 4.2 Correlations (r) between simulated sway measures and model parameters**

| | weight $w_1$ | weight $w_2$ | Weight $w_3$ | weight $w_4$ | weight $w_5$ | disturbance gain $k_n$ | sensory delay $\tau_d$ |
|---|---|---|---|---|---|---|---|
| MD | 0.181 | -0.247* | 0.119 | 0.124 | -0.262* | 0.832* | 0.187 |
| RMS | 0.176 | -0.247* | 0.150 | 0.112 | -0.297* | 0.850* | 0.177 |
| MAXD | 0.160 | -0.246* | 0.229* | 0.083 | -0.343* | 0.831* | 0.108 |
| MV | 0.162 | -0.276* | 0.298* | 0.112 | -0.335* | 0.878* | 0.153 |
| MFREQ | 0.124 | -0.267* | 0.409* | 0.099 | -0.355* | 0.812* | 0.109 |
| P50 | 0.112 | -0.150 | 0.074 | 0.073 | -0.259* | 0.679* | 0.265* |
| P95 | 0.133 | -0.227* | 0.257* | 0.083 | -0.328* | 0.906* | -0.003 |
| CFREQ | 0.170 | -0.295* | 0.260* | 0.188 | -0.267* | 0.839* | 0.174 |
| FREQD | 0.056 | -0.203 | 0.197 | 0.312* | 0.0917 | 0.338* | 0.115 |

Correlations noted by * were significant ($p<0.05$).

## 4.4 Discussion

One of the objectives of this study was to develop a balance control model based on an optimal control strategy that could accurately reflect postural sway during quiet upright stance. The simulation results showed that almost all simulated sway measures were completely within a one standard deviation range of the corresponding experimental data. Therefore, the balance control model appears able to simulate realistic COP-based measures of sway.

Since the proposed model was able to simulate realistic COP-based measures, it can be used to identify potential underlying causes of the aging effect on balance control. It is generally accepted that aging adversely affects the accuracy of control signals by increasing sensory noise and elevating sensory thresholds (Ahmed and Ashton-Miller, 2005; Gilsing et al., 1995; Tian et al., 2002). Accuracy of the control signal is influenced in the simulation model by the random disturbance gain ($k_n$). With larger disturbance gains, the accuracy of the control signal decreases. Since the predicted random disturbance gain among older adults was significantly larger than that of younger adults, the proposed model provides a plausible mechanism to explain age-related differences in upright balance control.

Sensory delay has also been generally considered to increase with aging (Ahmed and Ashton-Miller, 2005). From the simulation results, the mean sensory delay time among older adults was larger than that of younger adults, though not significantly ($p = 0.073$). In addition to disturbance gain and sensory delay, other model parameters also showed effects of age (Table 4.1). For example, the weight of ankle torque acceleration ($w_5$) was significantly larger in younger adults, so it might be concluded that ankle torque acceleration plays a more important role in balance control in younger versus older adults.

By examining the correlations between simulated sway measures and model parameters, we found that some model parameters ($w_2$, $w_3$, $w_5$, and $k_n$) may be predictable from more directly observable sway measures. For example, random disturbance gain ($k_n$) was positively (and significantly) correlated with all sway measures. Hence, knowing certain tendencies regarding sway measures, which can be determined experimentally, may aid in estimating the differences in underlying random disturbance magnitudes among different subject groups. In addition, we may also apply these relationships to eliminate redundant factors in the proposed model. For example, changes in the weighting of sway angular displacement ($w_1$) may not substantially affect any sway measures because it showed weak correlations with all of them. Since sway measures are generally used to characterize postural sway, it may not be necessary to consider the role of sway angles when analyzing postural control mechanisms.

Predicted sensory delay, accounting for the time delay in the feedback loop, was ~ 30ms. This time delay could be interpreted as the latency from the instant that mechanoreceptive afferents (e.g. in the foot) are stimulated, until the instant a sensory evoked potential is recorded in the somatosensory area of the brain (Masani et al., 2006). Applegate et al. (1988) reported that this time delay was in the range of 35.4-40.1 ms, which is comparable to our simulation results.

There are clearly other sources of delays, such as the motor command time delay in the postural control system, but these time delays are not in the feedback loop. In order to simplify the model – the more time delays that were introduced to the model, the more states that should be considered when designing the neural controller – we did not model these time delays. Note that errors may still be made in estimating sensory delay primarily due to two factors. First, the genetic algorithm cannot guarantee that exact global optimal solutions are found, so the predicted sensory delay may not be the exact time delay in the feedback loop. Second, the delayed sway angle considered in the model was only an approximation (see Eq. 4.3).

A PID control strategy has been widely used to design the neural controller in balance control models (Iqbal et al., 2004; Johansson et al., 1988; Maurer and Peterka, 2005). In particular, Maurer and Peterka (2005) obtained realistic simulations of COP-based sway measures using such a controller. The major difference between the presented model and that of Maurer and Perterka (2005) is in the control strategy used to define the neural controller. We assumed that the neural controller adopted an optimal control strategy. As a result, the inherent parameters of the two models are different. Since these model parameters are used to explain how the neural controller works, balance control mechanisms are explained from different perspectives. For example, we used weightings of several physical quantities relevant to sway to indicate which of these plays a more important role in balance control. In contrast, Maurer and Peterka (2005) interpreted the effect of active stiffness on balance control.

Kuo (1995, 2005) and van der Kooij et al. (1999) have also successfully applied optimal control theory when constructing balance control models. However, van der Kooij et al. (1999) only took into account the properties of human body dynamics when specifying the optimal feedback in their model. Sensory systems are also an important aspect of the closed loop

portion of the postural control system. In order to optimize the performance of the whole postural control system, properties of sensory systems should be considered by the neural controller. In Kuo's study (1995), the state equations accounted for both body dynamics and sensory properties. However, the system matrices were specified by measuring the feasible acceleration set (FAS). It is not easy to obtain the FAS, since it is derived from many complex factors, e.g musculoskeletal geometry and muscle properties. In contrast to these earlier models, the model presented here derived the controlled state equations (Eq. 4.8) from the transfer functions of human body dynamics and sensory systems, and the neural controller was modeled according to these state equations. In addition, no additional knowledge was necessary when specifying the sensory systems.

A strength of the model presented here is that it was able to accurately simulate sway behaviors. Further, we have presented an approach for determining what to optimize and how to optimize when modeling balance control during spontaneous sway. Modeling the neural controller as an optimal controller stems from a physiological basis, in that it is possible to incorporate physical quantities relevant to sway into the performance index defined in the optimal controller. It is also physiologically plausible that the state $x$ (see Eq. 8) can be fed back to the neural controller to generate the optimal control signal. Specifically, muscle spindles can sense the joint angular displacement and velocity (van der Kooij et al., 1999), and the state variables $T$ and $\dot{T}$ are internal states of the neural controller. At the same time, this model can be used to analyze potential balance control mechanisms for different groups of subjects by simply comparing their model parameters. In addition, this model may aid in predicting human physiological reactions used in maintaining balance, and facilitate evaluating the potential impact of intervention strategies for the improvement of balance.

The model presented here also has some limitations. First, only a few physical quantities that may have effects on spontaneous sway can be incorporated into the performance index. Second, the neural controller may not use an optimal control strategy to generate the motor plans that lead to spontaneous sway, though based on the simulation results, we may say that such a control strategy can at least partly explain the neural controller. Third, the presented model is only applicable for small amplitudes of planar sway motion, given only ankle torques were considered to contribute to maintaining balance (Kuo, 1995). Fourth, this model depends on experimental data to determine the parameters. Note that in the current work, the same anthropometry was assumed for both younger and older adults. This represents a limitation in implementation, though not necessarily in the modeling approach. Fifth, GAs are a heuristic approach and not good at local searching, which may not guarantee that the obtained set of model parameters were globally optimal.

It can also be argued that the real sensory systems are much more complex than is represented in the model, as a time delay, since to maintain upright stance body orientation information from visual, vestibular, and proprioceptive sensory systems should be integrated and fed back to the neural controller (Kuo, 2005; Peterka, 2002). Two reasons motivated our adoption of a simple time delay to represent sensory systems. First, the focus of this study was not on an investigation of the contributions of sensory systems to balance control. Second, it is easy to linearize sensory systems by simply using a time delay representation, so that the Ricatti equation can be used to calculate the optimal feedback gain. Several studies have also used this simplification to model sensory systems and obtained realistic results (Masani et al. 2006; Maurer and Peterka, 2005; Peterka, 2000). However, we admit that modeling sensory systems as a time delay might be too simple especially when the interest is in studying how sensory

systems work during quiet upright stance. Thus, in future research, a balance control model with more complex sensor dynamics should be investigated.

# Chapter 5 Effects of External Loads on Balance Control during Upright Stance: Experimental Results and Model-based Predictions


## Abstract

The purpose of this study was to identify the effects of external loads on balance control during upright stance, and to examine the ability of a new balance control model to predict these effects. External loads were applied to 12 young, healthy participants, and effects on balance control were characterized by center-of-pressure (COP) based measures. Several loading conditions were studied, involving combinations of load mass and height. A balance control model based on an optimal control strategy was used to predict COP time series, with an assumption that a given individual would adopt the same neural optimal control mechanisms under diverse external loading conditions. With the application of external loads, COP mean velocity in the anterior-posterior direction and RMS distance in the medial-lateral direction increased 8.1 and 10.4% respectively. Predicted COP mean velocity and RMS distance in the anterior-posterior direction also increased with external loading, by 11.1 and 2.9%, respectively. Both measured COP data and model-based predictions provided the same general conclusion, that application of larger external loads and loads more superior to the whole body center of mass lead to less effective postural control and perhaps a greater risk of loss of balance or falls. Thus, it can be concluded that the assumption about consistency in control mechanisms was partially supported, and it is the mechanical changes induced by external loads that primarily affect balance control.


## 5.1 Introduction

Falls are one of the most common incidents leading to injuries in daily activities and occupational settings. Fall-related injuries have substantial adverse impacts on functional ability and life quality. Unintentional falls often result from a ‘loss-of-balance’. An improved understanding of balance control may thus aid in understanding and preventing falls. A number of factors have been identified as influencing balance control, such as aging (Mackey and Robinovitch, 2006; Thelen et al., 1996; Vandervoort, 2002), localized muscle fatigue (Gribble and Hertel, 2004; Vuillerme et al., 2006), and decrements in the quality of sensory input (Cornilleau-Peres et al., 2005).

External loads also appear to affect balance control, and many daily and occupational activities require load carriage (e.g. military marches, Schiffman et al., 2006). Hence, further

investigation of how and why balance control is affected by external loads is warranted. Previous studies have suggested that external loads adversely affect balance control, since such loads resulted in increased postural sway during quiet erect stance (Chow et al., 2006; Ledin and Odkvist, 1993; Kincl et al., 2002; Schiffman et al., 2006). Increased postural sway indicates that the whole-body center-of-mass (COM) gets closer to the limits of the base of support (BOS) and thus leads to less stability. Existing studies of external loads, however, have been somewhat narrowly focused on the effects of external load mass on balance control. The location of any external loads would also seem relevant; while this has been investigated with respect to energy costs (Knapik et al., 1996), we are unaware of any evidence regarding whether load location affects balance control.

In addition to experimental studies, balance control models have been widely used to facilitate an understanding of underlying balance control mechanisms. For example, Ishida et al. (1997) adopted a balance control model to identify the roles of different sensory systems, and Maurer and Peterka (2005) applied a model based on a PID (proportional, integrative, and derivative) neural controller to examine the effects of aging on balance control. Validation of such mathematical models is often challenging. For example, some studies (Maurer and Peterka, 2005; Peterka, 2000) have examined whether balance control models could accurately simulate experimental center-of-pressure (COP) based measures, and Winter et al. (1998) compared simulated and measured relationships between sway amplitude and effective stiffness of balance control.

We recently presented a balance control model based on an optimal control strategy to simulate spontaneous sway behaviors, and used this model to identify aging effects on balance control (Qu et al., 2007). Our model was shown to generate reasonable simulations of measures

derived from COP time series. One can argue that a stronger test involves determining whether this (or related) model can make predictions of sway or COP behaviors under novel circumstances. In the current context, these circumstances are different configurations of an external load during quiet upright stance.

The primary purpose of this study was to determine whether, or to what extent, our optimal control model could predict changes in balance control behaviors under novel conditions. Such 'predictive ability' was assessed using a scenario involving application of external loads during quiet upright stance. This scenario was chosen since changes in mechanics due to loading could be estimated in a straightforward manner (see Methods). A secondary purpose was to determine the actual effects of external loads on balance control, and specifically the influences of load mass and height, by using the data obtained while participants were loaded. We hypothesized that increasing mass and/or height would challenge balance control, based on expected mechanical effects for an analogous inverted pendulum (as is frequently used to model upright stance). The effects of external loads on balance control were identified by COP-based measures, since the COP reflects the net motor control signal output necessary to keep the projection of the center-of-mass (COM) within the BOS (Cavanaugh et al., 2005; Prieto et al., 1993).

## 5.2 Methods

### 5.2.1 Participants and experimental procedures

Twelve participants (five female and seven male) were involved, with mean (SD) age = 29(6) years, stature = 169.4(11.2) cm, and body mass = 61.9(10.6) kg. None had any current or recent self-reported injuries, illness, or musculoskeletal disorders. All participants completed

an informed consent procedure approved by the Virginia Tech Institutional Review Board.

Each participant performed 15 trials involving quiet upright stance. In each trial, participants stood barefoot on a force platform (AMTI OR6-7-1000, Watertown, MA, USA), with eyes closed and arms at sides, and were requested to stand as still as possible. Trials lasted 90 seconds, with at least two minutes of rest between each. Triaxial ground reaction forces and moments were sampled at 60Hz, low-pass filtered (Butterworth filter, second order, 5Hz cutoff), and used to derive COP time series. The initial 20 and last 10 seconds of each time series were discarded.

Effects of external loads were investigated by manipulating two aspects of the load, specifically the mass and height. This was achieved using two load packs, placed dorsally and ventrally (Fig. 5.1). Total load mass was set to 0 (no packs), 10, and 20% of individual body mass, by inserting small metal cylinders into several pockets in the packs. These cylinders were placed symmetrically, to the extent possible, with respect to the frontal and sagittal planes. Load packs were placed at one of two heights, such that the COM of the external load was at height equal to the whole-body COM (= 58.8% of stature, Robertson et al., 2004), or at 15% of stature above the whole-body COM. These are referred to as ‘low’ and ‘high’ conditions, respectively. Since the no-load condition was identical for both heights, there were five combinations of external load mass and height examined. After an initial familiarization period, participants performed three trials in each combination, with the order of combinations randomized to minimize confounding related to learning effects.

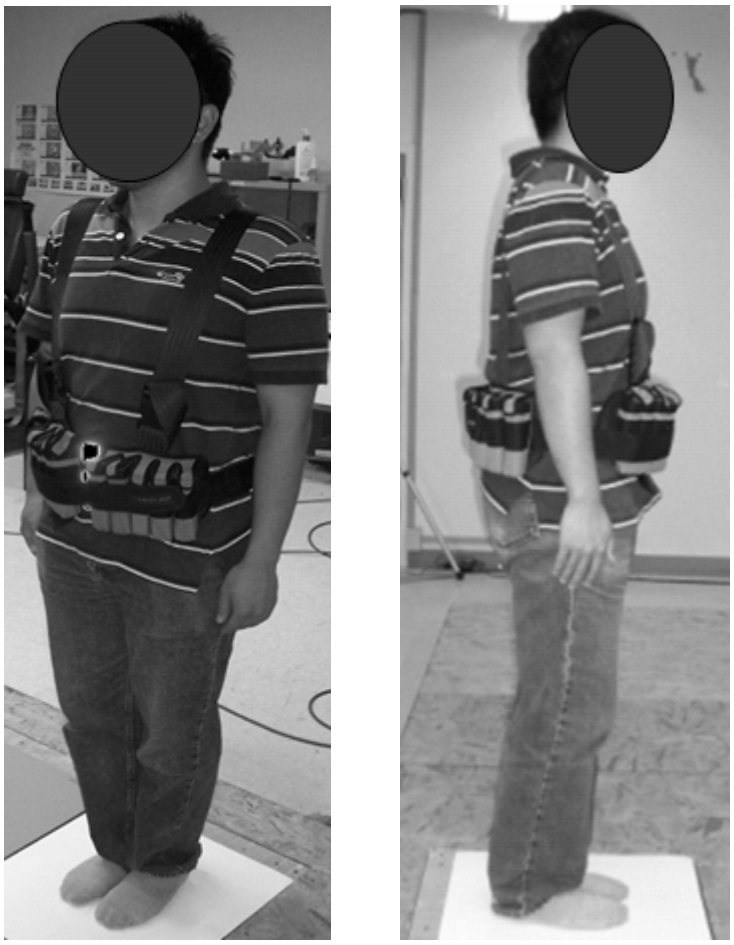

(a) (b)

**Figure 5.1 Participant wearing two load packs (load height equal to whole-body COM).**

### 5.2.2 Model description

Our existing balance control model (Qu et al., 2007) was used to predict the effects of external loads under the conditions described above. In this model, the human body is represented as a simple single-segment inverted pendulum during quiet upright stance, and the neural controller was assumed to be an optimal controller. The optimal neural controller is defined by optimal feedback gains, which are calculated by solving the Riccati equation, and generates ankle control torques by minimizing a certain performance criterion. This performance criterion was defined by several physical quantities relevant to sway, including delayed sway angle and ankle control torque. Several model parameters, such as the weightings

of relevant physical quantities, random disturbance gain, and sensory delay time, cannot be specified *a priori*. To determine the values of these unspecified model parameters, an optimization procedure was used with an objective defined as the scalar error between experimental and simulated COP-based measures. Specific terms in the scalar error were: mean distance (MD), root mean square distance (RMS), maximum distance (MAXD), mean velocity (MV), mean frequency (MFREQ), 50% power frequency (P50), 95% power frequency (P95), centroidal frequency (CFREQ), and frequency dispersion (FREQD). According to our earlier simulation results, this model was able to simulate COP-based measures, and helped to identify potential age-related changes in balance control.

### 5.2.3 Model-based predictions

Model-based predictions involved four sequential steps. First, several anthropometric measures were required: moment of inertia of the body about the ankle ($I$), body mass ($M$), height of whole-body COM ($h$), mass of the feet ($m_F$), height of the ankle ($h_F$), and anterior-posterior (A/P) distance between the ankle and the COM of the feet ($d_F$). Several measures were obtained directly from each participant prior to the experimental trials: $M$, stature ($l$) and foot length ($l_F$). The remaining measures were estimated from existing equations (Chaffin et al., 1999; Der Leva, 1996; Robertson et al., 2004) as follows:

$$\begin{cases} I = M \times l^2 \times [0.3^2 + (0.588 - 0.039)^2]; \\ h = l \times (0.588 - 0.039); \\ m_F = M \times 0.0137 \times 2(male) \quad or \quad m_F = M \times 0.0129 \times 2(female); \\ h_F = l \times 0.039; \\ d_F = l_F \times 0.4415(male) \quad or \quad d_F = l_F \times 0.4014(female). \end{cases} \tag{5.1}$$

Second, unspecified parameters in the model were determined. Using procedures described in Qu, et al. (2007), COP-based measures from the no-load trials were used to

determine these parameters for each participant.

Third, prior to using the model to predict the effects of external loads, anthropometric descriptors in the model were adjusted to account for the loads, using:

$$\begin{cases} M' = M + \Delta M \\ I' = I + \Delta M \times (h + \Delta h)^2 \\ h' = \dfrac{M \times h + \Delta M \times (h + \Delta h)}{M + \Delta M} \end{cases} \tag{5.2}$$

where $M'$, $I'$, and $h'$ are the adjusted values, $\Delta M$ is the external load mass, and $\Delta h$ is the external load height relative to whole-body COM. In the conditions with an external load, the five weights defined in the neural optimal controller, and the sensory time delay, were held at the values determined from the no-load trials. This was based on an assumption that a given individual would adopt the same neural optimal control mechanisms under diverse external loading conditions. In contrast, changes involving the application of external loads should affect external random disturbances, and we adjusted the random disturbance gain so that the ratio between the random disturbance gain and total mass (body+external loads) was held constant.

Fourth, the now fully-specified model was used to simulate sway behaviors under the four loaded conditions (see Qu et al., 2007 for a description of such simulation). Three sway trials with different initial random disturbance seeds were simulated for each loaded condition and each simulation trial was 90 seconds in duration (initial 20 and last 10 seconds removed). From the simulated COP time series, several measures were derived as described below. Note that the model employed is two-dimensional (sagittal plane), hence predicted COP measures are A/P only.

### 5.2.4 Dependent measures

Prieto et al. (1996) systematically presented a set of COP-based measures, which in general can be classified into two groups: time-domain and frequency-domain. A number of measures in both groups have been used in investigations of balance control (McClenaghan et al., 1996; Corbeil et al., 2003). However, these measures do not account for dynamic characteristics of COP time series (Norris et al., 2005), for which measures derived from statistical mechanics have been proposed (Collins and DeLuca, 1993; Delignieres et al., 2003; Duarte and Zatsiorsky, 2000). According to the classification of COP-based measures mentioned above, several measures were derived from the experimental and simulated COP time series, and used as dependent measures to characterize the effects of external loads on balance control. Most time-domain measures, including RMS, MD, and MAXD, appear to be highly correlated (Prieto et al., 1996). Among time-domain measures, MV has been found to be the most reliable (Lin et al., 2006). Thus, among time-domain measures, we chose RMS and MV for analysis. The selected frequency domain measures were CFREQ and FREQD, with CFREQ reflecting central frequency tendency and FREQD the variability in frequency content. Among potential statistical mechanics approaches, one considering the trajectory of the COP as fractional Brownian motion (fBm) appears most relevant and has been widely used when analyzing upright postural control (Genthon and Rougier, 2006; Meyer et al., 2004; Riley et al., 1998; Rougier, 1999a, 1999b). Thus, four statistical mechanics measures (Rougier, 1999a) derived from the fBm model were chosen (TT: transition time; TA: transition amplitude; $H_S$: short-term scaling exponent; $H_L$: long-term scaling exponent). Note that both TT and TA were defined by the transition point in the fBm model. Descriptions and units of dependent measures are given in Table 1.

**Table 5.1 Glossary of COP-based dependent measures**

| Acronym | Description | Unit |
|---|---|---|
| RMS | Root mean square distance | mm |
| MV | Mean velocity | mm/s |
| CFREQ | Centroidal frequency | Hz |
| FREQD | Frequency dispersion | -- |
| TT | Transition time | s |
| TA | Transition amplitude | $mm^2$ |
| $H_S$ | Short-term scaling exponent | -- |
| $H_L$ | Long-term scaling exponent | -- |

### 5.2.5 Analysis

In order to compare sway behaviors across individuals, COP-based measures from the loaded conditions were normalized by the corresponding average measures in the no-load condition. External load mass and load height, each at two levels, served as the two independent variables in subsequent analyses. Two-way analysis of variance (ANOVA) was performed to identify the effects of load mass and height on the normalized experimental COP-based measures. To compare loaded vs. unloaded conditions, the normalized experimental COP-based measures under loaded conditions were compared with a value of unity using t-tests. The same statistical analyses were also performed for the model-predicted COP-based measures. Significant effects were concluded when $p < 0.05$. Model-based prediction and experimental results were compared qualitatively, based on trends in COP-based measures versus external loads. A/P $H_L$ and medial-lateral (M/L) $H_L$ data from one participant were removed from these analyses, as they were more than 2.5 times the interquartile range away from the upper or lower quartile of the data, and thus considered outliers (McGill et al., 1978).

## 5.3 Results

Application of external loads led to significant changes in several COP-based measures (Table 5.3). Specifically, there were significant increases in A/P MV, A/P TA, M/L RMS, M/L

TT, and M/L TA, and a significant decrease in M/L $H_S$, at both levels of external load mass. Several measures significantly decreased only at the higher load mass: A/P FREQD, M/L CFREQ, and M/L $H_L$. When external load mass changed from 10% to 20% of body mass, significant changes occurred in A/P MV, A/P TA, M/L FREQD, and M/L TA. In addition to these significant effects, there were two trends apparent, including an increase in A/P RMS at the higher load mass ($p$=0.074), and a decrease in A/P FREQD at the lower load mass ($p$=0.069).

Three A/P measures and one M/L measure were significantly affected by external load height (Table 5.3). Specifically, A/P RMS and M/L MV became significantly larger, and A/P CFREQ and A/P $H_S$ became significantly smaller when the external load was raised above the COM. There were also two apparent trends in A/P TT ($p$=0.077) and M/L RMS ($p$=0.089), both of which increased at the higher load level. A significant mass×height interaction effect was found only for M/L MV. When external load mass changed from 10% to 20% of body mass, M/L MV decreased at the lower load level (from 0.974 to 0.952), but increased at the higher load level (from 0.992 to 1.068).

**Table 5.2 COP-based measures means (SD) under the no load condition**

| | | RMS | MV | CFREQ | FREQD | TT | TA | $H_S$ | $H_L$ |
|---|---|---|---|---|---|---|---|---|---|
| Experimental | A/P | 5.31(2.26) | 7.64(2.29) | 0.468(0.116) | 0.890(0.068) | 0.651(0.244) | 14.3(7.0) | 0.788(0.036) | 0.156(0.101) |
| | M/L | 5.21(2.07) | 9.30(3.00) | 0.512(0.139) | 0.842(0.065) | 0.638(0.407) | 24.0(3.1) | 0.785(0.065) | 0.117(0.108) |
| Predicted | A/P | 4.56(1.77) | 7.46(2.18) | 0.498(0.086) | 0.915(0.041) | 0.766(0.166) | 13.3(7.7) | 0.746(0.034) | 0.164(0.093) |

**Table 5.3 Normalized experimental COP-based measure means (SD)**

| | | External loads = 10% body mass | External loads = 20% body mass | Low external load level | High external load level | p-value | | | |
|---|---|---|---|---|---|---|---|---|---|
| | | | | | | 10% vs 20% | 10% vs 0% | 20% vs 0% | Low vs high |
| A/P | RMS | 1.03(0.28) | 1.05(0.30) | 0.98(0.24) | 1.10(0.32) | 0.65 | 0.19 | 0.074 | 0.013* |
| | MV | 1.05(0.14) | 1.11(0.14) | 1.07(0.15) | 1.09(0.13) | 0.009* | 0.001* | <0.001* | 0.49 |
| | CFREQ | 0.97(0.29) | 1.02(0.32) | 1.05(0.32) | 0.94(0.27) | 0.26 | 0.16 | 0.27 | 0.040* |
| | FREQD | 0.99(0.08) | 0.98(0.09) | 0.98(0.09) | 0.99(0.08) | 0.63 | 0.069 | 0.022* | 0.39 |
| | TT | 1.05(0.32) | 1.04(0.30) | 1.00(0.29) | 1.09(0.33) | 0.92 | 0.11 | 0.12 | 0.077 |
| | TA | 1.21(0.46) | 1.41(0.61) | 1.24(0.54) | 1.38(0.54) | 0.031* | <0.001* | <0.001* | 0.11 |
| | $H_S$ | 1.00(0.05) | 1.01(0.05) | 1.01(0.05) | 0.99(0.04) | 0.37 | 0.48 | 0.11 | 0.008* |
| | $H_L$ | 1.05(0.62) | 1.02(0.61) | 1.01(0.59) | 1.05(0.64) | 0.59 | 0.28 | 0.42 | 0.50 |
| M/L | RMS | 1.09(0.27) | 1.12(0.26) | 1.07(0.21) | 1.14(0.31) | 0.43 | 0.005* | <0.001* | 0.089 |
| | MV | 0.98(0.15) | 1.01(0.16) | 0.96(0.13) | 1.03(0.17) | 0.27 | 0.16 | 0.29 | 0.007* |
| | CFREQ | 0.97(0.24) | 0.91(0.24) | 0.93(0.26) | 0.94(0.23) | 0.13 | 0.14 | <0.001* | 0.73 |
| | FREQD | 1.03(0.07) | 1.00(0.08) | 1.01(0.06) | 1.02(0.08) | 0.040* | <0.001* | 0.39 | 0.60 |
| | TT | 1.19(0.81) | 1.28(0.72) | 1.24(0.81) | 1.22(0.72) | 0.48 | 0.026* | <0.001* | 0.87 |
| | TA | 1.14(0.70) | 1.44(0.86) | 1.20(0.74) | 1.38(0.85) | 0.028* | 0.043* | <0.001* | 0.17 |
| | $H_S$ | 0.980(0.08) | 0.98(0.08) | 0.99(0.08) | 0.98(0.08) | 0.77 | 0.013* | 0.031* | 0.40 |
| | $H_L$ | 1.02(0.81) | 0.82(0.88) | 0.84(0.75) | 1.00(0.93) | 0.17 | 0.42 | 0.048* | 0.30 |

* indicates p-value<0.05

Except for A/P $H_L$, all remaining predicted measures were significantly affected by both levels of external load mass (Table 5.4). A/P RMS, A/P MV, A/P TT and A/P TA increased, while A/P CFREQ, A/P FREQD, and A/P $H_S$ decreased, with the application of external loads. A significant increase in A/P $H_L$ was also found with the higher load mass. None of the predicted measures was significantly affected by external load height (Table 5.4), however changes in A/P RMS ($p$=0.053) and A/P CFREQ ($p$=0.058) approached significance. There were no significant mass × height interaction effects on any predicted measures.

**Table 5.4 Normalized predicted COP-based measure means (SD)**

| | | External loads = 10% body mass | External loads = 20% body mass | Low external load level | High external load level | p-value | | | |
|---|---|---|---|---|---|---|---|---|---|
| | | | | | | 10% vs 20% | 10% vs 0% | 20% vs 0% | Low vs high |
| A/P | RMS | 1.09(0.14) | 1.13(0.19) | 1.08(0.14) | 1.14(0.19) | 0.21 | <0.001* | <0.001* | 0.053 |
| | MV | 1.02(0.04) | 1.03(0.05) | 1.03(0.05) | 1.02(0.05) | 0.15 | <0.001* | <0.001* | 0.27 |
| | CFREQ | 0.87(0.19) | 0.86(0.20) | 0.89(0.19) | 0.83(0.19) | 0.73 | <0.001* | <0.001* | 0.058 |
| | FREQD | 0.99(0.04) | 0.99(0.03) | 0.98(0.04) | 0.99(0.04) | 0.86 | 0.002* | <0.001* | 0.47 |
| | TT | 1.31(0.40) | 1.42(0.69) | 1.36(0.54) | 1.36(0.59) | 0.24 | <0.001* | <0.001* | 0.94 |
| | TA | 1.37(0.55) | 1.60(0.97) | 1.47(0.87) | 1.50(0.71) | 0.086 | <0.001* | <0.001* | 0.83 |
| | $H_S$ | 0.97(0.06) | 0.97(0.06) | 0.96(0.06) | 0.97(0.06) | 0.91 | <0.001* | <0.001* | 0.68 |
| | $H_L$ | 1.13(0.71) | 1.24(0.84) | 1.09(0.86) | 1.29(0.67) | 0.40 | 0.058 | 0.008* | 0.12 |

* indicates p-value<0.05

Trends in the measured and predicted dependent measures versus external loads are illustrated in Figure 5.2. Most of the simulated trends were consistent with experimental findings. However, qualitative discrepancies between experimental and simulation results were found in the effects of load mass for A/P CFREQ, A/P TT, and A/P $H_L$, and in the effects of load height for A/P MV, A/P TT, and A/P $H_S$.

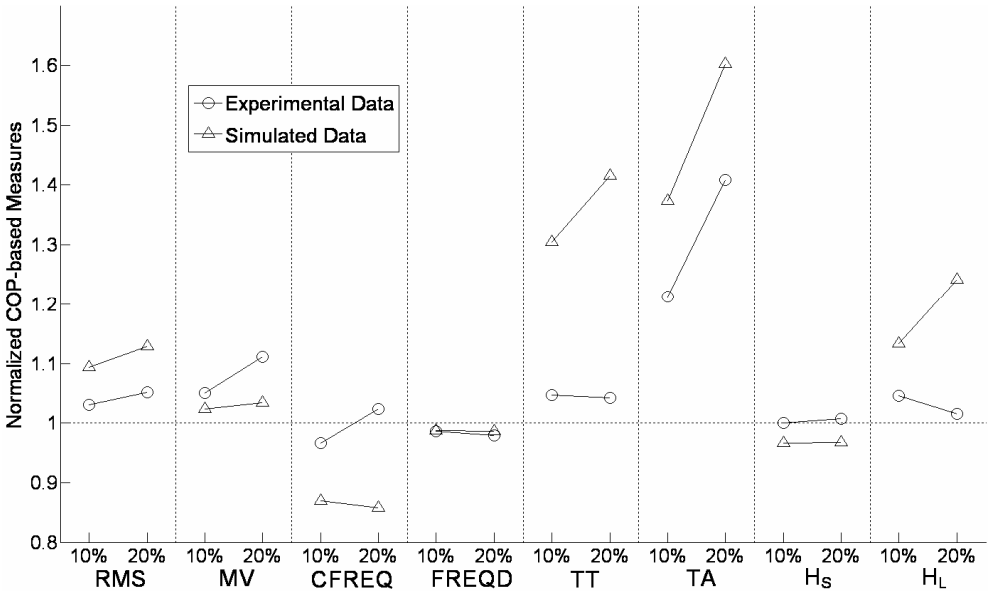


(a)

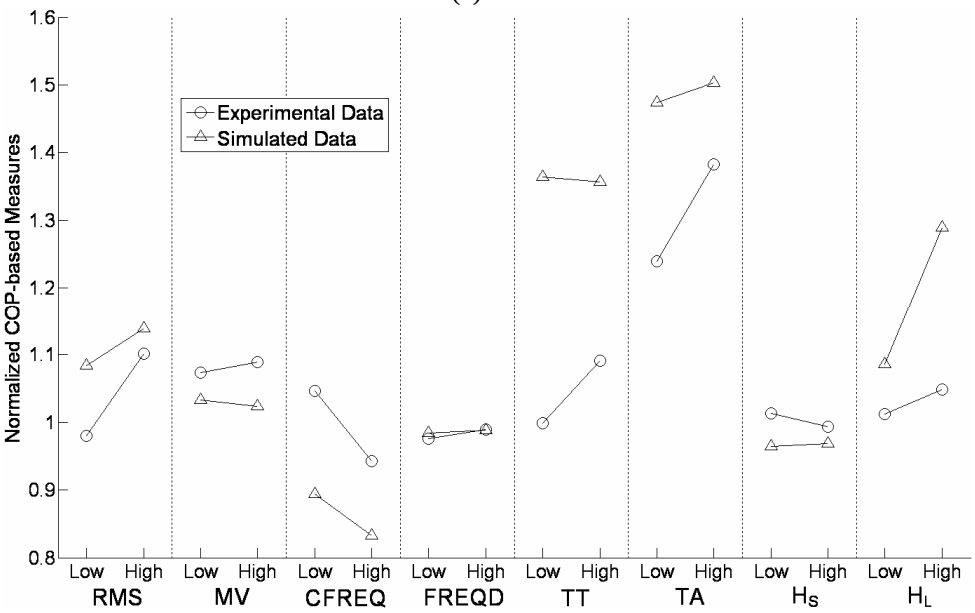


(b)

**Figure 5.2 (a) Average trends in experimental and simulated A/P COP-based measures versus external load mass. (b) Average trends in experimental and simulated A/P COP-based measures versus external load height.**

## 5.4 Discussion

One purpose of this study was to identify whether balance control (as assessed indirectly using COP) was influenced by different external loading conditions. With the application of external loads, A/P MV and M/L RMS both increased (Table 5.3 and Fig. 5.2 (a)). These

findings are consistent with previous studies (Punakallio et al., 2003; Schiffman et al., 2006), in which time-domain measures were shown to increase when carrying external loads. The present results also showed that RMS and MV, in both the A/P and M/L directions, tended to increase at the higher load level (Table 5.3 and Fig. 5.2 (b)). Since the COP is always in phase with the COM (Cavanaugh et al., 2005; Prieto et al., 1993), increases in these time-domain measures indicate that the COM more closely approached the boundary of the BOS with increasing load mass or load height. Thus, it can be inferred that there is a greater likelihood of fall-related incidents with heavier or higher external loads. Our initial hypothesis was also confirmed, that increasing mass and/or height would challenge balance control.

A/P CFREQ decreased when the load was moved above the COM, whereas M/L CFREQ decreased at the higher level of external load mass (e.g. 20% of body mass). A decrease in CFREQ indicates an increase in amplitude of lower frequency components. A/P and M/L stabilities are primarily maintained through muscular adjustments at the ankle and at the hip, respectively (Winter et al., 1996). Thus, changes in frequency content of ankle control forces and hip control forces may have led to the observed changes in A/P CFREQ and M/L CFREQ, respectively. Another explanation for the changes in A/P CFREQ and M/L CFREQ is that increased load mass and load height increase the moment of inertia of the body which results in the decrease in the natural frequency of the body. In addition, it can be surmised that variability in the frequency content of ankle control forces decreased when external load mass increased since there was an inverse relationship found between A/P FREQD and load mass.

Analysis of COP time series using an fBm model reveals two types of behavior (Rougier, 1999a). Specifically, over short term intervals, past and future displacements are positively correlated (persistent behavior and $H_S>0.5$), while over long term intervals, these displacements

are negatively correlated (anti-persistent behavior and $H_L$<0.5). In general, larger $H_S$ indicates more persistent postural control, whereas larger $H_L$ corresponds to less anti-persistent behaviors (Norris et al., 2005). The intersection of the short-term and long-term regions is the transition point whose coordinate is [TT, TA]. Hence, TT indicates the duration of persistent behaviors, while TA is the measure used to quantify the amplitude of sway movement over short term intervals.

As external load mass increased (i.e. from 0 -20% of body mass), both A/P TA and M/L TA increased. Hence, sway movement in either the A/P or M/L directions led to postures further from upright equilibrium, suggesting an increase in short-term instability. External loads also led to more persistent behaviors over a longer duration in the M/L direction, as indicated by increases in M/L $H_S$ and M/L TT in the loaded conditions, respectively. Persistent sway behaviors cause movements away from upright equilibrium (Collins and DeLuca, 1993). Thus, it might be further concluded that M/L balance control deteriorated over short-term intervals with the application of external loads.

In contrast, M/L $H_L$ decreased at the higher load mass, indicating more anti-persistent behaviors. In other words, in the presence of external loading M/L sway movement was more likely to return to upright equilibrium, and to be less random over long-term intervals. Thus, M/L balance control might be improved over long term intervals with heavier external loads. A possible explanation for these findings is that after experiencing decreased stability over short term intervals, humans may have the ability to adjust their balance control so as to improve stability over long term intervals. Thus, it can be hypothesized that the changes of M/L $H_L$ represent an adaptation of the postural control system to the decreased stability imposed by applied external loads.

Increasing external load height caused A/P postural sway to be less persistent or more random in the short-term (i.e. a decrease in A/P $H_S$). Contrasting this, A/P TT exhibited an increasing trend with external load height, suggesting that A/P persistent behaviors occurred over a longer duration. Given these contrasting results, it is unclear how A/P balance control was affected by load height over short-term intervals on the basis of these statistical mechanics measures.

It is important to note that a quantitative correspondence between measured and predicted outcomes was not expected in this study, mainly due to two factors. First, intra-individual differences in performance exist, and only three trials were conducted by each participant under a specific loading condition. Second, our model has some limitations that might induce errors. For example, the body was described simply as a single-segment inverted pendulum and only a limited set of physical quantities relevant to sway were considered in the model of optimal neural control. Thus, when evaluating the model performance, we sought only to determine whether the model could qualitatively reflect the observed trends in the COP-based measures as external loading conditions changed, and such trends were considered sufficient to reflect how the postural control strategies are adjusted according to different external loads. At the same time, even though the neural controller was assumed to be an optimal controller, the predicted postural sway should change with diverse loading conditions since external loads affect human body dynamics in the postural control system (Qu et al., 2007).

The model duplicated most of the significant effects of external load mass (and apparent trends) on the observed A/P COP-based measures, though more predicted measures were found to be significantly affected (see Table 5.3 and Table 5.4). In general, the predicted results indicated that heavier external loads challenged balance control, with A/P RMS, A/P MV, A/P TT

and A/P TA all predicted to increase with the application of external loads. In addition, when external load height increased, an increase in predicted A/P RMS ($p$=0.053) and a decrease in predicted A/P CFREQ ($p$=0.058) were evident as trends, and these trends were consistent with experimental findings. Since the predicted A/P RMS increased with an increase in external load height, we might predict that increasing height would challenge balance control as well as load mass. Similar to the measured data, the predicted results generally supported the initial hypothesis regarding the effects of external load mass and height. In other words, if the measured data were unavailable, model-based prediction would lead to the same general conclusion as did the empirical data. At the same time, as noted earlier, given the average trends in the dependent measures versus external loads (Fig. 5.2), our simulation results also matched most of the experimental findings. Hence, it might be concluded that although some discrepancies existed between the experimental and predicted results, our model was still able to provide some useful information on how balance control was affected by external loads.

Some limitations in this study should be noted. First, learning effects may have been present. However, since practice was provided before data collection, and the order of the different loading conditions randomly presented, these effects are thought unlikely to have substantially influenced the experimental findings. Second, the sample size (N=12) may have been insufficient to detect effects of external loading on some measures. Third, males and females are different in many aspects, for example, their anthropometric estimates (Eq. 1) are different. Hence, the application of external loads may lead to different responses between genders. Future work is warranted to determine if such differences are important. Fourth, some anthropometric measures and the body COM were estimated, and thereby served as a source of errors in the model-based prediction. Such errors should not be critical, though, since

effects of external loading were determined within-subjects.

Perhaps a more critical limitation is that we do not have direct evidence to support the two primary assumptions we made in this study. Specifically, the first assumption was that the same neural optimal control mechanisms would be employed under diverse conditions of external loading, based on which the model parameters defined in the neural optimal controller were held at the values determined from the no-load trials. The second was that external loads adversely affected the accuracy of control signals, and we implemented this by linearly increasing the random disturbance gain. During model simulations, only mechanical changes with external loads were taken into account. Due to the existence of discrepancies between the experimental and predicted results, these assumptions were not strongly supported. However, the predicted results did confirm the hypothesis that increasing mass and/or height would challenge balance control, and were consistent with the experimental findings. Hence, while there may be changes in neural optimal control mechanisms, and random disturbance gain may not change linearly with external loads, it is the mechanical changes induced by external loads that appear to primarily affect balance control.

Since a loss-of-balance often leads to unintentional falls, investigating effects on balance control caused by external loads may aid in better understanding and preventing fall-related injuries, especially for those occupational and daily activities involving load carriage. Results presented in this study were used to explain how balance control was adjusted according to the application of external loads and can provide a basis for developing intervention strategies for the improvement of balance. In addition, this study may also be used to investigate obesity effects on balance control.

# Chapter 6 An Investigation of Balance Control Mechanisms during Quiet Upright Stance using Alternative Balance Control Model Structures


## Abstract

Four two-dimensional balance control model structures were developed, based on alternative contemporary balance control theories. Specifically, the four models were derived from two assumptions regarding noise sources in postural control (i.e. afferent (sensory) vs. efferent (joint torque) noise) and whether or not passive control torques (stiffness and damping) were included. Model parameters were specified using experimental center-of-pressure (COP) data obtained during upright stance, and comparisons then made between simulated and actual COP-based measures. COP was simulated more accurately using models which assumed joint torque as the primary source of sway behaviors. Simulated active control torques were typically over seven times larger than passive, though some exceptions were found. These results suggest that sensory noise plays a relatively small role in driving body sway, and that active control torque is dominant in maintaining upright balance.


## 6.1 Introduction

Quiet upright stance is not perfectly quiet, given the existence of internal perturbations such as heart rate and muscle tremor (van der Kooij et al., 1999). Internal perturbations can be considered as noise in the postural control system, and internal control must be generated by the neural controller to counteract such noise and control upright posture. Different sources of noise in postural control have been assumed and/or adopted in the development of balance control models. Some studies have modeled this noise as existing in the efferent pathways, typically as random disturbance torques acting on joints (Maurer and Peterka, 2005; Peterka, 2000; Masani et al., 2006), whereas some others have indicated that such noise exists in the afferent pathways, specifically at sensory organs (Ahmed and Ashton-Miller, 2005; van der Kooij et al., 2001).

The relative roles or importance of active and passive control torques in the control of upright posture has also been an object of discussion and controversy. Active control torques

are generated by active muscle contraction regulated by the neural controller. In contrast, passive control torques are considered to stem from intrinsic tissue mechanical properties (i.e. stiffness or viscosity). Some authors have argued that upright posture is primarily controlled by active control torques (Morasso et al., 1999; Loram and Lakie, 2002; Lakie et al., 2003). However, Winter et al. (1998, 2001, and 2003) and Gage et al. (2004) suggested that passive control torques must play an important role in balance control.

According to different balance control theories mentioned above, four different two-dimensional balance control model structures are presented in this chapter. These balance control models are all based on an optimal control strategy, and model development and implementation followed the description provided earlier (Chapter 4). The objectives of this study were to evaluate the performance of these different model structures, and to determine which structure could best simulate spontaneous sway. Results were also used to make inferences regarding balance control mechanisms, specifically the degree to which afferent vs. efferent noise are involved in generating sway and whether or not passive control plays an important role in the control of upright posture.

## 6.2 Methods

In the balance control models presented here, the neural controller is assumed to be an optimal controller that can minimize a certain performance index defined by physical quantities relevant to sway. Human body dynamics are represented by a single-segment inverted pendulum model, and sensory systems are assumed to be able to provide accurate body orientation information to the neural controller but with a certain time delay. Experimental data are needed to specify model parameters, such as sensory delay time, and this specification is accomplished using an optimization procedure which adopted heuristic search approaches.

Several anthropometric measures were required when using these models, details on which were given in section 5.2.3. These model structures differed in either the sources of noise in postural control or active/passive control patterns. Cost functions in the optimization procedure, 95% confidence intervals of normalized simulated traditional center-of-pressure (COP) based measures, and a scalar error between simulated and experimental statistical mechanics COP-based measures were compared across model structures to evaluate their simulation performances.

### 6.2.1 Alternative model structures

Four alternative model structures were developed, as combinations of source of noise in postural control and active/passive control pattern (Fig 6.1). In the figure, TN, SN, NP and PA indicated joint torque noise, sensory noise, no passive control, and passive control, respectively. Only one noise source (either joint torque noise or sensory noise) was chosen in each model structure, and the noise was modeled as white noise. Specifically, the TN-NP model structure and TN-PA model structure adopted joint torque noise, whereas the SN-NP model structure and SN-PA model structure used sensory noise to drive sway motions. In addition, the TN-NP model structure and SN-NP model structure did not take the passive control torque into account. However, both passive stiffness and passive damping components were included in the TN-PA model structure and SN-PA model structure. Note that the TN-NP structure is identical to that used initially (Chapter 4).

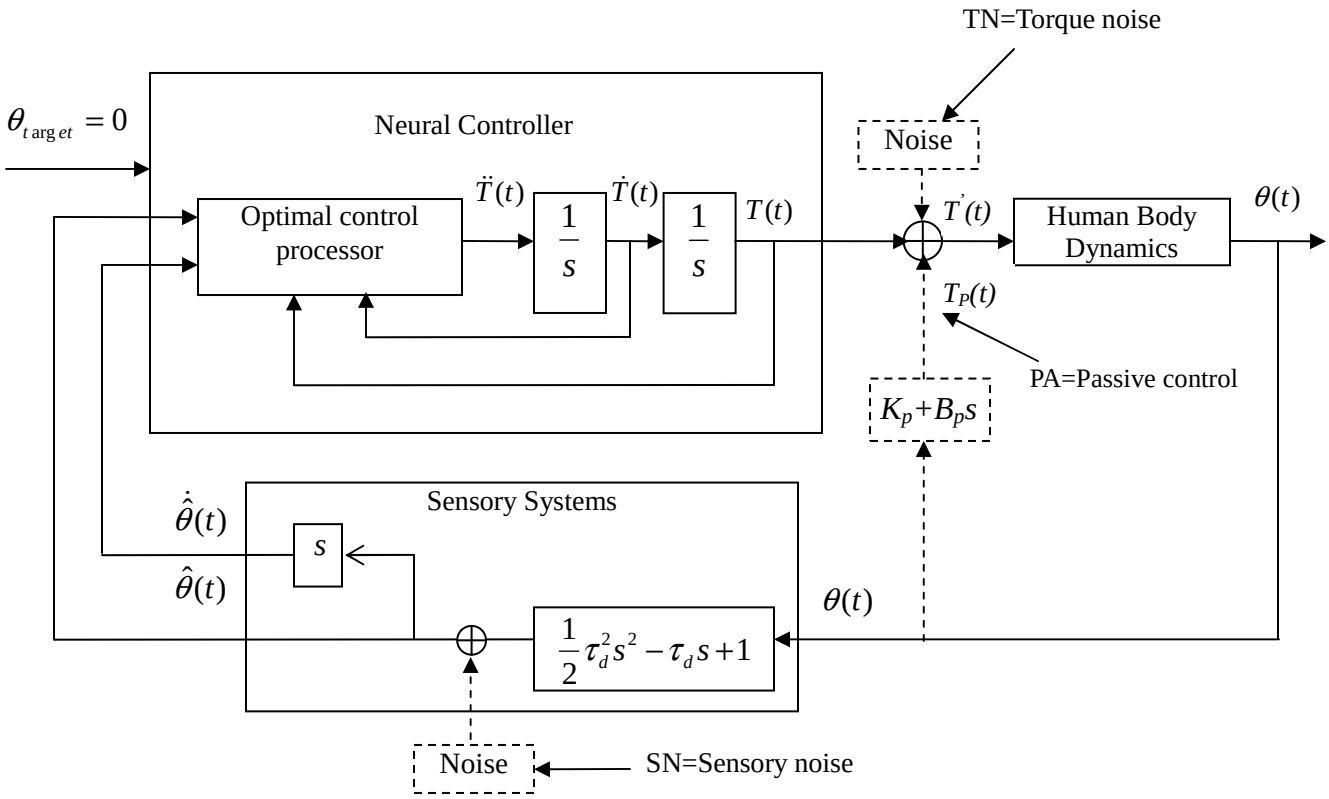


**Figure 6.1 Alternative model structures. (1) TN-NP model structure; (2) SN-NP model structure; (3) SN-PA model structure; (4) SN-PA model structure. NP = no passive control. θ = sway angular displacement; $\hat{\theta}$ = delayed sway angular displacement; $T'$ = ankle torque; $T$ = active control torque generated by the neural controller; $\theta_{target}$ = target sway angle; $\tau_d$ = sensory delay time; $K_P$ = passive stiffness parameter; $B_p$ = passive damping parameter; $T_P$ = passive control torque.**

### 6.2.2 Controlled state equations for different model structures

The controlled state equations for the TN-NP model structure and SN-NP model structure were given in the preliminary study (see Eq. 4.8). Unlike the situation in the TN-NP model structure and SN-NP model structure, passive control torques are included in the TN-PA model structure and SN-PA model structure. Therefore, to stabilize the postural control system, intrinsic passive mechanical properties need to be taken into account by the neural controller as well as those of body dynamics and sensory systems.

Since $T'=T+T_P$, the transfer function that can account for both body dynamics and

intrinsic passive mechanical properties is given by:

$$\frac{\theta(s)}{T(s)} = \frac{1}{Is^2 + B_{pas}s - (K_{pas} - Mgh)} \tag{6.1}$$

Derived from Eqs. 4.5 and 6.1, the transfer function from the torque generated by the neural controller to delayed sway angular displacement is:

$$\frac{\hat{\theta}(s)}{T(s)} = \frac{\frac{1}{2}\tau_d^2 s^2 - \tau_d s + 1}{Is^2 + B_{pas}s - (K_{pas} - Mgh)} \tag{6.2}$$

Using the differentiation operator to replace the Laplace '*s*', we then obtain:

$$\ddot{\hat{\theta}}(t) = \frac{Mgh - K_{pas}}{I}\hat{\theta}(t) - \frac{B_{pas}}{I}\dot{\hat{\theta}}(t) + \frac{1}{I}T(t) - \frac{\tau_d}{I}\dot{T}(t) + \frac{1}{2}\tau_d^2\ddot{T}(t) \tag{6.3}$$

Thus, the state equations accounting for intrinsic passive mechanical properties as well as the properties of body dynamics and sensory systems are as follows:

$$\dot{x}(t) = Ax(t) + Bu(t) \tag{6.4}$$

where $A = \begin{pmatrix} 0 & 1 & 0 & 0 \\ \frac{Mgh - K_{pas}}{I} & -\frac{B_{pas}}{I} & \frac{1}{I} & \frac{-\tau_d}{I} \\ 0 & 0 & 0 & 1 \\ 0 & 0 & 0 & 0 \end{pmatrix}$, $B = \begin{pmatrix} 0 \\ \frac{\tau_d^2}{2I} \\ 0 \\ 1 \end{pmatrix}$, the state is $x(t) = \begin{pmatrix} \hat{\theta}(t) \\ \dot{\hat{\theta}}(t) \\ T(t) \\ \dot{T}(t) \end{pmatrix}$, and the control signal is, $u(t) = \ddot{T}(t)$.

### 6.2.3 Optimal control processor and optimization procedure

As noted in section 4.2.2, the optimal control processor (see Fig. 6.1) is determined by an infinite-time linear quadratic regulator, which minimizes a performance index defined by several physical quantities relevant to sway. This performance index is the same as was used in the original model (Eq. 4.10). Optimal feedback gains can be obtained according to the state equations of the controlled part (Eq. 4.8 or Eq. 6.4) and weighting matrices (Eq. 4.11) and used

to define the optimal control processor (see Fig. 4.2 (b)). Some model parameters, including weightings of relevant physical quantities, gains of noise in postural control, and sensory delay times, cannot be specified before model simulation. Thus, an optimization procedure was performed to determine the values of these unspecified model parameters (please refer to section 4.2.3). The cost function of this optimization procedure was given by:

$$E = \sum_{i=1}^{N} \left( \frac{COPM_i - \hat{COPM}_i}{\hat{COPM}_i} \right)^2 \tag{6.5}$$

where N=9 is the number of COP-based measures, $COPM_i$ and $\hat{COPM}_i$ are the $i^{th}$ COP-based measure from the simulation results and from the experimental results, respectively (The COP-based measures used to define the cost function were given in section 4.2.3). Because a genetic algorithm (GA) is good at searching different parts of the feasible region to find which part contains the global optimum, and since simulated annealing (SA) has better performance at finding the local optimum, a GA and SA algorithm were implemented together to determine model parameters (Hillier and Lieberman, 2005). Specifically, a GA was first used to find the region that might include the global optimum, and then SA was used to search that region for the local optimum. In the GA, the number of chromosomes in a generation was set at 120; the crossover rate and mutation rate were set at 0.80~0.90 and 0.05~0.10, respectively, according to the generation number; and the maximum number of generation was set at 70. In the SA, the temperature was initialized at 30% of the initial cost function; the cooling rate was set at 0.80; the number of iterations between temperature changes was set at 20; and maximum number of iterations was set 100. These values were determined from trial and error. Note that since both the GA and SA were heuristic approaches, the solution obtained from the optimization procedure can not be expected to be globally optimal.

### 6.2.4 Participants and experimental procedures

Experimental data were required to specify model parameters, and were obtained from a prior experiment. Sixteen young participants (eight males and eight females) without injuries, illness, and musculoskeletal disorders were included in the study (age: 21±1.7 years; height: 171.4±7.0cm; weight: 66.4±11.3kg). Trials consisted of brief periods of quiet upright stance. During these, the participants stood barefoot on a force platform (AMTI OR6-7-1000, Watertown, Massachusetts, USA) as still as possible with their eyes closed. To ensure the same feet placement across trials, the feet were outlined on poster board placed on top of the force platform. Each trial was 75 seconds in duration, and the initial 10 seconds and last five seconds were removed. Three trials from each participant were performed, with at least one minute of rest between each. Triaxial ground reaction forces and moments were sampled at 100Hz, and subsequently low-pass filtered (5Hz cut-off). These forces and moments were used to derive center of pressure (COP) time series, which are commonly used to characterize sway behaviors (Baratto et al., 2002; Peterka, 2000; Prieto et al., 1996).

### 6.2.5 COP-based measures

The set of measures used to define the cost function (Eqn 6.7) are traditional measures. During model simulation, values of these traditional measures must be specified in advance, from experimental data, in order to calculate the cost function. Traditional measures are all summary statistics and cannot account for inherent dynamics characteristics of COP time series (Norris et al., 2005). In order to compensate for this limitation of traditional measures, several measures derived from statistical mechanics approaches have been proposed (e.g. Collins and DeLuca, 1993; Delignieres et al., 2003; Duarte and Zatsiorsky, 2000). These approaches are all

based on the stabilogram diffusion analysis (SDA) developed by Collins and DeLuca (1993).

Among the statistical mechanics approaches, one considering the trajectory of the COP as fractional Brownian motion (fBm) appears most relevant and has been widely used when analyzing upright postural control (Genthon and Rougier, 2006; Meyer et al., 2004; Riley et al., 1998; Rougier, 1999a; Rougier, 1999b). Descriptions of the fBm model were given in Chapter 5. Briefly, four statistical mechanics measures (TT: transition time; TA: transition amplitude; $H_S$: short-term scaling exponent; $H_L$: long-term scaling exponent) derived from the fBm model were chosen for analysis. Descriptions and units of COP-based measures are given in Table 6.1.

**Table 6.1 Glossary of COP-based dependent measures**

| Acronym | Description | Unit |
|---|---|---|
| MD | Mean distance | |
| RMS | Root mean square distance | mm |
| MAXD | Maximum distance | mm |
| MV | Mean velocity | mm/s |
| MFREQ | Mean frequency | Hz |
| P50 | 50% power frequency | Hz |
| CFREQ | Centroidal frequency | Hz |
| P95 | 95% power frequency | Hz |
| FREQD | Frequency dispersion | -- |
| TT | Transition time | s |
| TA | Transition amplitude | $mm^2$ |
| $H_S$ | Short-term scaling exponent | -- |
| $H_L$ | Long-term scaling exponent | -- |

### 6.2.6 Model simulation and Analysis

The proposed model structures were separately used to simulate selected experimental trials of quiet upright stance following the flows illustrated in Fig. 4.3. Each simulation trial was 75 second in duration with the initial 10 seconds and last five seconds removed. Separate comparisons of traditional COP-based measures were made between experimental data and simulated values generated by each model structure. To account for individual variability,

simulated measures were normalized by their corresponding experimental measures (i.e. a perfect prediction would yield a value of unity). Subsequently, 95% confidence intervals of the normalized measures were determined, and used to evaluate the simulated data yielded from each model structure. These confidence intervals are equivalent to two-tailed t-tests with $\alpha$=0.05.

Values of the cost function (Eq. 6.5) obtained from each of the different model structures were compared to evaluate the ability of different model structures to simulate traditional COP-based measures. These comparisons were done by using a repeated measure one-way ANOVA. Post-hoc pairwise comparisons were conducted using Tukey's honestly significant difference (HSD) criterion.

To evaluate predictions yielded by the different model structures, scalar errors between predicted statistical mechanics measures and their corresponding experimental measures were calculated. The definition of the scalar error is given by:

$$e = \left| \frac{m_{pre} - m_{ref}}{m_{ref}} \right| \tag{6.6}$$

where $m_{pre}$ is a predicted statistical mechanics measure for a given simulation trial, and $m_{ref}$ is the corresponding experimental measure. The ideal value for this scalar error is zero, since in that case the model duplicated the statistical mechanics measures exactly. Thus, a smaller scalar error indicates better prediction performance of a given model. Separate comparison of scalar errors across different model structures was performed for each statistical mechanics measures using one-way ANOVA and post-hoc pairwise comparisons (Tukey's HSD). In this approach, the models are being evaluated using fundamentally different COP-based measures than those that were used in specifying the model (i.e. determining model parameters). This

approach was considered a more rigorous test of the ability of the models to simulate behaviors.

## 6.3 Results

All 95% confidence intervals of traditional measures resulting from the TN-NP, TN-PA, and SN-NP model structures included unity (Fig. 6.2a, b, and c), indicating that there were no significant differences between the simulated and experimental measures. In contrast, the SN-PA model structure was only able to predict a smaller P95 since the confidence interval of P95 from this model structure was completely below the dotted line representing unity (Fig. 6.2d). The means of these normalized measures from the TN-NP and TN-PA model structures were typically closer to ideal value of unity than those from the SN-NP and SN-PA model structures.

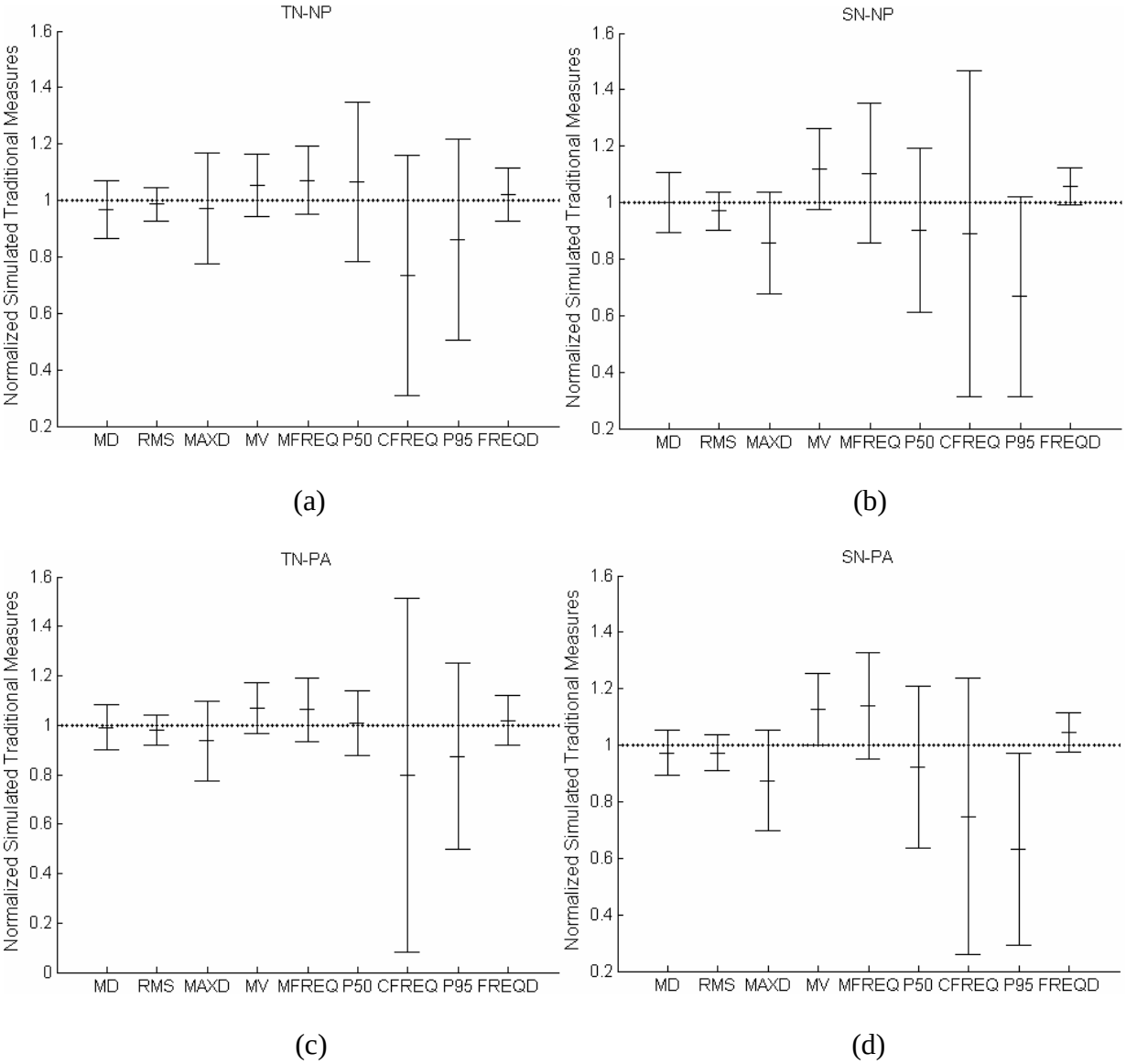


**Figure 6.2 Mean and 95% confidence intervals of the normalized simulated traditional measures resulting from different model structures: TN/SN = Torque / Sensory Noise: NP/PA = no passive / passive control included. Corresponding experimental references used for normalization are given in Table 6.3.**

**Table 6.2 Experimental traditional COP-based measures**

| Measures | MD | RMS | MAXD | MV | MFREQ | P50 | CFREQ | P95 | FREQD |
|---|---|---|---|---|---|---|---|---|---|
| Mean | 4.71 | 5.85 | 30.94 | 8.70 | 0.322 | 0.094 | 0.719 | 0.558 | 0.913 |
| SD | 1.84 | 2.23 | 9.95 | 2.47 | 0.114 | 0.064 | 0.278 | 0.178 | 0.051 |

There was significant main effect of model structures on the cost function ($F(3,173) = 27.45$, $p<0.0001$). Post-hoc comparison indicated that the cost functions obtained by simulating the TN-NP model structure (Mean (SD) = 0.441 (0.159)) or TN-PA model structure

(Mean (SD) = 0.478 (0.152)) were significantly smaller than those that resulted from simulating the SN-NP model structure (Mean (SD) = 0.572 (0.141)) or SN-PA model structure (Mean (SD) = 0.616 (0.107)). On average, the TN-NP model structure generated a smaller cost function than did the TN-PA model structure (0.441 vs. 0.478), but the difference between them was not significant (p =0.423).

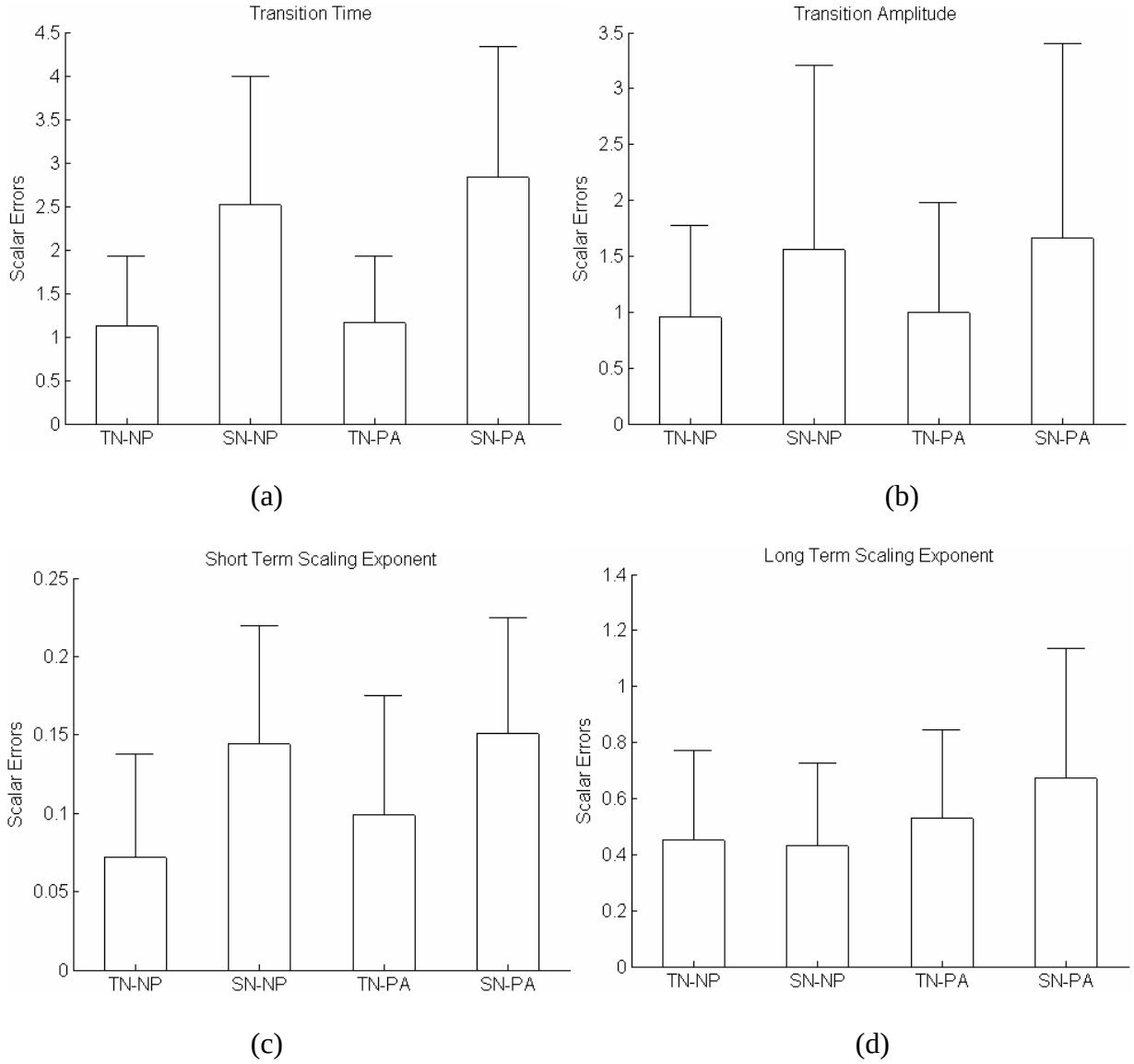


**Figure 6.3 (a) Scalar errors of transition time (TT); (b) Scalar errors of transition amplitude (TA); (c) Scalar errors of short term scaling exponent ($H_S$); (d) Scaling errors of long term scaling exponent ($H_L$). Error bars indicate one standard error.**

Fig. 6.3 shows the distributions of the scalar errors between predicted and experimental statistical mechanics measures. Significant main effects of model structures were found on the scalar errors of TT ($F(3,173) = 33.06$, $p<0.01$), TA ($F(3, 173) = 6.08$, $p<0.01$), $H_S$ ($F(3, 173) = 20.73$, $p<0.01$), and $H_L$ ($F(3,173) = 6.06$, $p<0.01$). Post-hoc analysis indicated that the TN-NP and TN-PA model structures provided significantly smaller scalar errors of TT, TA, and $H_S$ than did the SN-NP model structure and SN-PA model structures, and scalar errors of $H_L$ from the SN-PA model structure was significantly larger than those from the TN-NP and SN-NP model structures.

In the TN-PA and SN-PA model structures, passive joint torque generated by passive tissues was considered. Ratios between the passive and active joint torques are shown in Fig. 6.4 by using box plots. On average, these ratios were 0.034 and 0.056 for the TN-PA model structure and SN-PA model structure, respectively. Disregarding outliers, the maximum ratio was 0.090 for the TN-PA model structure, and 0.155 for the SN-PA model structure.

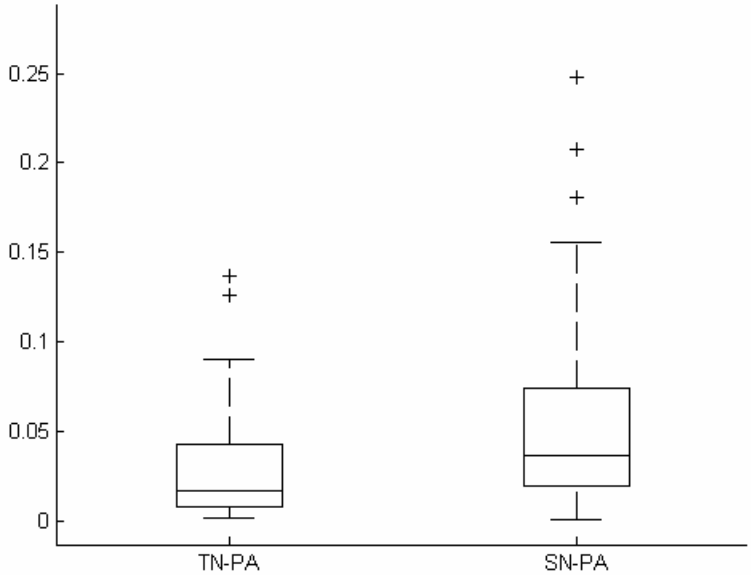


**Figure 6.4 Box plots of ratios between the passive and active joint control torques. Horizontal lines in the box represent lower quartile, median, and upper quartile of the data, respectively. Whiskers indicate 1.5 times of interquartile range (Velleman and Hoaglin, 1981). The '+' symbols indicate outliers that are beyond the whiskers.**

## 6.4 Discussion

According to different balance control theories, four balance control model structures were developed and evaluated in this study. These model structures differed in either the source of noise in postural control or active/passive control patterns. Mathematical models can be used to examine controversial theories, such as the relative roles of noise and passive control here. Thus, by evaluating the performances of different balance control model structures, we are able to examine the validity of various balance control theories. Performances of these model structures were evaluated in terms of their ability to accurately simulate COP-based measures.

When analyzing the 95% confidence intervals of the normalized traditional measures (Fig. 6.2), we found that all the confidence intervals resulting from the TN-NP and TN-PA model structures included unity. This finding indicates that any simulated traditional measure from both model structures was not significantly different from its corresponding experimental measure. However, the confidence interval of P95 from the SN-PA model structure was completely below the dotted line representing unity (Fig. 6.2), indicating that this model structure could only provide a smaller simulated P95 than the actual one. Simulated traditional measures from the TN-NP and TN-PA model structures also appeared to be more reasonable, since the means of normalized measures from them were typically closer to ideal value of unity than those from the rest model structures.

In addition, simulation performance was evaluated by the values of the cost function in the optimization procedure. The objective of the optimization procedure was to minimize the cost function so that the simulated traditional measures could best duplicate their corresponding experimental measures. Hence, a smaller cost function indicates better model performance.

The cost functions resulting from the TN-NP and TN-PA model structures were found to be significantly smaller than those from the SN-NP and SN-PA model structures, indicating that the TN-NP and TN-PA model structures could simulate traditional measures more accurately. Thus, from the perspective of simulating traditional measures, the TN-NP model structure and TN-PA model structure performed better than did the SN-NP model structure and SN-PA model structure.

When evaluating the performances of different model structures in predicting statistical mechanics measures, we found that the scalar errors of these measures (defined by Eq. 6.6) from the TN-NP and TN-PA model structures were typically smaller than those from the SN-NP and SN-PA model structures (Fig. 6.3). This finding indicates that the predicted statistical mechanics measures from the TN-NP and TN-PA model structures could better account for their experimental references. Thus, it might be further concluded that the TN-NP and TN-PA model structures could simulate postural sway more accurately than did SN-NP and SN-PA model structures. Note that experimental values of the statistical mechanics measures were only used after model specification and simulation, so the average scalar errors of TT and TA from the TN-NP and TN-PA model structures were even close to unity which did not indicate a very good prediction.

The common feature of the TN-NP and TN-PA model structures is that noise in postural control was modeled as a random disturbance torque acting on the ankle joint. In contrast, the SN-NP and SN-PA model structures introduced noise to sensory signals. The fact that the TN-NP and TN-PA model structures performed better does not deny the existence of sensory noise; however, it does at least suggest that compared with joint torque noise, sensory noise might play a less important role in driving body sway. Both sensory noise and joint torque

noise were modeled as white noise in this study. However, in reality, noise acting on the human body may not be perfect enough to be white noise. Thus, another possible explanation for why the TN-NP and TN-PA model structures performed better might be that joint torque noise has more common properties with white noise than does sensory noise.

Since no significant difference was found in the cost function or scalar errors of statistical mechanics measures between the TN-NP and TN-PA model structures, it might be concluded that these model structures performed the same given their ability to simulate upright postural sway. Similarly, the SN-NP and SN-PA model structures simulated COP-based measures at the same level of accuracy. The common feature of the TN-NP and SN-NP model structures is that they do not consider the contributions of passive components to balance control. In contrast, the TN-PA and SN-PA model structures take these contributions into account. In addition, when considering the simulation trials of both the TN-PA and SN-PA model structures, disregarding outliers, the maximum ratio between the passive and active control torques was only 0.155, indicating that active control torques are more important than passive control torques when maintaining upright posture. Our results are consistent with Peterka (2002), who applied a PID neural controller to simulate balance control, and found that the passive stiffness and damping parameters obtained from the simulation were only 1/10 the value of active stiffness and damping parameters. According to these simulation results, it might be concluded that active control torque plays a dominant role in balance control.

Some limitations in this study should be noted. First, some anthropometric measures were estimated, and thereby served as a source of errors in the model simulation. Second, both sensory noise and joint torque noise should exist at the same time; however, in this study, in order to compare the roles of these noise sources in balance control, they were introduced to the

model separately. Third, limitations within the presented balance control model based on an optimal control strategy also apply in this study (please refer to Chapter 4). For example, this model is only applicable for small amplitudes of planar sway motion given that only ankle torques were considered to contribute to maintaining balance (Kuo, 1995). In addition, since only two-dimensional balance control model structures were studied, the results can only account for the attributes of balance control in the sagittal plane. Thus, in future research, different three-dimensional balance control model structures should be investigated.

In summary, this study investigated afferent/efferent noise in postural control and active/passive control patterns during quiet upright stance by simulating alternative balance control model structures, and further proved that mathematical models are a useful tool to examine validity of difference balance control theories. The results from this study suggest that efferent noise plays a relatively important role in driving body sway, and that active control torque is dominant in maintaining upright balance.

# Chapter 7 A Three-dimensional Balance Control Model of Quiet Upright Stance Based on an Optimal Control Strategy


## Abstract

A three-dimensional balance control model of quiet upright stance is presented, based on an optimal control strategy, and evaluated in terms of its ability to simulate postural sway in both the anterior-posterior and medial-lateral directions. The human body was represented as a two-segment inverted pendulum during upright stance. In order to linearize body dynamics, several assumptions were made, for example that there was no transversal rotation during upright stance. The neural controller was assumed to be an optimal controller that generates ankle control torque and hip control torque according to certain performance criteria. An optimization procedure was used to determine the values of unspecified model parameters including random disturbance gains and sensory delay times. This model was used to simulate postural sway behaviors characterized by center-of-pressure (COP) based measures. No significant differences were found between any of the simulated COP-based measure and corresponding experimental references. Thus, the proposed three-dimensional balance control model appears to have the ability accurately simulate postural sway behaviors.


## 7.1 Introduction

Many existing balance control models have adopted a single-segment inverted pendulum to model the human body, and have focused on investigating postural sway only in the sagittal plane (e.g. Ishida et al., 1997; Johansson et al., 1988; Maurer and Peterka, 2005; Peeters et al., 1985). In these models, ankle control torque was the only neural output contributing to controlling upright posture. A single-segment inverted pendulum body model is applicable in some circumstances, especially when the sway amplitude is small and an ankle strategy dominates (Kuo, 1995). However, some researchers have argued that such an approach is oversimplified (e.g. Alexandrov et al., 2005; Hsu et al., 2007). For example, Hsu et al. (2005) noted that six major joints along the longitudinal axis of the body are coordinated to stabilize the spatial positions of the COM and head during quiet upright stance.

In addition to ankle control torque, hip control torque is also widely accepted as an important neural output to control upright posture. Many investigations have taken into account

the contribution of hip control torque in balance control by adopting a multi-segment inverted pendulum body model (e.g. Fujisawa et al., 2005; Kuo 1995; van der Kooij et al. 1999). However, these models still limit sway motions to the anterior-posterior (A/P) direction. Existing evidence indicates that medial-lateral (M/L) sway is important in some conditions, and that M/S sway measures are able to account for different balance control mechanisms. For example, sway excursion in the M/L direction was found to significantly increase with increased external loading during upright stance (Schiffman et al., 2006). McClenaghan et al. (1996) reported that significant age-related differences existed in some frequency-domain measures (e.g. CFREQ and P50) obtained from M/L postural sway. Thus, a simple two-dimensional balance control model that cannot simulate M/L postural sway is not able to sufficiently reflect how humans control upright posture.

The purpose of this study was to develop a balance control model that can accurately simulate postural sway in three-dimensional space. Similar to earlier models presented in this dissertation, the current model is also based on an optimal control strategy. Extending the previous efforts, however, human body dynamics are described by a two-segment inverted pendulum model in which there are two joints representing the ankle and the hip. Thus, the proposed three-dimensional balance control model should be able to account for both the ankle and hip strategies typically evidence in upright postural control (Kuo, 1995). Performance of the proposed three-dimensional balance control model was evaluated by comparing model simulations and experimental data for selected COP-based measures. We hypothesized that there would no significant differences between any of the simulated COP-based measure and corresponding experimental references.

## 7.2 Methods

In this model, human body dynamics were described by a two-segment inverted pendulum in three-dimensional space. Sensory systems were assumed to provide accurate ankle and hip sway angles to the neural controller but with an inherent time delay due to sensory processing, transduction, and transmission (van der Kooij et al., 1999). The neural controller was an optimal controller that can minimize a performance index defined by physical quantities relevant to sway in both the A/P and M/L directions. An optimization procedure using heuristic search approaches was performed to determine unspecified model parameters such as sensory delay times at the ankle and hip joints. 95% confidence intervals of normalized simulated COP-based measures were calculated and used to evaluate the proposed model in terms of its ability to simulate postural sway.

### 7.2.1 Postural control system

The postural control system model is illustrated in Fig. 7.1. Three portions comprise the closed loop: 1) the neural controller, 2) human body dynamics, and 3) sensory systems. Models of each of these three parts are discussed in more detail in subsequent sections. In addition, According to Chapter 6, modeling noise in postural control as random disturbance torques may have better simulation performances, so random disturbance torques were added to the ankle control torque and hip control torque generated by the neural controller to drive sway motions.

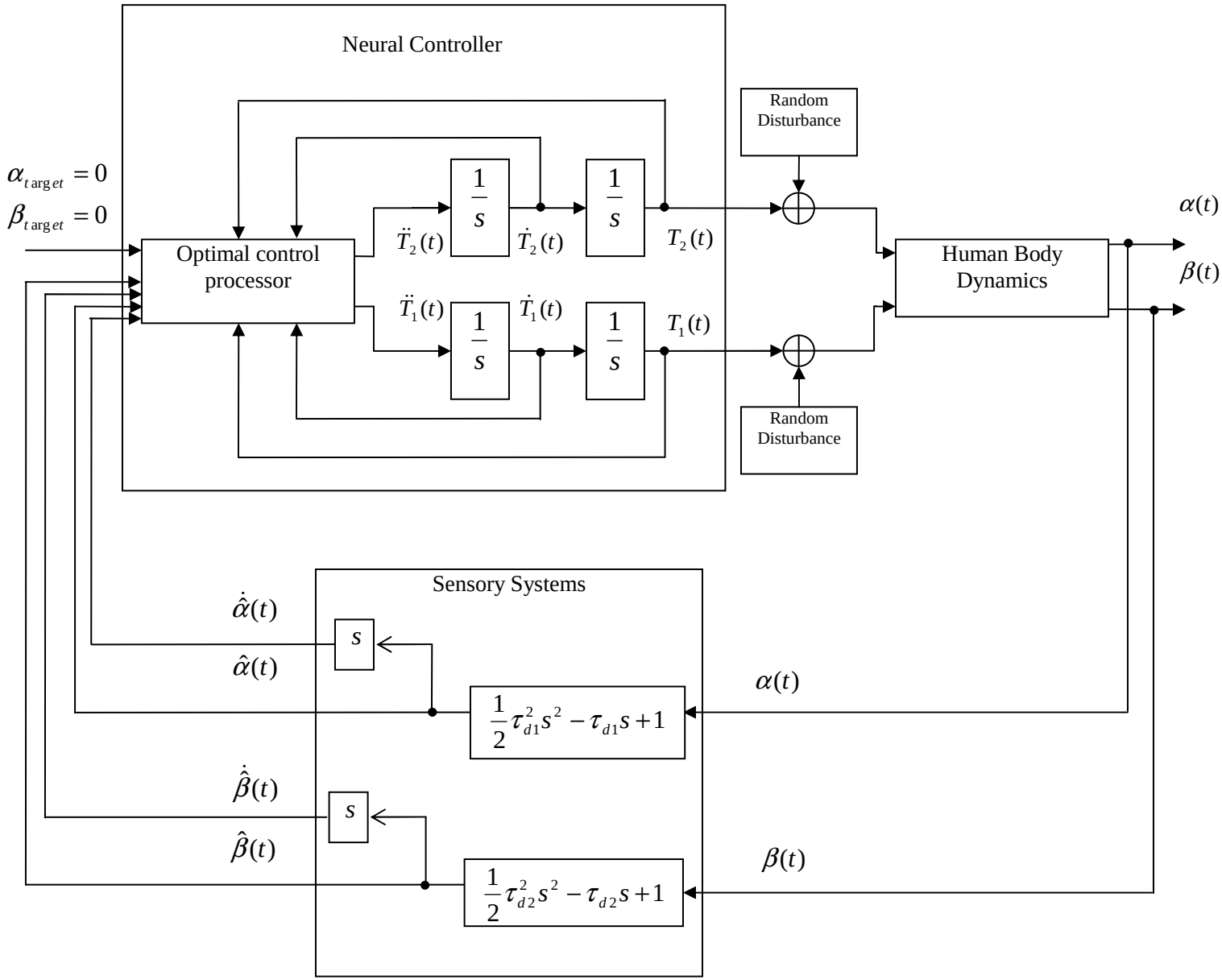


**Figure 7.1 Postural control system for the three-dimensional balance control model. $T_1$=ankle control torque; $T_2$=hip control torque; α=ankle sway angle; β=hip sway angle; $\tau_{d1}$=sensory delay time at the ankle; $\tau_{d2}$=sensory delay time at the hip.**

### 7.2.2 Human body dynamics and sensory systems

A two-segment inverted pendulum in three-dimensional space was used to describe human body dynamics (Fig. 7.2). The two rigid linked segments represent the legs and upper body, respectively; the joint connecting them corresponds to the hip joint.

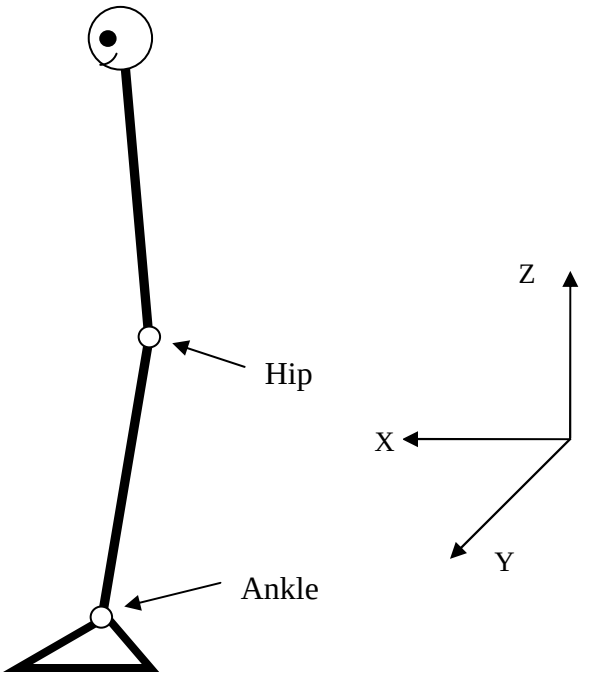


**Figure 7.2 A two-segment inverted pendulum model. X-axis is positive in the anterior direction; Y-axis is positive to the left; Z-axis is positive in the superior direction.**

In essence, the dynamics of this two-segment inverted pendulum are non-linear, yet optimal control formulations are only applicable to linear control systems. (Though non-linear optimal control theories have been proposed, these theories are not well formulated and cannot provide global optimal solutions). Given this, some assumptions are required in order to linearize the dynamics. McClenaghan et al. (1996) and Winter et al. (1996) have suggested that the ankle and hip strategies are applied primarily to control postural sway in the sagittal and frontal planes, respectively. Thus, the lower segment (legs), controlled primarily by ankle torques, was assumed to rotate only in the sagittal plane (along the A/P direction). Similarly,

the upper segment (upper body), controlled primarily by hip torques, was assumed to rotate only in the frontal plane (along the M/L direction). In addition, transversal rotations of the two segments have been ignored, since such movements are likely minimal during quiet upright stance (Gunther et al., 2008).

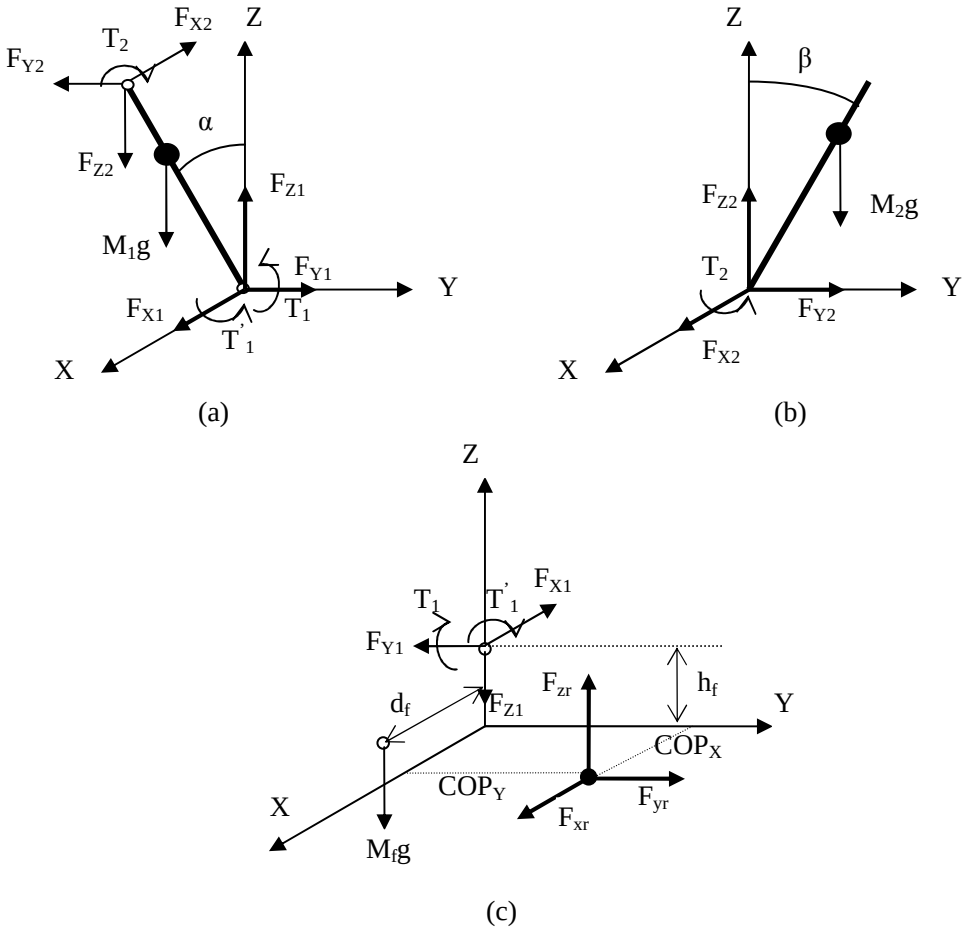


**Figure 7.3 (a) Force analysis of lower segment; (b) Force analysis of upper segment; (c) Force analysis of foot.**

Fig. 7.3 illustrates the force analysis of the two-segment inverted pendulum model. X-axis and Y-axis correspond to the A/P and M/L directions, respectively. According to this figure and the above assumptions, the equations of motion are given below, with Eqns. 7.1, 7.2, and 7.3 corresponding to a respective force analysis of the upper segment, lower segment, and

feet.

$$\begin{cases} I_2\ddot{\beta} = T_2 - m_2 g Y_{COM2} \\ F_{Z2} - m_2 g = m_2 \ddot{Z}_{COM2} \\ F_{Y2} = m_2 \ddot{Y}_{COM2} \\ F_{X2} = m_2 \ddot{X}_{hip} \end{cases} \tag{7.1}$$

$$\begin{cases} I_1\ddot{\alpha} = T_1 + F_{Z2} X_{hip} + m_1 g X_{COM1} - F_{X2} Z_{hip} \\ T_1^{'} + F_{Y2} Z_{hip} = T_2 \\ F_{Z1} - F_{Z2} - m_1 g = m_1 \ddot{Z}_{COM1} \\ F_{Y1} - F_{Y2} = 0 \\ F_{X1} - F_{X2} = m_1 \ddot{X}_{COM1} \end{cases} \tag{7.2}$$

$$\begin{cases} F_{Zr} = F_{Z1} + m_f g \\ F_{Xr} = F_{X1} \\ F_{Yr} = F_{Y1} \\ F_{Zr} COP_Y + F_{Yr} h_f = T_1^{'} \\ -F_{Zr} COP_X - F_{Xr} h_f - T_1 + m_f g d_f = 0 \end{cases} \tag{7.3}$$

where:

α is the sway angle of the lower segment in the sagittal plane

β is the sway angle of the upper segment in the frontal plane

$I_1$ and $I_2$ are the moments of inertia of the lower segment and upper segment, respectively

$m_1$ and $m_2$ are the masses of the lower segment and upper segment, respectively

$m_f$ is the mass of the feet

$h_f$ is the height of the ankle

$d_f$ is the distance between the ankle and the COM of the feet

$T_1$ is the ankle control torque whose direction is along Y axis

$T_1^{'}$ is the ankle control torque whose direction is along the X axis

$T_2$ is the hip control torque whose direction is along the X axis

$\{F_{X1}, F_{Y1}, F_{Z1}\}$, $\{F_{X2}, F_{Y2}, F_{Z2}\}$, and $\{F_{Xr}, F_{Yr}, F_{Zr}\}$ are the reactions forces on the ankle, hip and

ground, respectively

$\{X_{COM1}, Y_{COM1}, Z_{COM1}\}$, $\{X_{COM2}, Y_{COM2}, Z_{COM2}\}$, and $\{X_{hip}, Y_{hip}, Z_{hip}\}$ are the coordinates of the center of mass of lower segment (COM1), center of mass of upper segment (COM2), and the hip.

There is no hip torque about the Y-axis, because the upper segment was assumed to rotate only in the frontal plane. According to these equations, the COP location is given by:

$$COP_X = \frac{-(m_2\ddot{X}_{hip} + m_1\ddot{X}_{COM1})h_f - I_1\ddot{\alpha} + (m_2 g + m_2\ddot{Z}_{COM2})X_{hip} + m_1 g X_{COM1} - m_2\ddot{X}_{hip}Z_{hip} + m_f g d_f}{(m_1 + m_2 + m_f)g + m_2\ddot{Z}_{COM2} + m_1\ddot{Z}_{COM1}} \quad (7.4)$$

$$COP_Y = \frac{I_2\ddot{\beta} + m_2 g Y_{COM2} - m_2\ddot{Y}_{COM2}(Z_{hip} + h_f)}{(m_1 + m_2 + m_f)g + m_2\ddot{Z}_{COM2} + m_1\ddot{Z}_{COM1}} \quad (7.5)$$

Since it was assumed that the lower segment and the upper segment are restricted to rotations in the sagittal and frontal planes, respectively, ankle torque $T_1'$ can be determined by $T_1$ and $T_2$. Similarly, the force components in Eqns 7.1~7.3 can also be determined by $T_1$ and $T_2$. Thus, according to the assumptions made above, the neural controller only actively generates joint torques $T_1$ and $T_2$ to maintain balance.

The properties of human body dynamics can be formulated as:

$$\begin{cases} I_2\ddot{\beta} = T_2 - m_2 g Y_{COM2} \\ I_1\ddot{\alpha} = T_1 + F_{Z2}X_{hip} + m_1 g X_{COM1} - F_{X2}Z_{hip} \end{cases} \quad (7.6)$$

In addition, the coordinates of the COM1, COM2, hip and ankle are given by:

$$\begin{cases} X_{COM1} = h_1 \times \sin\alpha; Y_{COM1} = Y_{ankle}; Z_{COM1} = h_1 \times \cos\alpha; \\ X_{COM2} = X_{hip}; Y_{COM2} = -h_2 \times \sin\beta; Z_{COM2} = Z_{hip} + h_2 \times \cos\beta; \\ X_{hip} = l_1 \times \sin\alpha; Y_{hip} = Y_{ankle}; Z_{hip} = l_1 \times \cos\alpha; \\ X_{ankle} = 0; Y_{ankle} = 0; Z_{ankle} = 0. \end{cases} \quad (7.7)$$

where $h_1$ is the length of the COM1 relative to the ankle, $h_2$ is the COM2 relative to the hip, $l_1$ is the length of lower segment, and $l_2$ is the length of upper segment. We are only interested in

spontaneous sway, during which sway angles α and β are very small. Thus, in order to linearize human body dynamics, the following approximations were made: $sin\alpha \approx \alpha$, $sin\beta \approx \beta$, $cos\alpha \approx 1$, and $cos\beta \approx 1$. Given this, the linear human body dynamics are described as:

$$\begin{cases} I_2\ddot{\beta} = T_2 + m_2 g h_2 \beta \\ I_1\ddot{\alpha} = T_1 + m_2 g l_1 \alpha + m_1 g h_1 \alpha - m_2 l_1^2 \ddot{\alpha} \end{cases} \tag{7.8}$$

We also assumed that sensory systems feed back accurate sway angle measures to the neural controller with a certain time delay. Hence, two time-invariant sensory time delays, $\tau_{d1}$ and $\tau_{d2}$, were introduced to the model for α and β, respectively. In order to linearize the sensory systems, delayed joint angles $\hat{\alpha}$ and $\hat{\beta}$ were approximated by:

$$\hat{\alpha}(t) \approx \alpha(t) - \tau_{d1}\dot{\alpha}(t) + \frac{1}{2}\tau_{d1}^2\ddot{\alpha}(t)$$

$$\text{and} \quad \hat{\beta}(t) \approx \beta(t) - \tau_{d2}\dot{\beta}(t) + \frac{1}{2}\tau_{d2}^2\ddot{\beta}(t) \tag{7.9}$$

Thus, the state equations (Eqn. 7.10) that represent the properties of both body dynamics and sensory systems were derived from Eqn. 7.8 and Eqn. 7.9. (Please see section 4.4 for details on the derivation):

$$\dot{x}(t) = Ax(t) + Bu(t) \tag{7.10}$$

where $A = \begin{pmatrix} 0 & 1 & 0 & 0 & 0 & 0 & 0 & 0 \\ \frac{m_2 g l_1 + m_1 g h_1}{I_1 + m_2 l_1^2} & 0 & \frac{1}{I_1 + m_2 l_1^2} & \frac{-\tau_{d1}}{I_1 + m_2 l_1^2} & 0 & 0 & 0 & 0 \\ 0 & 0 & 0 & 1 & 0 & 0 & 0 & 0 \\ 0 & 0 & 0 & 0 & 0 & 0 & 0 & 0 \\ 0 & 0 & 0 & 0 & 0 & 1 & 0 & 0 \\ 0 & 0 & 0 & 0 & \frac{m_2 g h_2}{I_2} & 0 & \frac{1}{I_2} & \frac{-\tau_{d2}}{I_2} \\ 0 & 0 & 0 & 0 & 0 & 0 & 0 & 1 \\ 0 & 0 & 0 & 0 & 0 & 0 & 0 & 0 \end{pmatrix}$,

$$B=\begin{pmatrix} 0 & 0 \\ \frac{\tau_{d1}^2}{2(I_1+m_2l_1^2)} & 0 \\ 0 & 0 \\ 1 & 0 \\ 0 & 0 \\ 0 & \frac{\tau_{d2}^2}{2I_2} \\ 0 & 0 \\ 0 & 1 \end{pmatrix}$$, the state is $x(t)=\begin{pmatrix} \hat{\alpha} \\ \dot{\hat{\alpha}} \\ T_1 \\ \dot{T}_1 \\ \hat{\beta} \\ \dot{\hat{\beta}} \\ T_2 \\ \dot{T}_2 \end{pmatrix}$ and the control signal is $u(t)=\begin{pmatrix} \ddot{T}_1 \\ \ddot{T}_2 \end{pmatrix}$

According to Eqns. 7.8 and 7.9, sway angles α and β do not interact with each other, indicating that based on the assumptions we made above, sway motions in the sagittal plane and frontal plane are independent. Thus, state equations (Eq. 7.10) can be decomposed into two separate state equations that account for the properties of body dynamics in the A/P (Eq. 7.11) and M/L (Eq. 7.12) directions, respectively.

$$\dot{x}_1(t)=A_1x_1(t)+B_1u_1(t) \tag{7.11}$$

where $A_1=\begin{pmatrix} 0 & 1 & 0 & 0 \\ \frac{m_2gl_1+m_1gh_1}{I_1+m_2l_1^2} & 0 & \frac{1}{I_1+m_2l_1^2} & \frac{-\tau_{d1}}{I_1+m_2l_1^2} \\ 0 & 0 & 0 & 1 \\ 0 & 0 & 0 & 0 \end{pmatrix}$, $B_1=\begin{pmatrix} 0 \\ \frac{\tau_{d1}^2}{2(I_1+m_2l_1^2)} \\ 0 \\ 1 \end{pmatrix}$, the state is

$x_1(t)=\begin{pmatrix} \hat{\alpha} \\ \dot{\hat{\alpha}} \\ T_1 \\ \dot{T}_1 \end{pmatrix}$ and the control signal is $u_1(t)=\left(\ddot{T}_1\right)$

$$\dot{x}_2(t)=A_2x_2(t)+B_2u_2(t) \tag{7.12}$$

where $A_2=\begin{pmatrix} 0 & 1 & 0 & 0 \\ \frac{m_2gh_2}{I_2} & 0 & \frac{1}{I_2} & \frac{-\tau_{d2}}{I_2} \\ 0 & 0 & 0 & 1 \\ 0 & 0 & 0 & 0 \end{pmatrix}$, $B=\begin{pmatrix} 0 \\ \frac{\tau_{d2}^2}{2I_2} \\ 0 \\ 1 \end{pmatrix}$, the state is $x(t)=\begin{pmatrix} \hat{\beta} \\ \dot{\hat{\beta}} \\ T_2 \\ \dot{T}_2 \end{pmatrix}$ and the control

signal is $u_2(t) = \left(\ddot{T}_2\right)$

### 7.2.3 Anthropometry estimation

Different anthropometric data are required to implement this model, versus those required in the two-dimensional model (Chapter 5). Specifically, the three-dimensional balance control model requires: the moment of inertial of the lower body around the ankle ($I_1$), the mass of the lower body ($m_1$), the length of the lower body ($l_1$), and the length of the COM of the lower segment relative to the ankle ($h_1$), the moment of inertial of the upper body around the hip ($I_2$), the mass of the upper body ($m_2$), the length of the upper body ($l_2$), the length of the COM of the upper segment relative to the hip ($h_2$), the mass of the feet ($m_F$), the height of the ankle ($h_F$), and the distance between the ankle and the COM of the feet ($d_F$). According to some published results (Chaffin et al., 1999; de Leva, 1996; Robertson et al., 2004), an estimation of these anthropometric data was obtained using:

$$\begin{cases} m_1 = M \times (0.0435 + 0.1027) \times 2; m_2 = M \times 0.6708; \\ l_1 = l \times (0.530 - 0.039); l_2 = l \times (1 - 0.530); \\ h_1 = l_1 \times 0.6179; h_2 = l_2 \times 0.374; \\ I_1 = m_1 \times (l_1 \times 0.650)^2; I_2 = m_2 \times (l_2 \times 0.620)^2 \\ m_F = M \times 0.0137 \times 2(male) \quad or \quad m_F = M \times 0.0129 \times 2(\ female); \\ h_F = l \times 0.039; \\ d_F = l_F \times 0.4415(male) \quad or \quad d_F = l_F \times 0.4014(\ female). \end{cases} \tag{7.13}$$

### 7.2.4 Neural controller

The neural controller (Fig. 7.1) includes an optimal control processor and several integration units. The optimal control processor is defined by optimal feedback gains. Since sway motions in the sagittal and frontal planes are independent, we could calculate the optimal feedback for state equations 7.11 and 7.12 separately. The optimal control processor's structure

is given in Fig. 7.4.

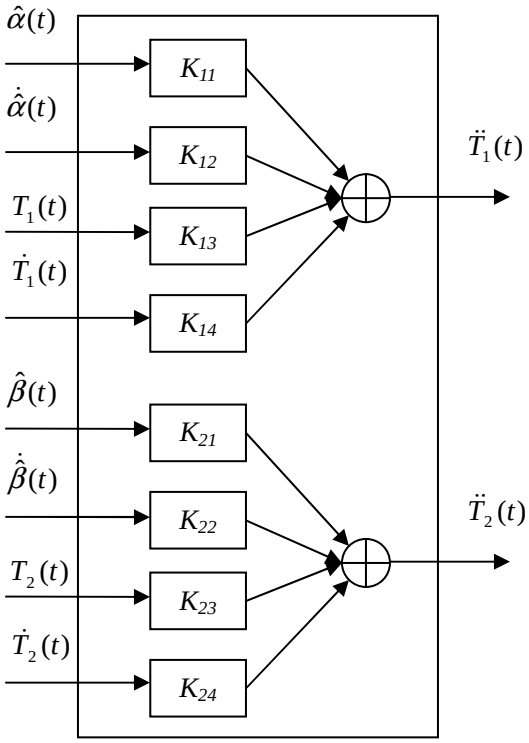


**Figure 7.4 Optimal control processor**

Performance indices for sway motions in the sagittal and frontal planes are defined by Eq. 7.14 and Eq. 7.15, respectively.

$$J_1 = \frac{1}{2}\int_0^\infty (w_{11}\hat{\alpha}^2(t) + w_{21}\dot{\hat{\alpha}}^2(t) + w_{31}T_1{}^2(t) + w_{41}\dot{T}_1{}^2(t) + w_{51}\ddot{T}_1{}^2(t))dt \qquad (7.14)$$

$$J_2 = \frac{1}{2}\int_0^\infty (w_{12}\hat{\beta}^2(t) + w_{22}\dot{\hat{\beta}}^2(t) + w_{32}T_2{}^2(t) + w_{42}\dot{T}_2{}^2(t) + w_{52}\ddot{T}_2{}^2(t))dt \qquad (7.15)$$

where $w_{ij}$ ( $i$=1~5, $j$=1 and 2) are weightings of physical quantities relevant to sway. Converting the above performance indices into standard form yields weighting matrices as follows:

$$Q_1 = \begin{pmatrix} w_{11} & 0 & 0 & 0 \\ 0 & w_{21} & 0 & 0 \\ 0 & 0 & w_{31} & 0 \\ 0 & 0 & 0 & w_{41} \end{pmatrix} \quad \text{and} \quad R_1 = w_{51} \qquad (7.16)$$

$$Q_2 = \begin{pmatrix} w_{12} & 0 & 0 & 0 \\ 0 & w_{22} & 0 & 0 \\ 0 & 0 & w_{32} & 0 \\ 0 & 0 & 0 & w_{42} \end{pmatrix} \quad \text{and} \quad R_2 = w_{52} \tag{7.17}$$

Note that as long as $J_1$ and $J_2$ are minimized, the sum of $J_1$ and $J_2$ must be also minimized. Therefore, we are able to calculate the optimal feedback gains for sway motions in A/P and M/L directions separately and still optimize the performance of the whole postural control system.

### 7.2.5 Optimization procedure

An optimization procedure was use to specify model parameters, including weights of relevant physical quantities, random disturbance gains and sensory delay times. The three-dimensional balance control model simulates postural sway in both the A/P and M/L directions. Thus, the cost function here should be defined by sway measures in both directions. Specifically, we chose two time-domain COP-based measures and two frequency-domain COP-based measures. These measures are traditional measures (Norris et al., 2005) and included root mean square displacement (A/P RMS and M/L RMS), mean velocity (A/P MV and M/L MV), centroidal frequency (A/P CFREQ and M/L CFREQ), and frequency dispersion (A/P FREQD and M/L FREQD). The definition of the cost function is given by:

$$E = \sum_{i=1}^{N} \left( \frac{COPM_i - \hat{COPM}_i}{\hat{COPM}_i} \right)^2 \tag{7.18}$$

where N=8 is the number of COP-based measures, and $COPM_i$ and $\hat{COPM}_i$ are the $i^{th}$ COP-based measures from the simulation and experimental results, respectively. A genetic algorithm (GA) and simulated annealing (SA) were used to specify model parameters (i.e. that minimized E). In the GA, the number of chromosomes in a generation was set at 140; the

crossover rate and mutation rate were set at 0.80~0.90 and 0.05~0.10, respectively, according to the generation number; and the maximum number of generation was set at 90. In the SA, the temperature was initialized at 30% of the initial cost function; the cooling rate was set at 0.80; the number of iterations between temperature changes was set at 40; and maximum number of iterations was set 200. These values were determined from trial and error. Note that since both the GA and SA were heuristic approaches, the solution obtained from the optimization procedure can not be expected to be globally optimal.

### 7.2.6 Participants and experimental procedures

Experimental data (COP time series) were required to specify model parameters. These data were obtained from a prior study, which has been described earlier (Chapter 6). In contrast to the earlier study, however, COP-based measures were used in both the A/P and M/L directions. In addition, the present analysis included COP time series obtained both before and after localized muscle fatigue. A commercial dynamometer (Biodex Medical Systems, Shirley, NY) was used to induce fatigue in the ankle plantarflexors (ankle fatigue) and lumbar extensors (torso fatigue). During fatiguing exercises, participants were requested to step on the Biodex and perform isotonic exertions which were set at 60% of the MVE (peak torque) at a speed of 12 repetitions/min. Fatigue was considered to be induced when participants could not complete the entire range of motion for three consecutive repetitions.

### 7.2.7 Model simulation and analysis

The flow of model simulation in this study was the same as described earlier for the two-dimensional balance control model (please refer to section 4.2.4). Having specified the model parameters, the three-dimensional balance control model was then used to predict both

traditional and some statistical mechanics COP-based measures that did not appear in the cost function. These statistical mechanics COP-based measures include transition time (A/P TT and M/L TT), transition amplitude (A/P TA and M/L TA), short term scaling exponent (A/P $H_S$ and M/L $H_S$), and long-term scaling exponent (A/P $H_L$ and M/L $H_L$). Descriptions and units of both traditional and statistical mechanics measures were given earlier (Table 6.1). Note that traditional and statistical mechanics measures derived from COP time series assess fundamentally different aspects of postural control (Norris et al., 2005). Specifying the model using the former, and evaluating it using the latter, was considered a fairly rigorous method to assess the performance of the three-dimensional balance control model. In addition, inclusion of post-fatigue COP data allowed for assessment of the model over a broader range of circumstances.

Quantitative evaluation of the three-dimensional balance control model was done by comparing simulated COP-based measures with corresponding experimental measures. Specifically, the simulated measures were normalized by their corresponding experimental measures, and 95% confidence intervals of these normalized simulated measures were obtained (perfect predictions would yield values of unity). These confidence intervals are equivalent to two-tailed t-tests with $\alpha=0.05$. There would be no significant differences between the simulated and experimental data if values of unity were included in the confidence intervals. Values of the cost function, defined as a scalar error between simulated and experimental data, were used to assess whether the model simulation ability differed with localized muscle fatigue (LMF). This comparison was done using a one-way ANOVA. Finally, pairwise correlations were obtained between the simulated COP-based measures and model parameters.

## 7.3 Results

For all traditional COP-based measures, 95% confidence intervals of the normalized simulated values included unity (Figure 7.5a). Means for the traditional measures were all within the range of 0.9-1.1, or very close to the ideal value of unity. These results suggest that the proposed model could simulate traditional COP-based measures reasonably well. In contrast, predictions of statistical mechanics measures were somewhat less favorable (Figure 7.5b). While mean values were generally close to unity, excepting TT, and confidence intervals contained unity, these intervals were quite broad. Among the statistical mechanics measures, $H_S$ was predicted substantially better (i.e. mean near unity and small confidence interval range). A non-significant ($p = 0.140$) effect of fatigue was found on the cost function, which had a mean (SD) value for pre-fatigue data of 0.439 (0.171), and respective values of 0.479 (0.145) and 0.456 (0.140) after ankle and torso fatigue.

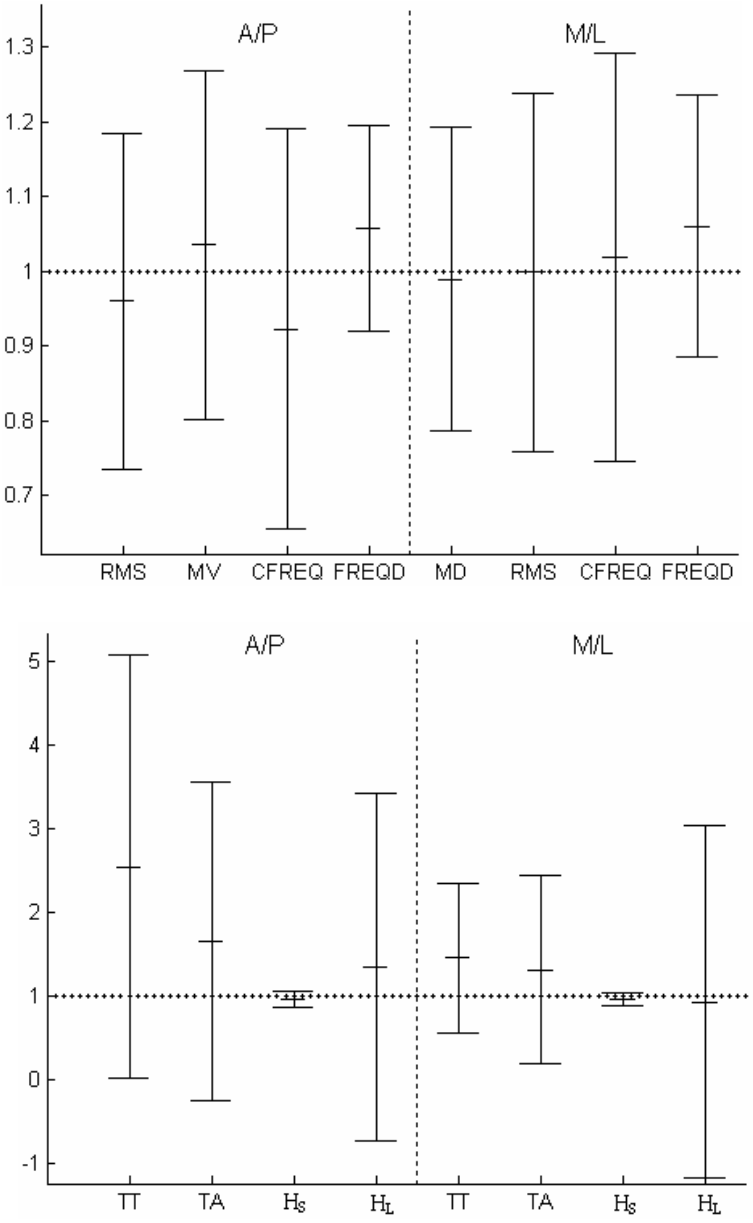


**Figure 7.5 Means and 95% confidence intervals of the normalized simulated COP-based measures (top: traditional measures; bottom: statistical mechanics measures). Dotted horizontal lines indicate unity, or perfect model predictions. Experimental references used for normalization are given in Table 7.1.**

**Table 7.1 Experimental COP-based measures**

| | | RMS | MV | CFREQ | FREQD | TT | TA | $H_S$ | $H_L$ |
|---|---|---|---|---|---|---|---|---|---|
| A/P | Mean | 6.68 | 10.52 | 0.549 | 0.903 | 0.579 | 26.33 | 0.817 | 0.198 |
| | SD | 2.95 | 3.55 | 0.139 | 0.061 | 0.297 | 26.23 | 0.041 | 0.100 |
| M/L | Mean | 6.31 | 13.08 | 0.582 | 0.844 | 0.477 | 34.35 | 0.829 | 0.148 |
| | SD | 2.19 | 4.95 | 0.153 | 0.079 | 0.122 | 31.50 | 0.030 | 0.109 |

Some patterns were evidence among the pairwise correlations between model parameters and COP-based measures (Table 7.2). Random disturbance gains ($k_{n1}$ and $k_{n2}$) were significantly correlated with all simulated COP-based measures except $H_S$. In contrast, some model parameters ($w_{11}$, $w_{21}$ and $w_{12}$) had no significant correlation with any of the simulated COP-based measures.

**Table 7.2 Correlations between model parameters and simulated sway measures**

| | $w_{11}$ | $w_{21}$ | $w_{31}$ | $w_{41}$ | $w_{51}$ | $k_{n1}$ | $\tau_{d1}$ | $w_{12}$ | $w_{22}$ | $w_{32}$ | $w_{42}$ | $w_{52}$ | $k_{n2}$ | $\tau_{d2}$ |
|---|---|---|---|---|---|---|---|---|---|---|---|---|---|---|
| A/P RMS | -0.107 | -0.130 | 0.007 | 0.147 | 0.159 | 0.314* | 0.201* | 0.142 | -0.077 | -0.084 | -0.033 | -0.062 | 0.392* | 0.084 |
| A/P MV | 0.036 | -0.059 | 0.297* | -0.115 | -0.142 | 0.793* | -0.076 | 0.051 | 0.177 | 0.183 | -0.195 | -0.196 | 0.860* | -0.046 |
| A/P CFREQ | 0.152 | 0.016 | 0.216* | -0.271* | -0.135 | 0.579* | -0.047 | -0.057 | 0.279* | 0.217* | -0.156 | -0.177 | 0.634* | -0.095 |
| A/P FREQD | -0.095 | -0.022 | -0.516* | 0.280* | 0.369* | -0.455* | 0.662* | 0.020 | -0.112 | -0.120 | 0.032 | 0.179 | -0.111* | 0.172 |
| A/P TT | -0.038 | -0.152 | -0.433* | 0.183 | 0.513* | -0.399* | 0.676* | 0.012 | -0.185 | -0.244* | 0.139 | 0.249* | -0.236* | 0.270* |
| A/P TA | 0.044 | -0.118 | 0.099 | -0.057 | 0.065 | 0.239* | 0.119 | 0.084 | 0.026 | 0.027 | -0.098 | -0.074 | 0.365* | 0.045 |
| A/P Hs | 0.146 | 0.058 | 0.309* | -0.478* | 0.059 | 0.028 | -0.022 | -0.009 | -0.009 | 0.152 | -0.081 | -0.036 | -0.033 | -0.148 |
| A/P $H_L$ | -0.107 | -0.139 | -0.481* | 0.311* | 0.473* | -0.358* | 0.609* | 0.069 | -0.294* | -0.340* | 0.209* | 0.243* | -0.280* | 0.306* |
| M/L RMS | 0.031 | -0.089 | 0.061 | 0.018 | -0.034 | 0.411* | 0.001 | 0.047 | 0.039 | -0.095 | -0.051 | 0.080 | 0.458* | 0.077 |
| M/L MV | 0.037 | -0.059 | 0.242* | -0.076 | -0.146 | 0.748* | -0.053 | 0.034 | 0.211* | 0.218* | -0.217* | -0.201* | 0.892* | -0.046 |
| M/L CFREQ | -0.032 | 0.040 | 0.161 | -0.043 | -0.111 | 0.555* | -0.067 | -0.080 | 0.259* | 0.339* | -0.158 | -0.274* | 0.700* | -0.132 |
| M/L FREQD | -0.128 | 0.092 | -0.391* | 0.185 | 0.282* | -0.352* | 0.228* | -0.228* | -0.183 | -0.338* | 0.421* | 0.405* | -0.450* | 0.407* |
| M/L TT | 0.057 | -0.085 | -0.202* | 0.093 | 0.087 | -0.219* | 0.177 | -0.054 | -0.093 | -0.183 | -0.151 | 0.743* | -0.336* | 0.667* |
| M/L TA | 0.086 | -0.075 | 0.140 | -0.077 | -0.103 | 0.518* | -0.016 | 0.131 | 0.085 | 0.128 | -0.352* | 0.081 | 0.515* | 0.119 |
| M/L $H_S$ | 0.185 | 0.074 | 0.078 | -0.279* | -0.115 | 0.102 | -0.082 | 0.082 | -0.036 | 0.222* | -0.349* | 0.175 | 0.000 | 0.050 |
| M/L $H_L$ | -0.010 | -0.122 | -0.230* | 0.200 | 0.134 | -0.283* | 0.168 | -0.152 | -0.123 | -0.466* | 0.286* | 0.596* | -0.304* | 0.407* |

*Significant ($p<0.05$) correlations

## 7.4 Discussion

In this study, a three-dimensional balance control model based on an optimal control strategy was developed, and evaluated in terms of its ability to simulate postural sway in both the A/P and M/L directions. Since COP-based measures are most commonly used to characterize postural sway (Baratto et al., 2002; Peterka, 2000; Prieto et al., 1996), we adopted COP-based measures to evaluate the simulation performance of the model. In general, COP-based measures can be classified into three groups: time-domain measures, frequency-domain measures, and statistic mechanical measures (e.g. Norris et al., 2005; Prieto et al., 1996). Each of these type were incorporated, including two time-domain measures (RMS and MV), two frequency-domain measures (CFREQ and FREQD), and four statistical mechanics measures (TT, TA, $H_S$, and $H_L$). Given this range of measures, results obtained from this study can be expected to reasonably account for diverse aspects of balance control mechanisms.

Predictions generated by the model appeared to be fairly accurate. Specifically, there were no significant differences between any simulated traditional measures and their experimental references, most of the means for these measures were near unity (0.9~1.1). In addition, the simulated measures were fairly consistent, having narrow confidence intervals, despite being generated across a range of participants and for conditions before and after localized muscle fatigue. Good performance was also found overall in predicting statistical mechanics measures. Again, there were no significant differences between measured and predicted values, however there was substantially more variability across participants and fatigue

conditions. According to these results, the three-dimensional balance control model appears able to accurately simulate postural sway behaviors. Such a model can be use to further investigate balance control mechanisms, especially when individual differences and task conditions (e.g., aging and LMF) affect balance control.

It is important to note the essential difference between the traditional and statistical mechanics measures derived from COP time series, and that each was used differently here. Experimental values of traditional measures must be available in advance, and were used to calculate the cost function. In contrast, experimental values of the statistical mechanics measures were only used after model specification and simulation. Thus, it seems unlikely that simulated traditional measures and simulated statistical mechanics measures would have the same level of accuracy. This argument may help explain why the widths of the 95% confidence intervals of the statistical mechanics measures were typically larger than those of the traditional measures (Fig. 7.5).

No significant or substantial difference was found in the cost function of the optimization procedure across several LMF conditions, suggesting that the ability of the model to accurately simulate COP-based measures is not affected by LMF. This was expected, since none of the model parameters or subparts of the model were specifically designed to reflect the presence or absence of LMF. LMF likely affected the COP time series, and the derived COP-based measures (Corbeil et al., 2003), yet the model has sufficient degrees of freedom (unspecified model parameters) to account for such changes such that simulation accuracy is not affected.

Several significant correlations were found between model parameters and COP-based

measures, and can be used to predict and/or specify how internal postural control changes affect balance control. For example, the sensory delay time at the hip ($\tau_{d2}$) had significantly positive correlations with TT and $H_L$ in both the A/P and M/L directions. An increased TT indicates that the open-loop control scheme has a longer duration, while an increased $H_L$ suggests that, over long-term intervals, postural control has become less anti-persistent. Both a longer open-loop control scheme and less anti-persistent postural control might result in a more unstable postural control system since the body posture tend to be further away from the equilibrium. Thus, it might be concluded that when the sensory delay time at the hip increased, the postural control system would become more unstable.

Similar analysis can be performed for other model parameters as well. In general, when the statistical mechanics measures increased, the postural control system tended to become more unstable. However, relationships between the statistical mechanics measures and some model parameters were not always consistent. For example, TA significantly increased with increases in random disturbance gains ($k_{n1}$ and $k_{n2}$), while TT and $H_L$ significantly decreased. In such cases, it cannot be determined whether larger random disturbance torques would lead to a more unstable postural control system simply by analyzing statistical mechanics measures. Additional COP-based measures should be considered. For instance, when random disturbance gains became larger, time-domain sway measures significantly increased, indicating that the projection of the whole body COM moved closer to the boundary of the BOS. Thus, a more unstable postural control system should have larger random disturbance joint torques.

The postural control system is a complex, and in most situations an automatic, control

system. It is generally accepted that the neural controller generates active joint control torques according to feedback regarding body orientations to maintain balance. Thus, balance control has always been analyzed from a control perspective (e.g., Iqbal et al., 2004; Ishida et al., 1997; Johansson et al., 1988). Existing control theories, however, are more effective in solving linear control problems, whereas the postural control system is obviously nonlinear. A two-dimensional single-segment inverted pendulum model has been used most often to represent the human body when modeling balance control because it is easy to be linearized. In contrast, three-dimensional balance control models have been rarely used previously due to its complexity, although such a model may be more valid.

In the present study, a linearized three-dimensional balance control model was developed. Several assumptions were made during linearization. For example, we assumed that the lower segment and upper segment only rotate in the sagittal and frontal planes, respectively, based on earlier evidence for the use of an ankle and hip strategy to control postural sway in these planes (Winter et al., 1996). Although these assumptions have some experimental support, we have to admit that the proposed model was limited by such assumptions since they are simplifications of a more complex reality. In addition to the limitations caused by these assumptions, some limitations in the two-dimensional balance control model also exist in the proposed three-dimensional balance control model, such as the model's dependence on the availability of experimental balance data to specify free model parameters. However, this model can be still considered valid to some extent due to its good performance in simulating and predicting COP-based measures, and provides a new step towards investigating three-dimensional balance

control models.

# Chapter 8 Model-based Assessments of the Effects of Aging and Localized Muscle Fatigue on Balance Control


## Abstract

The purpose of this study was to employ a three-dimensional balance control model to identify the effects of aging and localized muscle fatigue (LMF) on balance control. Data were obtained from a prior study which included both younger and older participants. Trials of quiet upright stance were performed by each participant; analyzed here were trials pre-fatigue, post-ankle-fatigue, and post-torso-fatigue. COP-based measures and unspecified model parameters were used to identify effects of age and fatigue. Compared with younger adults, COP mean velocities in the anterior-posterior medial-lateral directions increased 45.5% and 48.9%, respectively, in older adults. COP frequency dispersion in the anterior-posterior direction increased 4.7% with torso fatigue. When comparing the measured and simulated results, though discrepancies existed, most of the aging and localized muscle fatigue effects on simulated COP-based measures were qualitatively consistent with experimental findings. Changes in both COP-based measures and model parameters were used to infer potential mechanisms that cause the observed effects of aging and LMF.


## 8.1 Introduction

Recent studies have shown that aging affects the way in which humans maintain balance. For example, it is generally accepted that aging can deteriorate the accuracy of afferent balance control signals, and increase sensory delays (Tian et al., 2002). Era and Heikkinen (1985) found significant age-related changes in total sway displacement, which is proportional to mean velocity. Maki et al. (1990) investigated COP-based measures with 64 healthy young and elderly adults, and found that these measures demonstrated significant aging-related decreases in stability. In addition, McClenaghan et al. (1996) analyzed spectral characteristics of postural forces and pointed out that aging effects exist in spectral parameters obtained from M/L postural

forces. Prieto et al. (1996) also evaluated postural steadiness measures and found that COP-based measures, such as COP mean velocity and COP range, changed with age.

Localized muscle fatigue (LMF) also has effects on balance control. For example, Yaggie and McGregor (2002) isokinetically fatigued plantarflexors and dorsiflexors as well as invertors and evertors of the ankle, and found that both A/P sway and M/L sway increased significantly after fatigue. Corbeil et al. (2003) also induced muscular fatigue of ankle plantarflexors and found that this fatigue resulted in increased postural sway and a decreased long-term scaling exponent. The study done by Davidson et al. (2004) suggested that time-domain postural sway measures increased with lumbar extensor fatigue. Additionally, Hsiao and Simeonov (2001) identified that fatigue deteriorates the ability of the nervous system to regulate balance efficiently, and emphasized the necessity of understanding the effects of fatigue on balance control and fall prevention. Besides the studies mentioned above, there are also many investigations into fatigue effects (e.g., Burdet and Rougier, 2004; Caron, 2003; Gribble and Hertel, 2004; Miller and Birds, 1976), the results from which all demonstrate that fatigue has adverse effects on balance control.

In summary, changes in balance control with aging and LMF may lead to an increased risk of falling (e.g., Mackey and Robinovitch, 2006; Pline et al., 2006). Hence, understanding the mechanisms by which humans maintain balance, especially for the aged or in the presence of LMF, would be very helpful for the prevention of fall injuries.

To maintain balance, it is generally accepted that the projection of the COM should be kept inside the base of support (BOS). Therefore, to study how humans maintain balance, we

may investigate the oscillations of the COM during body sway. However, the locations of the COM cannot be easily measured. The COP is always in phase with the COM, and reflects the net motor control signal output necessary to keep the projection of the COM within the BOS (Cavanaugh et al., 2005; Prieto et al., 1993). In addition, COP-based and COM-based measures have been found to be highly correlated (Hasan et al., 1996). Most importantly, the COP can be measured easily using a force platform. A number of studies have already applied COP-based measures to identify aging or LMF effects on balance control (e.g., Corbeil et al., 2003; Norris et al., 2005).

As discussed in previous chapters, balance control models are a useful tool to investigate balance control. The first purpose of this study was to examine the ability of the proposed three-dimensional balance control model to simulate the effects of aging and LMF on balance control. These effects were quantified using COP-based measures derived from experimental data, and these same data were used to evaluate the simulation performance of a three-dimensional balance control model. The second purpose was to identify potential postural control mechanisms that cause the observed aging and LMF effects, by investigating intrinsic model parameters.

## 8.2 Method

### 8.2.1 Participants and experimental procedures

Thirty-two individuals (16 males and 16 females) without injuries, illness, and

musculoskeletal disorders participated in the study. These participants were evenly classified into two groups according to age (Table 8.1).

**Table 8.1 Demographic information on participants**

| | Old participants | | Young participants | |
|---|---|---|---|---|
| | Mean | SD | Mean | SD |
| Age (year) | 63 | 6.2 | 21 | 1.7 |
| Height (cm) | 167.4 | 12 | 171.4 | 7.0 |
| Body mass (kg) | 77.5 | 20.4 | 66.4 | 11.3 |

Several localized muscle fatigue conditions were tested, including ankle fatigue, knee fatigue, torso fatigue, and shoulder fatigue. Only ankle fatigue and torso fatigue were used for analysis in this study, because the control inputs in the proposed three-dimensional balance control model are the ankle control torque and hip control torque, and these torques are affected by ankle fatigue and torso fatigue, respectively. Further, fatigue at these two locations was found to have the most substantial effects on postural control as assessed by COP- and COM-based measures (Singh et al. 2005). A commercial dynamometer (Biodex Medical Systems, Shirley, NY) was used to induce fatigue in the ankle plantarflexors (ankle fatigue) and lumbar extensors (torso fatigue). During fatiguing exercises, participants performed isotonic exertions at 60% of their maximum voluntary isokinetic contraction at a speed of 12 repetitions/min. Fatigue was considered to be induced when participants could not complete the entire range of motion for three consecutive repetitions. COP data were then collected within 45 seconds after the fatiguing exercises. For details on COP data collection, please refer to section 7.2.3. Besides post-ankle-fatigue and post-torso-fatigue sway trials, a single pre-fatigue sway trial was also randomly selected from among three performed by each

participant.

### 8.2.2 Dependent COP-based measures

Numerous studies have demonstrated that postural sway increases with aging or LMF by using time-domain COP-based measures (Corbeil et al., 2003; Murry et al, 1975; Vuillerme et al., 2006). Glass and Mackey (1977) noted that altered periodicity was an indicator of reduced physiological functional ability, which might be caused by aging or LMF. Both time-domain and frequency-domain COP-based measures are traditional measures that were generally considered unable to account for the dynamic characteristics of the postural control system. Thus, statistical mechanics measures have been proposed (Collins and De Luca, 1993) and used to differentiate between individuals who differ in age or LMF conditions (Norris et al, 2005; Corbeil et al., 2003). We selected eight COP-based measures of different types to determine the effects of external loads on balance control (Chapter 5). In this study, we used these measures to investigate the effects of aging or LMF. These measures included RMS, MV, CFREQ, FREQD, TT, TA, $H_S$, and $H_L$. The descriptions and units of these measures were given in Table 6.1.

### 8.2.3 Model simulation and analysis

Ninety-six experimental trials of upright stance were simulated using the three-dimensional balance control model (described in Chapter 7). These trials were evenly classified into two groups (old and young) according to the age of the participants. In addition,

when taking LMF into account, 32 trials were under the pre-fatigue condition; 32 trials were under the post-ankle-fatigue condition; and the remaining 32 trials were under the post-torso-fatigue condition. Based on the experimental and simulation results from these 96 trials, two-way repeated measures ANOVAs were performed to identify significant ($p<0.05$) changes in COP-based measures and model parameters with aging or LMF. Since LMF had three levels (pre-fatigue, post-ankle-fatigue and post-torso-fatigue), post-hoc pairwise comparisons were conducted using the Tukey's honestly significant difference (HSD) criterion. To validate the three-dimensional balance control model, model-based predictions and experimental results were compared qualitatively according to the trends in COP-based measures versus aging or LMF.

## 8.3 Results

### 8.3.1 Fatigue and aging effects on COP-based measures

Significant main effects of aging were found on MV, CFREQ, FREQD, TT, and $H_L$ in both the A/P and M/L directions (Fig. 8.1). More specifically, A/P MV, M/L MV, A/P CFREQ, and M/L CFREQ increased, while A/P FREQD, M/L FREQD, A/P TT, M/L TT, A/P $H_L$, and M/L $H_L$ decreased with aging. There were also significant main effects of LMF on A/P FREQD, M/L FREQD, A/P TA, and M/L $H_L$ (Fig. 8.2). Post-hoc comparisons indicated that torso fatigue led to increases in A/P FREQD and A/P TA, and decreases in M/L FREQD and M/L $H_L$. In addition, significant differences between the post-ankle-fatigue and post-torso-fatigue

conditions were also found in A/P FREQD and A/P TA.

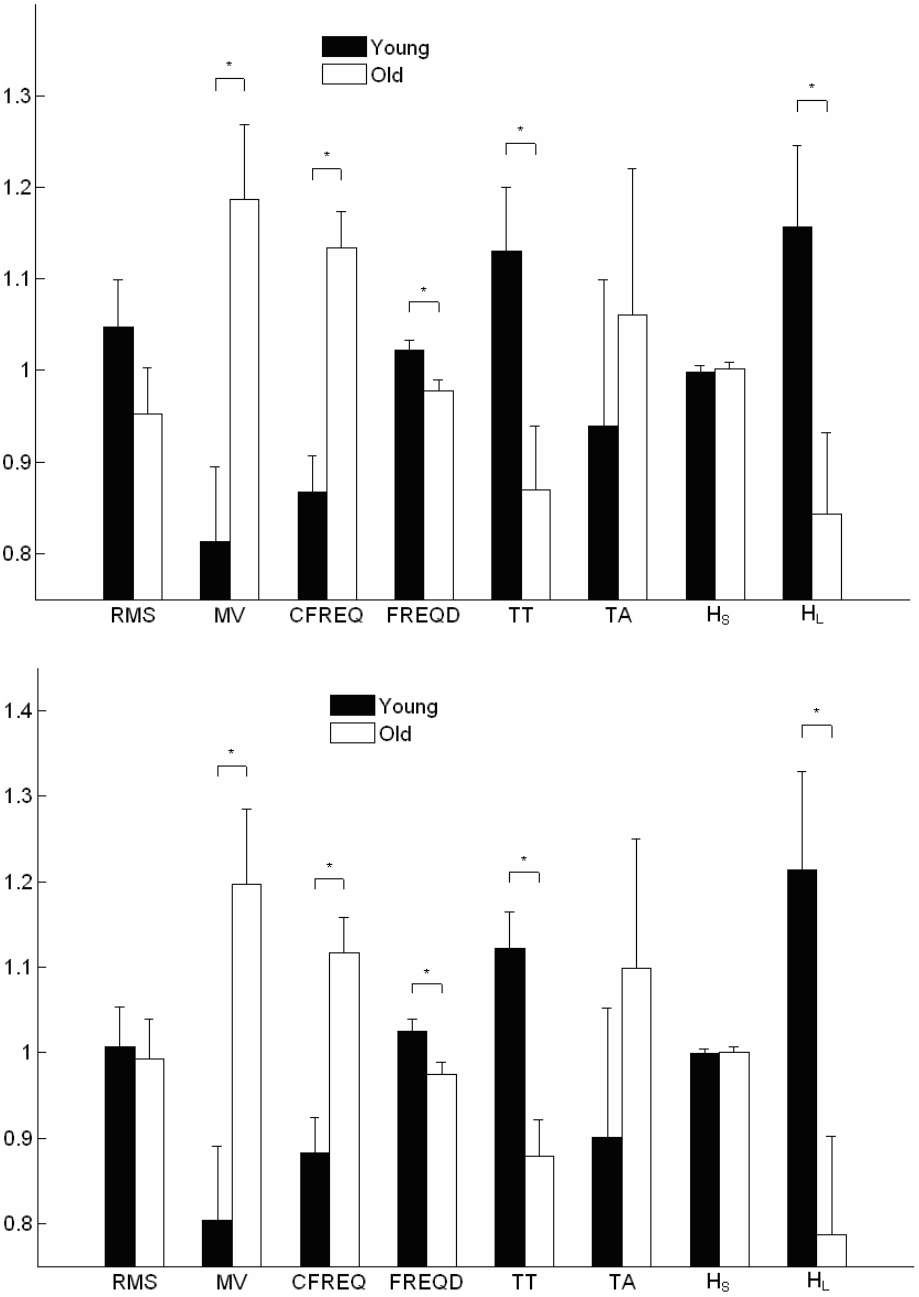


**Figure 8.1 Effects of aging on experimental COP-based measures (top: A/P; bottom: M/L). Significant differences (p-value<0.05) are noted by *, and error bars indicate one standard error. The values of experimental COP-based measures here were normalized by their corresponding averages (Table 8.6) in order to have the distributions of all measures illustrated in the same figure.**

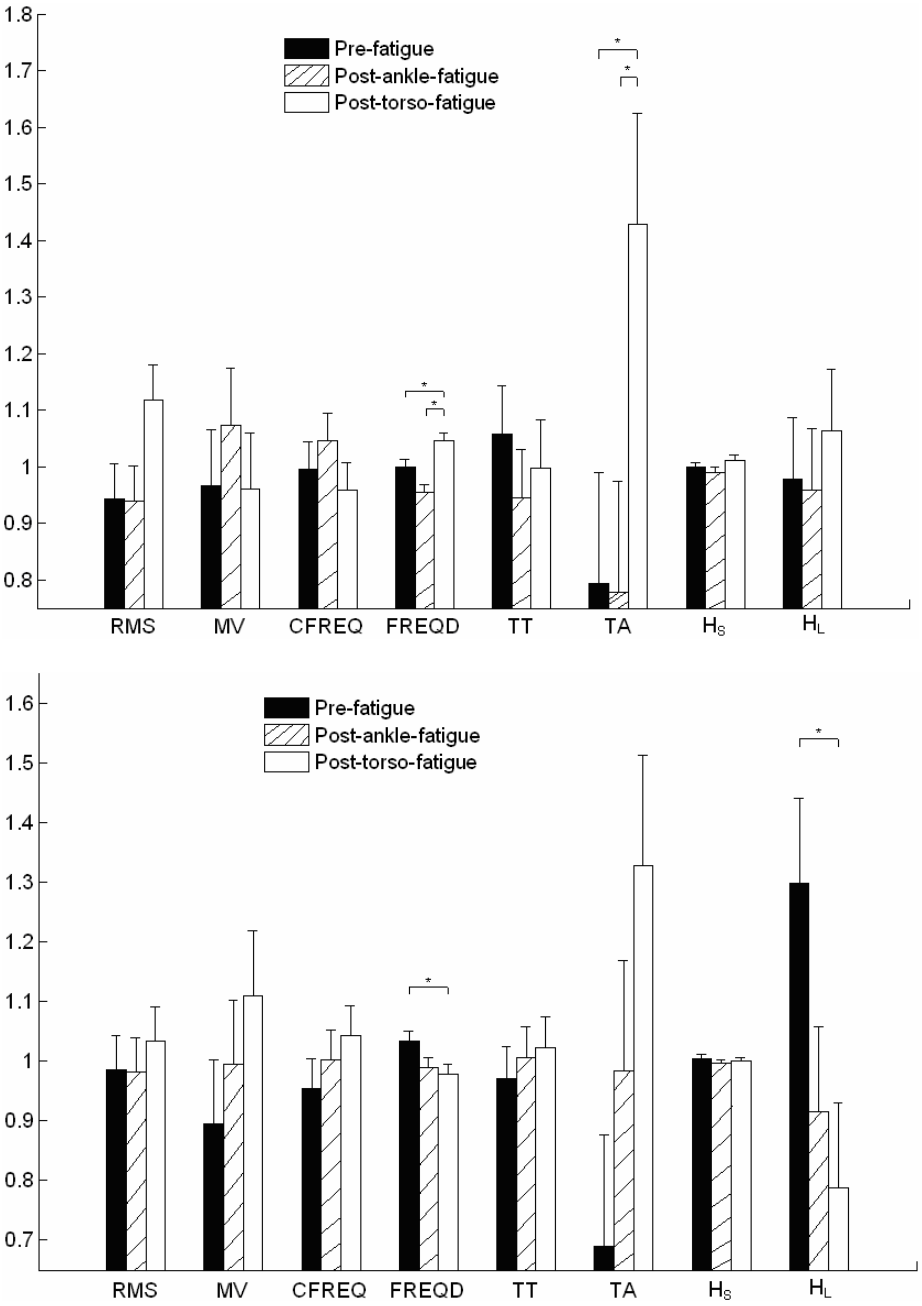


**Figure 8.2 Effects of LMF on experimental COP-based measures (top: A/P; bottom: M/L). Significant differences (p-value<0.05) are noted by *, and error bars indicate one standard error. The values of experimental COP-based measures here were normalized by their corresponding averages (Table 8.2) in order to have the distributions of all measures illustrated in the same figure.**

**Table 8.2 Means (SD) of experimental COP-based measures**

| Measures | RMS | MV | CFREQ | FREQD | TT | TA | $H_S$ | $H_L$ |
|---|---|---|---|---|---|---|---|---|
| A/P | 6.55(2.37) | 15.09(8.82) | 0.63(0.19) | 0.85(0.07) | 0.51(0.25) | 28.03(31.52) | 0.81(0.04) | 0.17(0.11) |
| M/L | 6.26(1.99) | 16.28(10.27) | 0.66(0.20) | 0.82(0.08) | 0.43(0.14) | 38.13(40.49) | 0.83(0.03) | 0.12(0.10) |

Analysis of variance of the simulated measures revealed that significant main effects of aging occurred for A/P MV, A/P CFREQ, A/P TT, A/P $H_L$, M/L MV, M/L CFREQ, and M/L $H_L$, and significant LMF effects for A/P FREQD, A/P TA, A/P $H_L$, and M/L FREQD (Fig. 8.3 and Fig. 8.4). Specifically, A/P MV, M/L MV, A/P CFREQ, M/L CFREQ increased, and A/P TT, A/P $H_L$, and M/L $H_L$ decreased with aging. A/P FREQD and A/P TA increased, and M/L FREQD decreased with torso fatigue. A/P FREQD, A/P $H_L$, and M/L FREQD decreased with ankle fatigue.

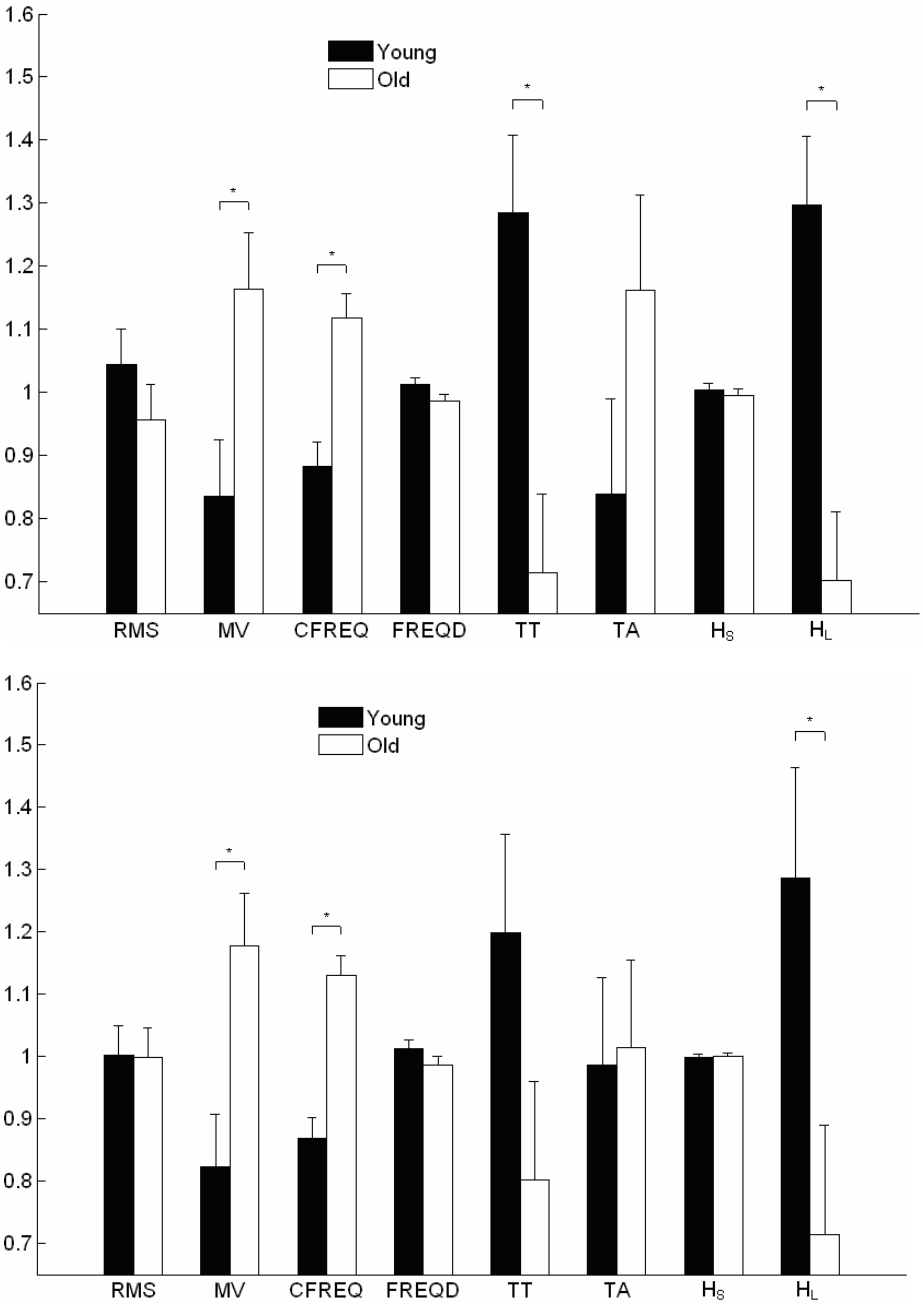


**Figure 8.3 Effects of aging on simulated COP-based measures (top: A/P; bottom: M/L). Significant differences (p-value<0.05) are noted by *, and error bars indicate one standard error. The values of simulated COP-based measures here were normalized by their corresponding averages (Table 8.7) in order to have the distributions of all measures illustrated in the same figure.**

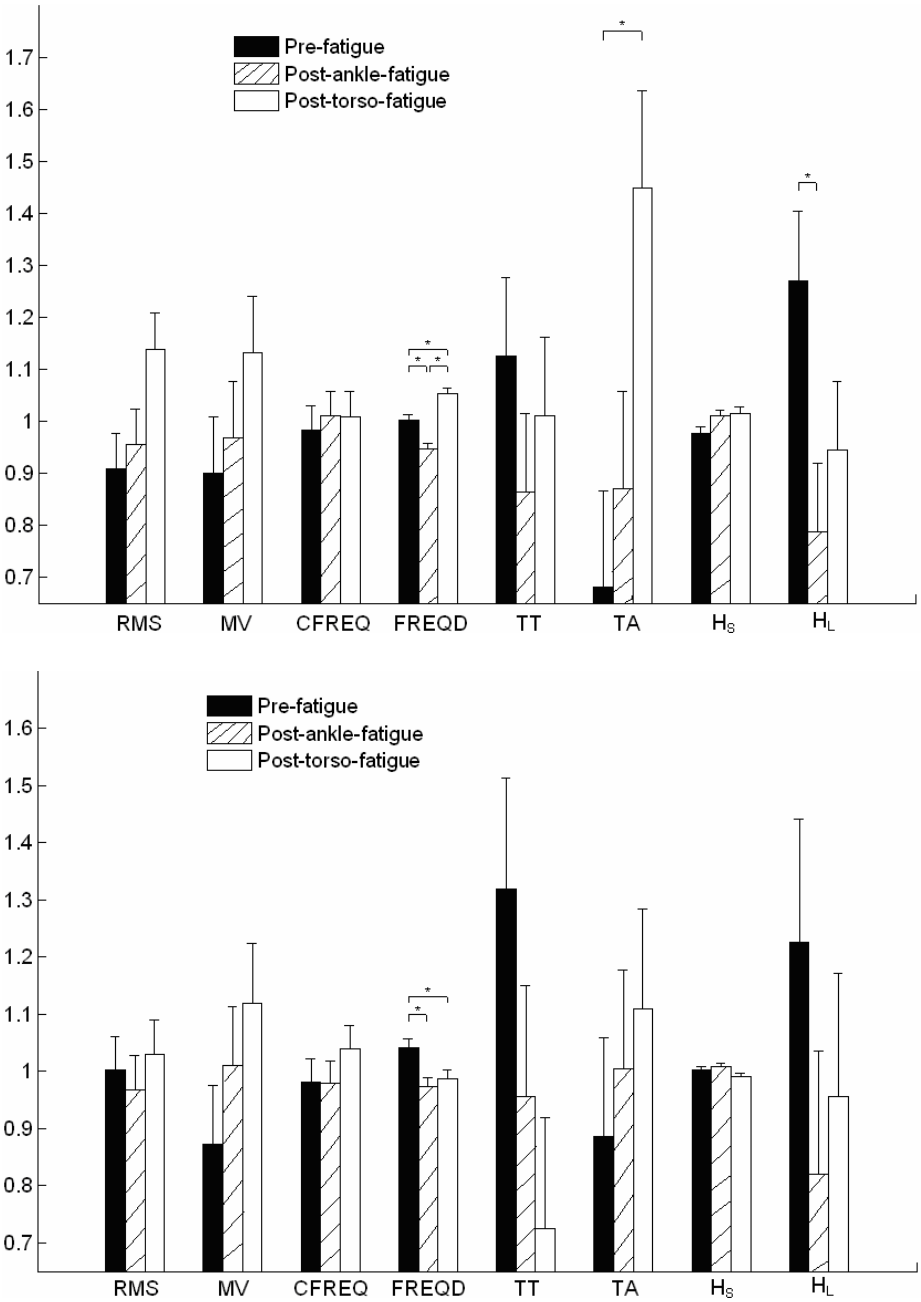


**Figure 8.4 Effects of LMF on simulated COP-based measures (top: A/P; bottom: M/L). Significant differences (p-value<0.05) are noted by *, and error bars indicate one standard error. The values of simulated COP-based measures here were normalized by their corresponding averages (Table 8.3) in order to have the distributions of all measures illustrated in the same figure.**

**Table 8.3 Means (SD) of simulated COP-based measures**

| Measures | RMS | MV | CFREQ | FREQD | TT | TA | $H_S$ | $H_L$ |
|---|---|---|---|---|---|---|---|---|
| A/P | 6.18(2.49) | 13.26(8.29) | 0.55(0.16) | 0.88(0.07) | 1.85(1.64) | 47.30(52.37) | 0.77(0.05) | 0.24(0.20) |
| M/L | 6.23(2.02) | 16.19(9.89) | 0.66(0.17) | 0.87(0.08) | 0.87(0.99) | 48.78(46.89) | 0.80(0.03) | 0.11(0.14) |

### 8.3.2 Comparison between experimental and simulated measures

Among the dependent COP-based measures that significantly changed with aging, the proposed three-dimensional balance control model was able to accurately predict changes in A/P MV, A/P CFREQ, A/P TT, A/P $H_L$, M/L MV, M/L CFREQ, and M/L $H_L$. However, no significant differences were found in the simulated A/P FREQD, M/L FREQD, and M/L TT between younger and older adults. In addition, except for A/P $H_S$, all simulated COP-based dependent measures showed the same average change trends with their corresponding experimental measures.

Almost all significant changes in experimental COP-based dependent measures caused by LMF were reflected in the simulated data. The only exception occurred in M/L $H_{L,}$ which significantly decreased with torso fatigue according to the measured data. Although the simulated M/L $H_L$ showed a decreasing trend with torso fatigue, this trend was not statistically significant. The proposed model also predicted that ankle fatigue significantly affected A/P FREQD, A/P $H_L$, and M/L FREQD, which is not consistent with the experimental findings.

### 8.3.3 Fatigue and aging effects on model parameters

Several model parameters significantly changed with aging (Fig. 8.5), including the weights of ankle sway angular velocity ($w_{21}$) and hip control torque ($w_{32}$), and random

disturbance gains and sensory delay times at the ankle ($k_{n1}$, $\tau_{d1}$) and hip ($k_{n2}$, and $\tau_{d2}$). Specifically, all of these parameters became larger in older adults. At the same time, LMF only significantly affected the sensory delay time at the hip ($\tau_{d2}$), which increased with torso fatigue (Fig. 8.6).

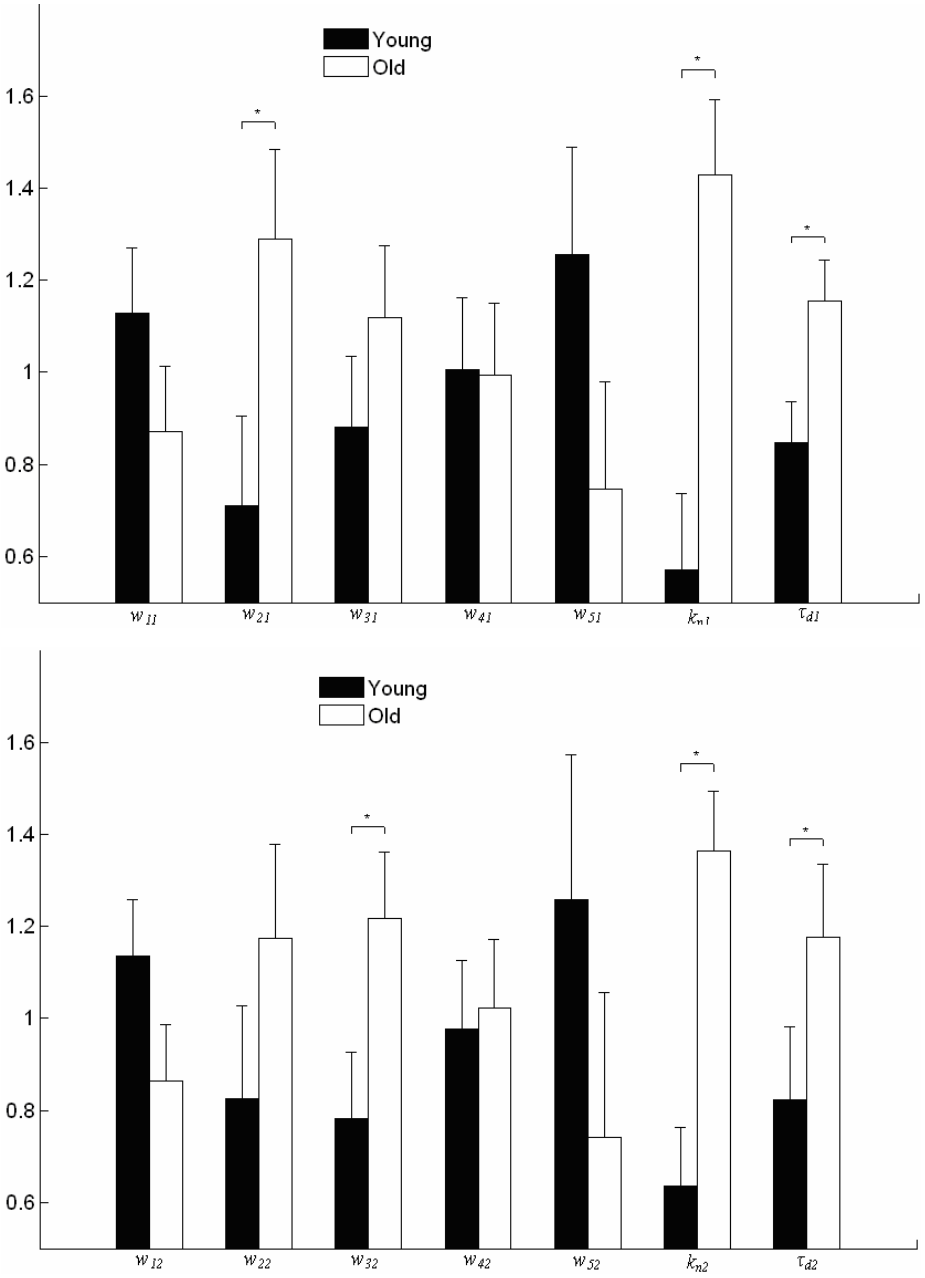


**Figure 8.5 Effects of aging on model parameters. Significant differences (p-value<0.05) are noted by *, and error bars indicate one standard error. The values of model parameters**

**here were normalized by their corresponding averages (Table 8.4) in order to have the distributions of all measures illustrated in the same figure.**

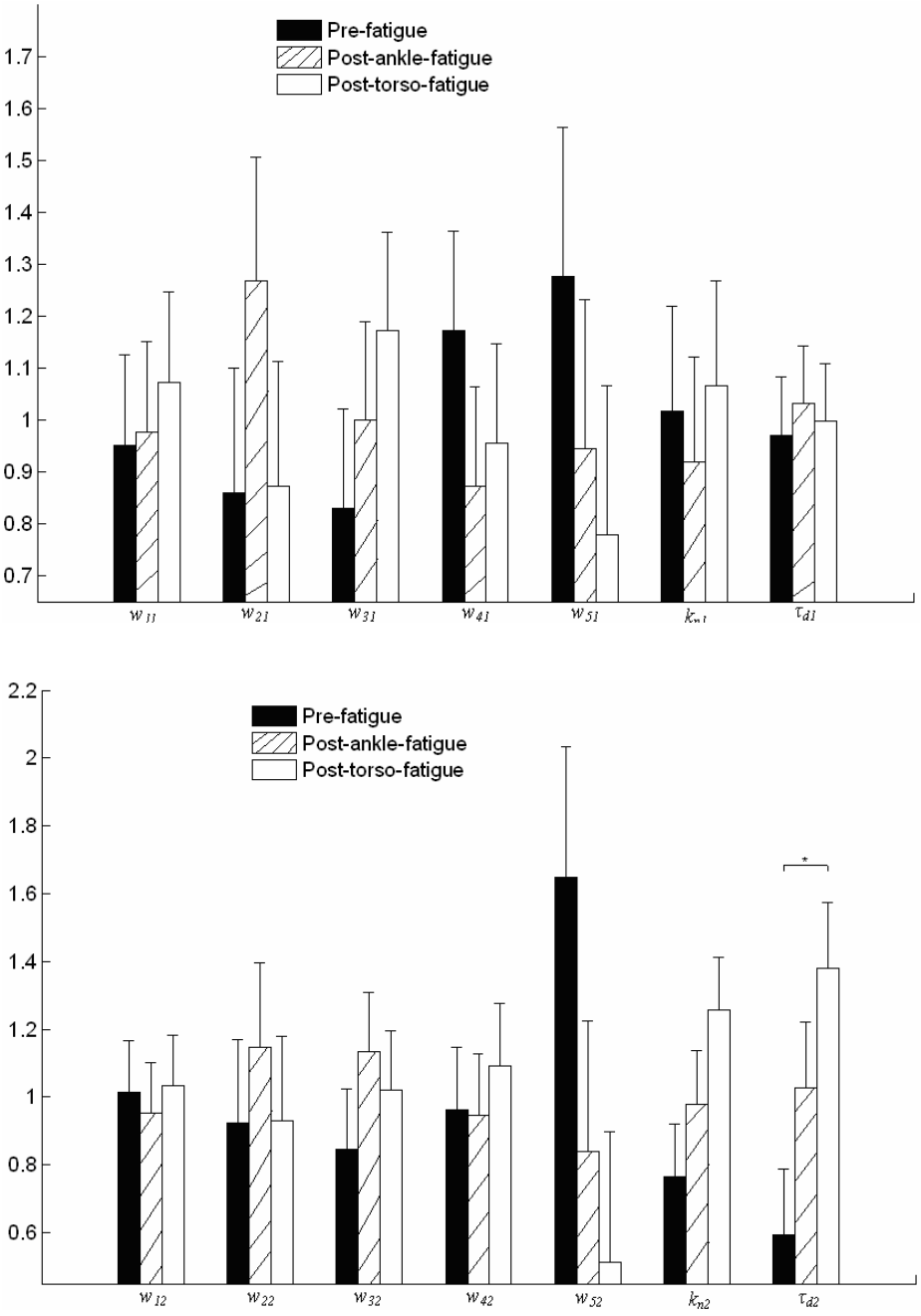


**Figure 8.6 Effects of LMF on normalized model parameters. Significant differences (p-value<0.05) are noted by *, and error bars indicate one standard error. The values of model parameters here were normalized by their corresponding averages (Table 8.4) in order to have the distributions of all measures illustrated in the same figure.**

**Table 8.4 Means (SD) of model parameters in the three-dimensional balance control model**

| Ankle Parameters | | Hip Parameters | |
|---|---|---|---|
| $w_{11}$ | 0.330(0.318) | $w_{12}$ | 0.377(0.327) |
| $w_{21}$ | 0.165(0.226) | $w_{22}$ | 0.107(0.149) |
| $w_{31}$ | 0.168(0.179) | $w_{32}$ | 0.201(0.204) |
| $w_{41}$ | 0.244(0.260) | $w_{42}$ | 0.249(0.265) |
| $w_{51}$ | 0.093(0.149) | $w_{52}$ | 0.066(0.147) |
| $k_{n1}$ | 192.9(230.3) | $k_{n2}$ | 235.7(226.4) |
| $\tau_{d1}$(ms) | 42.1(26.8) | $\tau_{d2}$(ms) | 17.0(19.1) |

## 8.4 Discussion

One purpose of this study was to investigate the effects of aging and LMF on balance control. Since COP data have been widely used to characterize sway behaviors, we adopted 16 COP-based measures that were able to sufficiently reflect properties of COP trajectories as dependent measures to quantify these effects. MV in both the A/P and M/L directions were found to significantly increase with aging, while there were no age-related changes in A/P RMS and M/L RMS (Fig. 8.1). These findings are in agreement with previous studies (Maki et al., 1990; Prieto et al., 1996). Time-domain COP-based measures can be used to estimate the displacement amplitude of COM. Since aging led to significant increases in A/P MV and M/L MV, the displacement amplitude of COM may become larger and get closer to the boundary of the BOS in older adults. Thus, older adults would seem to be at a higher risk of a loss of balance and subsequent fall.

COP-based measures accounting for central spectral tendency (A/P CFREQ and M/L CFREQ) became significantly larger in older adults (Fig. 8.1), indicating an increase in the

amplitude of higher frequency components in the A/P and M/L postural forces. In addition, it can be surmised that variability in the frequency content of the A/P and M/L postural forces decreases with aging, since both A/P FREQD and M/L FREQD became significantly smaller in older adults (Fig. 8.1). We also found that TT and $H_L$ in both directions significantly decreased with aging (Fig. 8.1). Smaller TT and smaller $H_L$ indicate a shorter open-loop control scheme and more anti-persistent postural control over long-term intervals, respectively. In addition, postural control tends to be more persistent in a larger region over short-term intervals for older adults, as indicated by the increases in TA and $H_S$ with aging (Fig. 8.1).

Ankle fatigue did not appear to affect balance control, since no significant differences were found in any COP-based dependent measure between the pre-fatigue and post-ankle-fatigue conditions (Fig. 8.2). Torso fatigue resulted in a significant increase of A/P FREQD and a significant decrease of M/L FREQD, indicating that variability in the frequency content of the A/P and M/L postural forces increased and decreased, respectively, with torso fatigue (Fig. 8.2). In addition, since both A/P TA and M/L $H_L$ significantly changed with torso fatigue as well (Fig. 8.2), we may conclude that, in the presence of torso fatigue, individuals adopt a persistent control strategy over a larger region in the sagittal plane over short-term intervals, whereas in the long-term region they would adopt a less anti-persistent M/L postural control strategy.

Another purpose of this study was to examine the ability of the proposed three-dimensional balance control models to accurately simulate aging and LMF effects. As noted earlier, though some discrepancies exist, most of the aging and LMF effects on simulated COP-based measures were qualitatively consistent with experimental findings. These results

indicate that the proposed three-dimensional balance control models could accurately simulate aging and LMF effects to some degree, and further supports the argument that these models can be used to investigate how humans maintain balance. In addition, identifying the changes in COP-based measures with either aging or LMF is the initial step in developing interventions to reduce age- or LMF-related falls (McClenaghan et al., 1996). Since the proposed models were able to accurately predict most changes in COP-based measures, they will also be useful tools for the development of fall interventions. At the same time, use of mathematical models can help avoid the need for collecting actual balance control data in some cases.

Changes of model parameters with aging and LMF may reflect how the neural controller adjusts underlying control mechanisms to maintain upright balance under different conditions of interest. It has been generally accepted that aging adversely affects the accuracy of control signals by increasing sensory noise and elevating sensory thresholds (Ahmed and Ashton-Miller, 2005; Gilsing et al., 1995; Tian et al., 2002). Accuracy of the control signal is influenced in the simulation model by the random disturbance gain ($k_n$). With larger disturbance gains, the accuracy of the control signal decreases. In addition, sensory delay has also been generally considered to increase with aging (Ahmed and Ashton-Miller, 2005). Since the random disturbance gains and sensory delays significantly increased with aging, the proposed balance control models were able to provide a plausible control mechanism that explained the effects of aging.

It has been suggested that muscle fatigue slows neural transmission (Basmajian and DeLuca, 1985), and decreases the position sense acuity (Björklund et al., 2000). Thus, in the

present study, random disturbance gains and simulated sensory delays should have significantly increased with LMF as well. However, only sensory delay $\tau_{2d}$ was found to significantly increase with torso fatigue. This unexpected result may be explained by the fact that different protocols were adopted to induce fatigue between the current study and previous ones. Other factors, such as the use of heuristic methods to search optimal solutions and approximation of delayed sway angles, may also have led to this result.

In addition to random disturbance gain and sensory delay, other model parameters were used to weight the physical quantities relevant to sway. A larger weight might indicate that the neural controller places more emphasis on the corresponding physical quantity when maintaining upright balance. For example, the weight of ankle torque acceleration ($w_{51}$) was larger in younger adults, so it might be concluded that ankle torque acceleration plays a more important role in balance control in younger versus older adults. Note that it is still impossible for us to specify the exact relevant physical quantities that the neural controller may take into account when maintaining balance, and that heuristic methods cannot give exact optimal solutions in the optimization procedure. Thus, we cannot completely rely on the simulated weighting model parameters to indicate the relative importance of different relevant physical quantities. The simulation results only provide us with a preliminary understanding of these physical quantities' role in balance control. Further investigation should be done to confirm the simulation findings.

In summary, this study investigated the effects of aging and LMF on balance control using both measures of postural sway (experimental and simulated) and intrinsic parameters of a

balance control model. The proposed three-dimensional balance control model was able to accurately predict seven out 10 significant aging effects and three of four significant LMF effects on dependent COP-based measures. Changes of model parameters with aging and LMF can also provide insights into complex postural control during quiet upright stance. Thus, this model might aid in further investigating balance control mechanisms and evaluating the potential impact of intervention strategies for the improvement of balance.

# Chapter 9 Conclusion and Future Research

## 9.1 Research Contributions

The research presented in this dissertation focused on two areas: lifting motion simulation and balance control modeling. A novel approach to predict lifting motions based on fuzzy logic control was proposed. This approach may be useful not only in ergonomic design, but also in the investigation of possible control mechanisms adopted by the neural controller to plan motions. Meanwhile, two-dimensional and three-dimensional balance control models based on an optimal control strategy were developed. These models were able to accurately simulate COP-based measures, and were successful in accounting for the effects of aging, localized muscle fatigue, and external loads on balance control. Thus, these models may be applicable in the development and evaluation of interventions intended to maximize the capacity of the postural control system and to minimize losses of balance and associated fall events.

## 9.2 Strengths and Limitations

### 9.2.1 Lifting Motion Simulation

The presented lifting motion simulation model based on fuzzy logic control was able to simulate two-dimensional lifting motions. Based on the results, some hypotheses regarding how the neural controller works may be offered. In essence, the presented model is data-based, since recorded motion data are needed to generate fuzzy rules. Yet unlike existing data-based models, this model is able to investigate how the neural controller plans motions by interpreting

fuzzy rules. These fuzzy rules are not based on any assumptions, but rather stem from observed motion data. Thus, the presented model may have a higher level of construct validity than optimization-based models.

However, several limitations still exist when using this model. First, due to the properties of linguistic terms, there is no way to obtain the exact rules between fuzzy inputs and outputs. Possible rules can be only roughly estimated by analyzing actual motion trajectories. Second, we assumed that the neural controller adopted the same strategy for different but similar lifting motions. This may not necessarily be true in reality, as humans may have many options to complete a given motion task and the motion planning may have a stochastic component. Third, some features of the predicted motions, such as motion duration, must be specified externally. While durations may be externally specified or predictable in some cases (e.g. assembly line tasks), this is clearly not true for all tasks of interest. Fourth, this model may be computationally inefficient since an optimization procedure was adopted to determine the values of membership function parameters and fuzzy rules had to be specified manually. Fifth, several assumptions were made during model simulation for simplicity. For example, we assumed that motions of five joints were independent. These assumptions might not be valid in reality, but were required in this initial model development in order to improve computational efficiency.

### 9.2.2 Balance Control Modeling

One strength of the balance control models presented in this dissertation is that they were able to accurately simulate sway behaviors. Further, we have presented an approach for

determining what to optimize and how to optimize when modeling balance control during spontaneous sway. Modeling the neural controller as an optimal controller stems from a physiological basis, in that it is possible to incorporate physical quantities relevant to sway into the performance index defined in the optimal controller. It is also physiologically plausible that the state *x* (see Eq. 4.8 or Eq. 6.4 for the two-dimensional balance control model; Eq. 7.10 for the three-dimensional balance control model) can be fed back to the neural controller to generate the optimal control signal. Specifically, muscle spindles can sense the joint angular displacement and velocity (van der Kooij et al., 1999), and the state variables related to joint torques are internal states of the neural controller. At the same time, these models can be used to analyze potential balance control mechanisms for different groups of subjects by simply comparing their model parameters (e.g., sensory delay time). In this dissertation, for example, the presented models were able to identify possible underlying age-related and localized-muscle-fatigue-related differences in balance control mechanisms. In addition, these models may aid in predicting human physiological reactions used in maintaining balance, and facilitate evaluating the potential impact of intervention strategies for the improvement of balance.

The models presented here also have some limitations. First, only a few physical quantities that may affect spontaneous sway can be incorporated into the performance index. Second, the neural controller may not use an optimal control strategy to generate the motor plans that lead to spontaneous sway. Based on the simulation results, we may say that the optimal control strategy can at least partly explain the neural controller; however, this does not mean that

the neural controller necessarily adopts such a control strategy. Third, given that approximations were made to some trigonometric functions, the presented models are only applicable for small amplitudes of planar sway motion. Fourth, these models depend on experimental data to determine the parameters. Fifth, heuristic approaches were used in the optimization procedure, and thus do not guarantee that the obtained set of model parameters was globally optimal.

## 9.3 Future Research

### 9.3.1 Lifting Motion Simulation

Currently, simulation of any novel lifting motion uses the root lifting motion from the same participant to generate fuzzy rules, and only two-dimensional lifting motions were simulated. The presented model should also be able to simulate motions across individuals (e.g., using a root motion and novel motion from different individuals), and be applicable to two-dimensional and three-dimensional motions of other types (so long as some root motions are available). Thus, in future research, the ability of the presented model to simulate lifting motions across individuals and to simulate two-dimensional and three-dimensional motions of other types should be investigated. At the same time, sensitivity analyses, generalizability, and investigations of the effects of some tasks attributes on the observable trends in fuzzy variable trajectories are also worthy areas of future investigation.

### 9.3.2 Balance Control Modeling

Modeling sensory systems as a time delay might be too simple, especially when the interest is in studying how sensory systems work during quiet upright stance. In future research, a balance control model with more complex sensor dynamics should be investigated. In addition, as we discussed above, some other control strategies have been adopted when modeling balance control, such as PID control strategy and sliding model control strategy. The exact control strategy adopted by the neural controller is still controversial. Thus, it would be of interest to compare the ability of balance control models with different control strategies to simulate sway behaviors in future research, which may help to identify the actual control strategy.

# References


Abdel-Malek, K., Mi, Z., Yang, J., Nebel, K. (2006) Optimization-based trajectory planning of the human upper body. *Robotica 24*: 683-696.

Ahmed, A.A., Ashton-Miller, J.A. (2005) Effect of age on detecting a loss of balance in a seated whole-body balancing task. *Clinical Biomechanics 20*: 767-775.

Alexandrov, A.V., Frolov, A.A., Massion, J. (2001) Biomechanical analysis of movement strategies in human forward trunk bending. I. modeling. *Biological Cybernetics 84*: 425-434.

Applegate C., Gandevia S.C., Burke D. (1988) Changes in muscle and cutaneous cerebral potentials during standing. *Experimental Brain Research 71*: 183–188.

Bajpai, A.C., Mustoe, L.R., Walker, D., 1978. Advanced Engineering Mathematics. John Wiley & Sons, New York, pp195-198.

Baratto, L., Morasso, P.G., Re, C., Spada, G. (2002) A new look at posturaographic analysis in the clinical context: sway-density versus other parameterization techniques. *Motor Control 6*: 246-270.

Basmajian, J.V., DeLuca, C.J. (1985) *Muscles alive: their functions revealed by electromyography*. Baltimore: Williams & Wilkins.

Bays, P.M., Wolpert, D.M. (2007) Computational principles of sensorimotor control that minimize uncertainty and variability. *Journal of Physiology 578*: 387-396.

Beck, D.J., Chaffin, D.B. (1992) An evaluation of inverse kinematics models for posture prediction. In Mattila, M. and Karwowski, W. (Eds), *Computer Applications in Ergonomics, Occupational Safety and Health.* Armsterdam: Elsevier.

Bernard, J.A. (1988) Use of rule-based system for process control. *IEEE Control Systems Magazine* 8: 3-13.

Björklund, M., Crenshaw, A. G., Djupsjöbacka, M., Johansson, H. (2000) Position sense acuity is diminished following repetitive low-intensity work to fatigue in a simulated occupational setting. *European Journal of Applied Physiology 81*: 361-367.

Bolognani, S., Zigliotto, M. (1996) Fuzzy logic control of a switched reluctance motor drive. *IEEE Transaction on Industry Application 32*: 1063-1068.

Bottaro A., Casadio, M., Morasso, P.G., Sanguineti, V. (2005) Body sway during quiet standing: Is it the residual chattering of an intermittent stabilization process? *Human Movement Science 24*: 588-615.

Breteler, M.D.K., Gielen, S.C.A.M., Meulenbroek, R.G.J. (2001) End-point constraints in aiming movements: effects of approach angle and speed. *Biological Cybernetics 85*: 65-75.

Brumagne, S., Cordo, P., Verschueren, S. (2004) Proprioceptive weighting changes in persons with low back pain and elderly persons during upright standing. *Neuroscience Letters 366*: 63-66.

Buckles, B.P., Petry, F.E. (1992) *Genetic Algorithms*. Los Alamitos, Calif: IEEE computer society press.

Burdet, C., Rougier, P. (2004) Effects of utmost fatigue on undisturbed upright stance control. *Science & Sports 19*: 308-316.

Carver, S., Kiemel, T., Jeka, J.J. (2006) Modeling the dynamics of sensory reweighting. *Biological Cybernetics 95*: 123-134.

Carver, S., Kiemel, T., van der Kooij, H., Jeka, J.J. (2005) Comparing internal models of the dynamics of the visual environment. *Biological Cybernetics 92*: 147-163.

Caron, O. (2003) Effects of local fatigue of the lower limbs on postural control and postural stability in standing posture. *Neuroscience Letters 340*: 83-86.

Castro, J.L. (1995) Fuzzy logic controllers are universal approximators. *IEEE Transactions on Systems, Man and Cybernetics 25*: 629-635.

Casadio, M., Morasso, P.G., Sanguineti, V. (2005) Direct measurement of ankle stiffness during quiet standing: implications for control modeling and clinical application. *Gait & Posture 21*: 410-424.

Cavanaugh, J.T., Guskiewicz, K.M., Stergiou, N. (2005) A nonlinear dynamic approach for evaluating postural control. *Sports medicine 35*: 935-950.

Cenciarini, M., Peterka, R.J. (2006) Stimulus-dependent changes in the vestibular contribution to human postural control. *Journal of Neurophysiology 95*: 2733-2750.

Chaffin, D. B., Erig, M. (1991) Three-dimensional biomechanical static strength prediction model sensitivity to postural and anthropometric inaccuracies. *IIE Transactions, 23*, 215-227.

Chaffin, D.B., Andersson, G.B.J., Martin B.J. (1999) *Occupational Biomechanics*. New York: John Wiley & Sons.

Chaffin, D.B., Faraway, J.J., Zhang, X. (1999) *Simulating reach motions.* Paper presented at *the Proceedings of the SAE Digital Human Modeling for Design and Engineering International Conference and Exposition.*

Chaffin, D.B. (Eds.). (2001) *Digital human modeling for vehicle and workplace design*. Warrendale, PA: Society of Automotive Engineers, Inc.

Chaffin, D.B. (2005) Improving digital human modeling for proactive ergonomics in design. *Ergonomics 48*: 478-491.

Chang, C., Brown, D.R., Bloswick, D.S., Hsiang, S.M. (2001) Biomechanical simulation of manual lifting using spacetime optimization. *Journal of Biomechanics 34*: 527-532.

Chow, D., Kwok, M., Cheng, J., Lao, M., Holmesm A., Au-Yang, A., Yao, F., Wong, M.S. (2006) The effect of backpack weight on the standing posture and balance of schoolgirls with adolescent idiopathic scoliosis and normal controls. *Gait Posture 24*: 172-181.

Collins, J.J., De Luca, C.J. (1993) Open loop and closed loop control of posture: A random-walk analysis of center of pressure trajectories. *Experimental Brain Research 95*: 308-318.

Collins, J.J., De Luca, C.J., Burrows, A., Lipsitz, L.A. (1995) Age-related changes in open-loop and closed-loop postural control mechanisms. *Experimental Brain Research 104*: 480-492.

Corbeil, P., Blouin, J.S., Begin, F., Nougier, V., Teasdale, N. (2003) Perturbation of the postural control system induced by muscular fatigue. *Gait & Posture 18*: 92-100.

Cornilleau-Peres, V., Shabana, N., Droulez, J., Goh, J.C.H., Lee, G.S.M., Chew, P.T.K. (2005) Measurement of the visual contribution to postural steadiness from the COP movement: methodology and reliability. *Gait & Posture 22*: 96-106.

Craig, J. J. (1989) *Introduction to robotics: mechanics and control* (2nd ed.). Reading, MA: Addison-Wesley.

Davidson, B.S., Madigan, M.L., Nussbaum, M.A. (2004) Effects of lumbar extensor fatigue and fatigue rate on postural sway. *European Journal of Applied Physiology 93*: 183-189.

Delignieres, D., Deschamps, T., Legros, A., Caillou, N. (2003) A methodological note on nonlinear time series analysis: is the open- and closed-loop model of Collins and De Luca (1993) a statistical artifact? *Journal of Motor Behavior 35*: 86-97.

De Silva, C.W. (1995) *Intelligent control – fuzzy logic applications*. Boca Raton, FL: CRC Press.

Der Leva, Paolo (1996) Adjustments to Zatsiorsky-seluyanov's segment inertia parameters. *Journal of Biomechanics 29*: 1223-1230.

Dessing, J.C., Caljouw, S.R., Peper, C.E., Beek, P.J. (2004) A dynamic neural network for hitting an approaching object. *Biological Cybernetics 91*: 377-387.

Dornan, J., Fernie, G.R., Holliday, P.J. (1978) Visual inputs: Its importance in the control of postural sway. *Archives of Physical Medicine and Rehabilitation 59*: 586-591.

Du Pasquier, R.A., Blanc Y., Sinnreich M., Landis T., Burkhard P., Vingerhoets F.J.G. (2003) The effect of aging on postural stability: a cross sectional and longitudinal study. *Neurophysiologie Clinique 33*: 213-218.

Duarte, M., Zatsiorsky, V.M. (2000) On the fractal peoperties of natural human standing. *Neuroscience Letters 283*: 173-176.

Dysart, M. J., Woldstad, J. C. (1994) *Development and validation of a posture prediction algorithm for a static lifting task.* Paper presented at the *Proceedings of the Triennial Congress of the International Ergonomics Association - IEA '94*.

Dysart, M. J., Woldstad, J. C. (1996) Posture prediction for static sagittal-plane lifting. *Journal of Biomechanics 29*: 1393-1397.

Era, P., Heikkinen, E. (1985) Postural sway during standing and unexpected disturbance of balance in random samples of men of different ages. *Journals of gerontology 40*: 287-295.

Fagg, A.H., Shah, A., Barto, A.G., (2002) A computational model of muscle recruitment for wrist movement. *Journal of Neurophysiology 88*: 3348-3358.

Faraway, J.J (1997) Regression analysis for a functional response. *Technometrics 39*: 254-261.

Faraway, J.J, Zhang, X., Chaffin, D.B. (1999) Rectifying postures reconstructed from joint angles to meet constraints. *Journal of Biomechanics 32*: 733-736.

Faraway, J.J. (2003) *Data-based motion prediction.* Paper presented at *the Proceedings of SAE Digital Human Modeling for Design and Engineering Conference and Exposition*.

Ferry, M., Martin, L., Termoz, N., Cote, J., Prince, F. (2004) Balance control during an arm raising movement in bipedal stance: which biomechanical factor is controlled? *Biological Cybernetics 91***,** 104-114.

Fitzpatrick, R., Burke, D., Gandevia, S.C. (1996) Loop gain of reflexes controlling human standing measured with the use of postural and vestibular disturbances. *Journal of Neurophysiology 76*: 3994-4008.

Flash, T., Hogan, N. (1985) The coordination of arm movements: an experimentally confirmed mathematical model. *Journal of Neuroscience 7*: 1688-1703.

Frymoyer, J.M., Cats-Baril, W. (1987) Predictors of low-back pain disability. *Clinical Orthopaedics and Related Research 221*: 89-98.

Fujisawa, N., Tasuda, T., Inaoka, H., Fukuoka, Y., Ishida, A., Minamitani, H. (2005) Human standing posture control system depending on adopted strategies. *Medical & Biological Engineering & Computing 43*: 107-114.

Gage, W.H., Winter, D.A., Frank, J.S., Adkin, A.L. (2004) Kinematic and kinetic validity of the inverted pendulum model in quiet standing. *Gait & Posture 19*: 124-132.

Gatev, P., Thomas, S., Kepple, T., Halett, M. (1999) Feedforward ankle strategy of balance during quiet stance in adults. *Journal of Physiology 514*: 915-928.

Genthon, N., Rougier, P. (2006) Does the capacity to appropriately stabilize trunk movements facilitate the control of upright standing? *Motor Control 10*: 232-243.

Gilsing, M.G., van der Bosch, C.G., Lee, S.G., Ashton-Miller, J.A., Alexander, N.B., Schultz, A.B., Ericson, W.A. (1995) Association of age with the threshold for detecting ankle inversion and eversion in upright stance. *Age Ageing 241*: 58-66.

Glass, L., Mackey, M.C. (1977) Oscillation and chaos in physiological control systems. *Science* 197: 287-289.

Gleicher, M. (1997) *Motion editing with spacetime constraints.* Paper presented at *the Proceedings of the 1997 symposium on Interactive 3D graphics.*

Gleicher, M. (2001) *Motion path editing.* Paper presented at *the Proceedings of the 2001 symposium on Interactive 3D graphics*.

Gribble, P.A. and Hertel, J. (2004) Effects of lower-extremity muscle fatigue on postural control. *Archives of Physical Medicine and Rehabilitation 85*: 589-592.

Guez, A., Ahmad, Z. (1990) Improving the solution of the inverse kinematic problem in robotics using neural networks. *Journal of Neural Network Computing 1*: 21-32.

Gundogdu, O. (2000). *Quantification and assessment of objective function performance in manual materials handling.* Unpublished Ph.D. Dissertation, Rensselaer Polytechnic Institute, Troy, NY.

Gunther, M., Otto, D., Muller, O., Blickhan, R. (2008) Transverse pelvic rotation during quiet human stance. *Gait & Posture 27*: 361-367.

Hasan, S.S., Robin, D.W., Szurkus, D.C., Ashmead, D.H., Peterson, S.W., Shiavi, R.G. (1996) Simultaneous measurement of body center of pressure and center of gravity during upright stance. Part II: Amplitude and frequency data. *Gait & Posture 4*: 11-20.

Hassoun, M. (1995) *Fundamentals of artificial neural networks.* Cambridge, MA. The MIT Press.

Hermens, F., Gielen, S. (2004) Posture-based or trajectory-based movement planning: a comparison of direct and indirect pointing movements. *Experimental Brain Research 159*: 340-348.

Hessburg, T., Tomizuka, M. (1994) Fuzzy logic control for lateral vehicle guidance. *IEEE Control Systems Magazine 14*: 55-63.

Hicheur, H., Vielledent, S., Richardson, M.J.E. (2005) Velocity and curvature in human locomotion along complex curved paths: a comparison with hand movements. *Experimental Brain Research 162*: 145-154.

Hillier, E.S, Lieberman, G.J (2005) *Introduction to operations research.* McGraw Hill, New York.

Horak, F.A. (2006) Postural orientation and equilibrium: what do we need to know about neural control of balance to prevent falls? *Age and Ageing 35-S2*: ii7-ii11.

Hsiang, S.H., Ayoub, M.M. (1994) Development of methodology in biomechanical simulation of manual lifting. *International Journal of Industrial Ergonomics 13*: 271-288.

Hsiang, S.M., McGorry, R.W. (1997) Three different lifting strategies for controlling the motion patterns of the external load. *Ergonomics 40*: 928-939.

Hsiao, H., Simeonov, P. (2001) Preventing falls from roofs: a critical review. *Ergonomics 44*: 537-561.

Hsu, W.L., Scholz, J.P., Schoner, G., Jeka, J.J., Kiemel, T. (2007) Control and estimation of posture during quiet stance depends on multijoint coordination. *Journal of Neurophysiology 97*: 3024-3035.

Iqbal, K., Roy, A. (2004) Stabilizing PID controllers for a single-link biomechanical model with position, velocity, and force feedback. *Journal of Biomechanical Engineering 126*: 838-843.

Iguchi, N., Sakaguchi, Y., Ishida, F. (2005) The minimum endpoint variance trajectory depends on the profile of the signal-dependent noise. *Biological Cybernetics 92*: 219-228.

Ishida, A., Imai, S., Fukuoka, Y. (1997) Analysis of the posture control system under fixed and sway-referenced support conditions. *IEEE Transactions on Biomedical Engineering 44*: 331-336.

Isik, C. (1987) "Identification and fuzzy rule-based control of a mobile robot motion," Paper presented at *the Proceedings of IEEE International Symposium on Intelligent Control,* Philadelphia, USA.

Jo, S., Massaquoi, S.G. (2004) A model of cerebellum stabilized and scheduled hybrid long-loop control of upright balance. *Biological Cybernetics 91*: 188-202.

Johansson, R., Magnusson, M., Akesson, M. (1988) Identification of human postural dynamics. *IEEE Transactions on Biomedical Engineering 35*: 858-869.

Jung, E.S., Kee, D., Chung, M.K. (1995) Upper body reach posture prediction for ergonomic evaluation models. *International Journal of Industrial Ergonomics 16*: 95-107.

Jung, E. S., & Park, S. (1994). Prediction of human reach posture using a neural network for ergonomic man models. *Computers and Industrial Engineering, 27*: 369-372.

Kajita, S., Kanehiro, F., Kaneko, K. (2001) *The 3D linear inverted pendulum mode: A simple modeling for a biped walking pattern generation.* Paper presented at *the Proceedings of the 2001 IEEE/RSJ International Conference on Intelligent Robots and Systems*.

Kawato, M. (1996) Trajectory formation in arm movements: minimization principles and procedures. In Zelaznik, H.N. (Eds.), *Advances in Motor Learning and Control*. Champaign, IL: Human Kinetics.

Kiemel, T., Oie, K.S., Jeka, J.J. (2002) Multisensory fusion and the stochastic structure of postural sway. *Biological Cybernetics 87*: 262-277.

Kiemel, T., Oie, K.S., Jeka, J.J. (2006) Slow dynamics of postural sway are in the feedback loop. *Journal of Neurophysiology 95*: 1410-1418.

Kincl, L.D., Bhattacharya, A., Succop, P.A., Clark, C.S. (2002) Postural sway measurements: A potential safety monitoring technique for works wearing personal protective equipment. *Applied Occupational and Environmental Hygiene 17*: 256-266.

Knapik, J., Harman, E., Reynolds, K. (1996) Load carriage using packs: a review of physiological, biomechanical and medical aspects. *Applied Ergonomics 27*: 207-216.

Kuo, A.D. (1995) An optimal control model for analyzing human postural balance. *IEEE Transactions on Biomedical Engineering, 42*: 87-101.

Kuo, A.D. (2005) An optimal state estimation model of sensory integration in human postural balance. Journal of Neural Engineering 2, S235-S249.

Lakie, M., Caplan, N., Loram, I.D. (2003) Human balancing of an inverted pendulum with a compliant linkage: neural control by anticipatory intermittent bias. *Journal of Physiology 551*: 357-370.

Laughton, C.A., Slavin, M., Katdare, K., Nolan, L., Bean, L.F., Kerrigan, D.C., Phillips, E., Lipsitz, L.A., Collins, J.J. (2003) Aging, muscle activity, and balance control: physiologic changes associated with balance impairment. *Gait & Posture 18*: 101-108.

Lee, S., Zhang, X. (2005) Development and evaluation of an optimization-based model for power-grip posture prediction. *Journal of Biomechanics 38*: 1591-1597.

Ledin, T., Fransson, P.A., Magnusson, M. (2004) Effects of postural disturbances with fatigued triceps surae muscles or with 20% additional body weight. *Gait & Posture 19*: 184-193.

Ledin, T., Odkvist, L.M. (1993) Effects of increased inertial load in dynamic and randomized perturbed posturography. *Acta Otolaryngol 113*: 249-252.

Lim, C.M., Hiyama, T. (1991) Application of fuzzy logic control to a manipulator. *IEEE Transaction on Robotics and Automation 7*: 688-691.

Lin, C.J., Ayoub, M.M., Bernard, T.M. (1999) Computer motion simulation for sagittal plane lifting activities. *International Journal of Industrial Ergonomics 24*: 141-155.

Lin D, Hyang S, Nussbaum, M.A., Madigan M.L. (2006) Reliability of COP-based postural sway measures. *Paper presented at the Proceedings of the 50th Human Factors and Ergonomics Society Conference, San Francisco, USA.*

Loram, I.D., Lakie, M. (2002) Human balancing of an inverted pendulum: position control by small, ballistic-like, throw and catch movements. *Journal of Physiology 540*: 1111-1124.

Lord, S.R., Clark, R.D., Webster, I.W. (1991) Postural stability and associated physiological factors in a

population of aged persons. *Journal of gerontology 46*: M69-76.

Mackey, D.C., Robinovitch, S.N. (2006) Mechanisms underlying age-related differences in ability to recover balance with the ankle strategy. *Gait & Posture 23*: 59-68.

Maki, B.E., Holliday, P.J., Fernie, G.R. (1990) Aging and postural control: A comparison of spontaneous- and induces-sway balance tests. *Journal of the American Geriatrics Society 38*: 1-9.

Marler, R.T. (2004) *Development of real-time multi-objective optimization-based posture prediction* (Technical Report No. VSR-04.02).

Martin, L., Cahouet, V., Ferry, M., Fouque, F. (2006) Optimization model predictions for postural coordination modes. *Journal of Biomechanics 39*: 170-176.

Masani, K., Vetter, A.H., Popovic, M.R. (2006) Controlling balance during quiet standing: Proportional and derivative controller generates preceding motor command to body sway position observed in experiments. *Gait & Posture 23*: 164-172.

Maurer, C., Peterka, R.J. (2005) A new interpretation of spontaneous sway measures based on a simple model of human postural control. *Journal of Neurophysiology 93*: 189-200.

Mavrikios D., Karabatsou, V., Alexopoulos, K., Pappas, M., Gogos, P., Chryssolouris, G. (2006) An approach to human motion analysis and modeling. *International Journal of Industrial Ergonomics 36*: 979-989.

McClenaghan, B.A., Williamsb, H.G., Dickerson, J., Dowda, M., Thombs, L., Eleazer, P. (1996) Spectral characteristics of aging postural control. *Gait & Posture 4*: 112-121.

McGill, R., Tukey, J. W., Larsen, W. A. (1978) Variations of Boxplots. *The American Statistician 32*: 12-16.

Meyer, P.F., Oddsson, L.I.E., DeLuca, C.J. (2004) The role of plantar cutaneous sensation in unperturbed stance. *Experimental Brain Research 156*: 505-512.

Mi, Z. (2004) *Task-based prediction of upper body motion*. Unpublished Ph.D. Dissertation, University of Iowa, Iowa City, IA.

Miller P.K. and Bird, A.M. (1976) Localized muscle fatigue and dynamic balance. *Perceptual and motor skills 42*: 135-138.

Morasso, P.G. (1981) Spatial control of arm movements. *Experimental Brain Research 42*: 223-227.

Morasso, P.G., Schieppati, M. (1999) Can muscle stiffness alone stabilize upright standing? *Journal of*

*Neurophysiology 83*: 1622-1626.

Morasso, P.G., Sanguineti, V. (2002) Ankle muscle stiffness alone cannot stabilize balance during quiet standing. *Journal of Neurophysiology 88*: 2157-2162.

Murry, M.P., Siereg, A.A., Sepic, S.B. (1975) Normal postural stability and steadiness: quantitative assessment. *Journal of Bone and Joint Surgery 57*: 510-516.

Naidu, D.S. (2003) *Optimal Control Systems*. Boca Raton, FL: CRC Press.

Norris, J.A., Marsh, A.P., Smith, I.J., Kohut, R.I., Miller, M.E. (2005) Ability of static and statistical mechanics posturographic measures to distinguish between age and fall risk. *Journal of Biomechanics 38*: 1263-1272.

Ohta, K., Svinin, M.M., Luo, Z., Hosoe, S. (2004) Optimal trajectory formation of constrained human arm reaching movements. *Biological Cybernetics 91*:23-36.

Ostergaad, J. J. (1977) Fuzzy logic control of a heat exchange process. In Gupta, M.M., Saridis, G.N. and Gaines, B. R. (Eds), *Fuzzy Aotomata and Decision Processes* (pp285-320). Amsterdam: North-Holland .

Park, W. (2003) *Memory-based human motion simulation.* Unpublished Ph.D. Dissertation, University of Michigan, Ann Arbor, MI.

Park, W. (2004) Toward memory-based human motion simulation: development and validation of a motion modification algorithm. *IEEE Transactions on Systems, Man and Cybernetics – part A: Systems and Humans 34*: 376-386.

Park, W., Chaffin, D.B., Marin, B.J., Faraway, J.J. (2005) A computer algorithm for representing spatial-temporal structure of human motion and a motion generalization method. *Journal of Biomechanics 11*: 2321-2329.

Park, W., Singh, D., Martin, B.J. (2006) A memory-based model for planning target reach postures in the presence of obstructions. *Ergonomics 49*: 1565-1580.

Peeters, H.P.M, Caberg, H.B., Mol, J.M.F. (1985) Evaluation of biomechanical models in posturography. *Medical & Biological Engineering & Computing 23*: 469-473.

Perez, M.A. (2005) *Prediction of whole-body lifting kinematics using artificial neural networks*. Unpublished

Ph.D. Dissertation, Virginia Tech, Blacksburg, VA.

Peterka, R.J. (1995) Simple model of sensory interaction in human postural control. In Mergner T. and Hlavacka F. (Eds.), *Multisensory control of posture* (pp281-288). Plenum Press, New York.

Peterka, R.J. (2000) Postural control model interpretation of stabilogram diffusion analysis. *Biological Cybernetics 82*: 335-343.

Peterka, R.J. (2002) Sensorimotor integration in human postural control. *Journal of Neurophysiology 88*: 1097-1118.

Peterka, R.J., Loughlin, P.J. (2004) Dynamic regulation of sensorimotor integration in human postural control. *Journal of Neurophysiology 91*: 410-423.

Pline, K.M., Madigan, M.L., Nussbaum, M.A. (2006) Influence of fatigue time and level on increases in postural sway. *Ergonomics 49*: 1639-1648.

Prieto, T.E., Myklebust, J.B., Hoffmann, R.G., Myklebust, B.M. (1993) Characterization and modeling of postural steadiness in the elderly: a review. *IEEE Transactions on Rehabilitation Engineering 1*: 26-34.

Prieto, T.E., Myklebust, J.B., Hoffmann, R.G., Lovett, E.G., Myklebust, B.M. (1996) Measures of postural steadiness: differences between healthy young and elderly adults. *IEEE Transactions on Biomedical Engineering 43*: 956-966.

Punakallio, A., Lusa, S., Luukkonen, R. (2003) Protective equipment affects balance abilities differently in younger and elder firefighters. *Aviation, space, and environmental medicine 74*: 1151-1156.

Qu, X., Nussbaum, M.A., Madigan, M.L. (2007) A balance control model of quiet upright stance based on an optimal control strategy. *Journal of Biomechanics 40*: 3590-3597.

Riley, M.A., Balasubramaniam, R., Mitra, S., Turvey, M.T. (1998) Visual influence on center of pressure dynamics in upright posture. *Ecological Psychology 10*: 65-91.

Robertson, D.G.E, Caldwell, G.E, Hamill J., Kamen, G., Whittlesey, S.N. (2004) *Research Methods in Biomechanics*. Human Kinetics, Champaign, IL.

Rosenbaum, D.A., Loukopoulos, L.D., Meulenbroek, R.G.M., Vaughan, J., Engelbrecht, S.E. (1995). Planning reaches by evaluating stored postures. *Psychological Review, 102*, 28-67.

Rosenbaum, D.A., Meulenbroek, R.J., Vaughan, J., Jansen, C. (2001) Posture-based motion planning: Applications to grasping. *Psychological Review 108*: 709-734.

Rougier, P. (1999a) Automatic determination of the transition between successive control mechanisms in upright stance assessed by modeling of the center of pressure. *Archives of Physiology and Biochemistry 107*: 35-42.

Rougier, P. (1999b) Influence of visual feedback on successive control mechanisms in upright quiet stance in humans assessed by fractional Brownian motion modeling. *Neuroscience Letters 266*: 157-160.

Schiffman, J.M., Bensel, C.K., Hasselquist, L., Gregorczyk, K.N., Piscitelle, L. (2006) Effects of carried weight on random motion and traditional measures of postural sway. *Applied Ergonomics 37*: 607-614.

Shin, Y.J., Gobert, D., Sung, S.H., Powers, E.J., Park, J.B. (2005) Application of cross time-frequency analysis to postural sway behavior: the effects of aging and visual systems. *IEEE Transactions on Biomedical Engineering 52*: 859-868.

Singh, N.B., Nussbaum, M.A., Lin, D., Madigan, M.L. (2006) Effects of localized muscle fatigue induced at different joints on postural control. *Paper presented at the Proceedings of the 49th Human Factors and Ergonomics Society Conference, Orlando, USA.*

Soechting JF, Buneo CA, Herrmann U, Flanders M (1995) Moving effortlessly in three dimensions: does Donder's law apply to arm movement? *Journal of Neuroscience 15*: 6271-6280.

Thelen, D.G. (2003) Adjustment of muscle mechanics model parameters to simulate dynamic contractions in older adults. Journal of Biomechanical Engineering 125: 70-77.

Thelen D.G., Schultz, A.B., Alexander, N.B., Ashton-Miller, J.A. (1996) Effects of age on rapid ankle torque development. *Journals of gerontology. Series A, Biological sciences and medical sciences 51*: M226-232.

Tian, J.R., Crane, B.T., Wiest, G., Demer, J.L. (2002) Effect of aging on the human initial interaural linear vestibule-ocular reflex. *Experimental Brain Research 145*: 142-149.

Ulusoy, I., Parnianpour, M., Berme, N., Simon, S.R. (2001) A neural network system with reinforcement learning to control a dynamic arm model. *Biomedical Engineering – Applications Basis &*

*Communications 13*: 117-123.

Uno, Y., Kawato, M., Suzuki, R. (1989) Formation and control of optimal trajectory in human multijoint arm movement. *Biological Cybernetics 61*: 89-101.

van der Kooij, H., Jacobs, R., Koopman, B., Grootenboer, H. (1999) A multisensory integration model of human stance control. *Biological Cybernetics 80*: 299-308.

van der Kooij, H., Jacobs, R., Koopman, B., van der Helm, F. (2001) An adaptive model of sensory integration in a dynamic environment applied to human stance control. *Biological Cybernetics 84*: 103-115.

Vandervoort, A.A. (2002) Aging of the human neuromuscular system. *Muscle Nerve 25*: 17-25.

Vandervoort, A. A., Chesworth, B. M., Cunningham, D. A., Paterson, D. H., Rechnitzer, P. A., and Koval, J. J. (1992) Age and Sex Effects on Mobility of the Human Ankle. *Journal of gerontology 47*: M17–21.

Vaughan, J., Rosenbaum, D. A., Harp, C. J., Loukopoulos, L. D., Engelbrecht, S. E. (1998). Finding final postures. *Journal of Motor Behavior, 30,* 273-284.

Velleman, P.F., Hoaglin, D.C. (1981) Applications, Basics, and Computing of Exploratory Data Analysis. Boston, MA: Duxbury Press.

Verriest, J. P., Rezgui, M. A., Wang, X. (1994) *Experimental validation of arm reach movement simulation. Paper presented at the Proceedings of Triennial Congress of the International Ergonomics Association - IEA '94*.

Vuillerme, N., Burdet, C., Isableu, B., Demetz, S. (2006) The magnitude of the effect of calf muscles fatigue on postural control during bipedal quiet standing with vision depends on the eye-visual target distance. *Gait & Posture 24*: 169-172.

Wang, X., Verriest, J.P. (1998) A geometric algorithm to predict the arm reach posture for computer-aided ergonomic evaluation. *The Journal of Visualization and Computer Animation 9*: 33-47.

Wang, X. (1999) A behavior-based inverse kinematics algorithm to predict arm prehension postures for computer-aided ergonomic evaluation. *Journal of Biomechanics 32*: 453-460.

Winter, D.A. (1990) *Biomechanics and Motor Control of Human Movement* (2nd ed.). New York: John Wiley & Sons, Inc.

Winter, D.A., Prince, F., Frank, J.S., Powell, C., Zabjek, K.F. (1996) Unified theory regarding A/P and M/L

balance in quiet stance. *Journal of Neurophysiology 75*: 2334-2343.

Winter, D.A., Patla, A.E., Prince, F., Ishac, M. (1998) Stiffness control of balance in quiet standing. *Journal of Neurophysiology 80*: 1211-1221.

Winter, D.A., Patla, A.E., Prince, F., Ishac, M. (2001) Ankle muscle stiffness in the control of balance during quiet standing. *Journal of Neurophysiology 85*: 2630-2633.

Winter, D.A., Patla, A.E., Ishac, M., Gage, W.H. (2003) Motor mechanisms of balance during quiet standing. *Journal of Electromyography and Kinesiology 13*: 49-56.

Witkin A., Kass, M. (1988) Spacetime constraints. *Computer Graphics 27*: 335-342.

Witkin, A., Popovic, Z. (1995) *Motion warping. Paper presented at the SIGGRAPH 95 Conference Proceedings*.

Woldstad, J. C. (1997) *Further evaluations of a revised posture prediction algorithm for static lifting*. Paper presented at the Advances in Occupational Ergonomics and Safety II.

Yaggie, J.A., McGregor, S.J. (2002) Effects of isokinetic ankle fatigue on the maintenance of balance and postural limits. *Archives of physical medicine and rehabilitation 83*: 224-228.

Yang, J.F., Winter, D.A., Wells, R.P. (1990) Postural dynamics in the standing human. *Biological Cybernetics 62*: 309-320.

Zadeh, L.A. (1973) Outline of a new approach to the analysis of complex systems and decision processes. *IEEE Transactions on Systems, Man and Cybernetics 3*: 28-44.

Zhang, X., Chaffin, D.B. (1997) Task effects on three-dimensional dynamic postures during seated reaching movements: an investigative scheme and illustration. *Human Factors 39*: 659-671.

Zhang, X., Kuo, A.D., Chaffin, D.B. (1998) Optimization-based differential kinematic modeling exhibits a velocity-control strategy for dynamic posture determination in seated reaching movements. *Journal of Biomechanics 31*: 1035-1042.

Zhang, X., Chaffin, D.B. (2000) A three-dimensional dynamics posture prediction model for simulating in-vehicle seated reaching movements: development and validation. *Ergonomics 43*: 1314-1330.